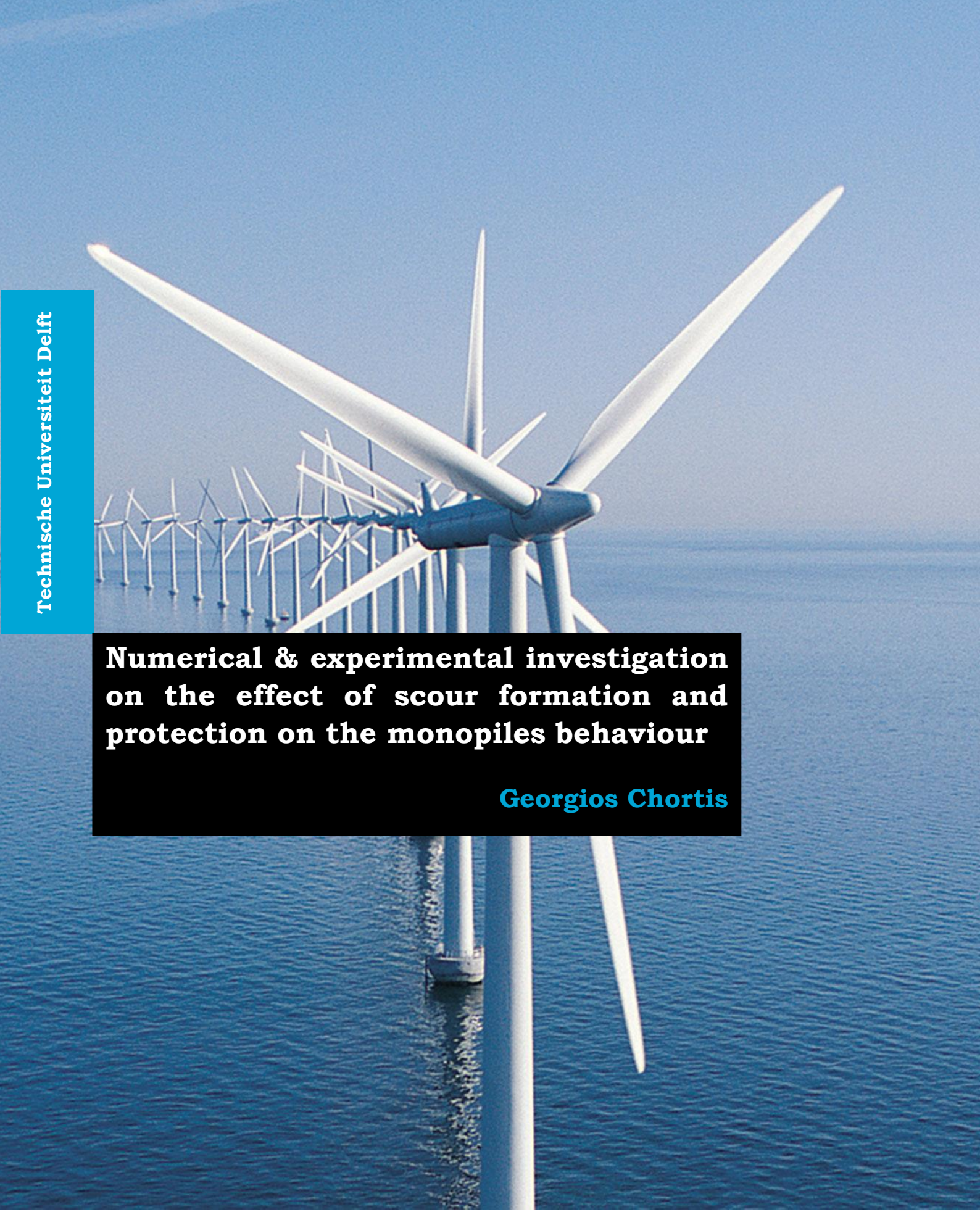

Technische Universiteit Delft

Numerical & experimental investigation on the effect of scour formation and protection on the monopiles behaviour

Georgios Chortis

TU Delft Delft University of Technology

Challenge the future

Numerical & experimental investigation on the effect of scour formation and protection on the monopiles behaviour

by

Georgios Chortis

in partial fulfillment of the requirements for the degree of

Master of Science

in Civil Engineering

at the department of Geoscience & Engineering within the Faculty of Civil Engineering & Geosciences of the Delft University of Technology.

Supervisor:	Dr. A. Askarinejad	TU Delft
Thesis committee:	Dr. Ir. R.B.J. Brinkgreve	TU Delft
	Prof. Dr. K.G. Gavin	TU Delft
	Dr. F. Pisanò	TU Delft

The cover photo depicts a series of offshore wind-turbines, founded on monopiles. (https://wonderfulengineering.com)

An electronic version of this thesis is available at http://repository.tudelft.nl/.

TU Delft Delft University of Technology

Αρχάς είναι των όλων ατόμους και κενόν, τα δ' άλλα πάντα νενομίσθαι.
(Δημόκριτος, 460-370 π.Χ.)

Nothing exists except atoms and void; everything else is opinion.
(Democritus, 460-370 B.C.)

Preface

This MSc thesis was focused on the behavior of the monopiles, when used as a foundation for offshore windfarms. The investigation was conducted both by physical and numerical modelling, combining two basic branches of modern geotechnical engineering. Working in the laboratory, and especially in the centrifuge, proved to be a unique period of my studies, as performing experiments in an environment of 100g is a life-time experience. Numerical simulations in PLAXIS 3D with a sophisticated hypoplastic model offered me also a great deal of skills and knowledge, which I had to acquire in order to progress my research.

I had the chance to work with Dr. Amin Askarinejad, as my daily supervisor, whom I would like to thank for granting me the opportunity to work in such an exciting project and for an excellent co-operation in the whole duration of the project. I owe a lot of gratitude to Prof. Dr. K.G. Gavin, Dr. Ir. R.B.J. Brinkgreve and Dr. F. Pisanò, who are the members of the committee, assessing my work. They have gained my respect not only for their guidance during the project, but also for standing as an example to me, for treating me as an equal engineer, despite their superior experience and knowledge over me. The team of technicians, Ronald van Leeuwen, Kees van Beek and Han de Visser, had an essential contribution in performing my centrifuge experiments, therefore I thank them too. I have also to note the Qiang Li's help, who introduced me in the centrifuge experiments. Special thanks need to be granted to Dr. Luke Prendergast. He was a co-author in three of the four papers submitted by the work of this thesis, and I had gained a new perception in crucial matters of geo-engineering thanks to our co-operation and his comments.

During the MSc thesis and the two-year master program in general, I had the chance to meet new friends, some of whom I now consider family, who stood to me in all the difficulties arisen in this period. Therefore, I need to express my huge gratitude to Antonis, Dimitris, Dionysia, Eleni, Konstantinos, Nikiforos and Vassilis, whose contribution in building a friendly and trusted environment around me is invaluable. Konstantinos and Vassilis, my fellow students in the master, offered me high quality judgement and critical thinking in the whole duration of my studies, which proved to be a valuable asset in providing a high quality work. Eleni is not only my roommate, but also a friend eager to support me in any situation needed. Dimitris and Nikiforos are part in almost every good memory I have from my staying in Netherlands, while Antonis is like an academic mentor to me, by introducing me to the TU Delft. I would also like to thank my brother, who was the first to inspire me to follow the engineering path, and my family as they gave me the opportunity to study in TU Delft and the means to hopefully become an accomplished engineer.

I dedicate my work to all the people that inspire and motivate me to do my best in every project I commit myself to.

Giorgos Chortis
October 2018

Abstract

Offshore wind farms are rapidly developing in Western Europe as an alternative means of clean energy. The foundation of wind-turbines in the shallow water of the Northern Sea is almost exclusively (over 87%) performed by short rigid monopiles, as an efficient and relatively cheap solution. Scour formation, meaning the soil removal around the pile due to the actions of the waves and currents, is a potential hazard for the functionality and the integrity of the structures supporting the turbines. This thesis investigates the effect of scour formation in the soil-pile capacity and examines the possible contribution of the scour protection layers in the stiffness of the system both under static and cyclic loading. The methodology followed included 18 main static and cyclic centrifuge experiments and 9 basic cyclic numerical analyses. The physical modelling included an aluminum pile, equipped with strain gauges in order to calculate bending moments and ultimately derive the "p-y curves", which was embedded in a dense dry Geba sand. Numerical analyses have been conducted in PLAXIS 3D, with a symmetrical fully drained model, in prototype scale, with the same set of materials (Geba sand, aluminum pile).

The results have shown that scour formation can diminish the lateral soil capacity in the ultimate limit state (ULS). Scour depth is the most critical characteristic of the scour hole geometry, but the scour width at a specific depth can also make the difference between structure's integrity and failure. Therefore, the term "local" scour is deemed insufficient, as it cannot be described by a unique geometry. A valid design against scour is recommended to include a series of analyses with combinations of scour depth and width in realistic ranges. Experimental derived "p-y curves" have been compared with the ones proposed by the API method, concluding that the API overestimated both the initial response and the ultimate capacity of the soil reaction. It is proposed to update the existing regulations for the rigid piles and add rotational springs to simulate the effects of the considerable shear developing in the tip of rigid monopiles. The effect of the scour width in the "p-y curves" was observed to be limited in the shallower depth of the pile, as going deeper resulted almost to the same soil response regardless of the type of scour. The cyclic centrifuge experiments focused on the load type, investigating different scenarios of "one-way" and "two-way" load patterns. It was shown that the "one-way" case is more favorable in terms of accumulating deformations compared to the "two-way" case which experienced higher residual displacements, as long as the same maximum load was applied. This was attributed to the smaller dissipation of energy and hence destruction of the soil structure by the "one-way" loading. However, when the maximum load applied in a "two-way" experiment is considerably smaller than the equivalent of the "one-way" test, smaller deformations observed in the "two-way" test, implying the significance of the maximum load. The last section of this thesis, the numerical analyses, focused on the scour protection effect in the mechanical properties of the soil-pile system when subjected to cyclic loading. It was shown that a typical protection layer can highly increase the stiffness of the system and hence decrease the accumulated displacements. The length of the protection layer is not crucial, as change in its magnitude does not alter considerably the reduction of the accumulated displacements, in contrast with the thickness which has a larger impact on the stiffness of the system. It is concluded that scour protection layers can considerably increase the soil resistance around the monopile, allowing for smaller embedment length, so their contribution in the soil-pile stiffness should be taken into account for a more economic design.

Contents

Figures

Tables

Chapter 1

Introduction

The constant increase of the global population along with the evolution of the human needs requires more energy to be produced. On the same context, renewable energy sources are becoming more popular as they considered to be an eco-friendly and yet sustainable alternative for supplying the world with at least part of the demanded energy. As a result, the offshore windfarms have been developed rapidly especially in Western and Northern Europe, leading in lot of research in optimizing their construction. Foundation is a key aspect, and the monopiles have prevailed as the most efficient type of foundation, since they have been chosen in over 75% of the existing wind farms according to Doherty & Gavin (2012) and over 87% according to Wind Europe (2017). However, despite their dominance, there are still mechanisms that can affect their response during the lifetime of the windfarms, that require further investigation.

1.1 Problem Statement & Motivation

The offshore foundation is a challenging branch of geo-engineering. Though a vast series of offshore projects have been constructed especially in the past 50 years, wind turbine's monopiles are relatively a new approach of founding structures in the sea bed. A typical monopile in the aforementioned cases is rigid, with a diameter of 5.0 to 6.0 m and a length of about 30 m, leading to a ratio L/D around 5. However, long and slender piles, with a ratio of L/D more than 20 have prevailed in the past, leading to a lot of understanding for the mechanisms of such piles, which is yet not sufficiently applicable to rigid piles. Therefore, the behavior of the rigid piles needs further investigation, with respect to the prevailing conditions that occur in offshore structures, which affect the stability and the sustainability of the piles.

Scour formation around the pile is a crucial factor that may diminish the offered soil resistance, leading to failure mostly due to serviceability limit state, as excessive deformations are produced during the functionality of the wind turbine. Despite the high chance of formation of large enough scour holes around the monopiles, this phenomenon cannot yet be explicitly predicted, and its effect on the pile capacity based on the scour hole geometry is not yet clear. On the same context, scour protection layers are widely used as preventive measures against scour formation. However, the literature review in this matters has focused in the properties of these layers, without though investigating the possible contribution on the pile capacity, due to the extra overburden pressures around the pile.

The loading scheme that the monopile will endure during its lifetime is another important component to be investigated. A typical offshore wind turbine has to withstand more than 10000 cycles, with a load occurring by the combination of the wind, the waves, the currents and the functionality of the wind turbine. The type of load, meaning its amplitude, the direction or its symmetry, may influence the monopile response. Investigating the realistic loading schemes that may occur will allow for better understanding the monopile response and defining the worst loading scenarios.

As already mentioned, a vast number of offshore projects have been constructed in the past, before the development of the windfarms. *P-y curves* have been a rather popular tool in these cases to simulate the lateral behavior of the piles, as they offered a number of advantages while remaining quite simple to be used. However, this method has been developed for different kind of piles than the rigid ones (mostly slender, long piles) which may render them inappropriate for the wind turbines' monopiles.

Therefore, an evaluation in the suitability of the p-y curves method should be performed, based on some real case or experimental measurements.

1.2 Objectives & Goals

The goal of the current thesis is to expand the knowledge around the behavior of the monopiles, when subjected to lateral loading, by focusing on the points discussed above. The first objective is to investigate the effect of the scour hole formation to the pile lateral capacity. To succeed in this point, the different possible geometry of the scour holes should be investigated, as they are not characterized only by their depth but also by their wideness in the horizontal direction. The second objective, still relevant to scour, is analyzing the scour protection layer's influence in the monopile, and specifically to the lateral capacity and the soil-pile stiffness. The width of the protective layer along with its thickness that corresponds to an extra overburden pressure around the pile affects the stress regime and possibly the pile behavior.

Third objective of this thesis is further investigate the influence of the cyclic load characteristics on the lateral soil capacity of the monopile. A lot of research has been conducted in this topic, yet for a relatively insufficient number of cycles, comparing to the ones that the monopile should endure in its lifetime. In addition to this, the amplitude of the load and especially the ratio between the maximum and the minimum load are considered to have an influence in the monopile response, but not in an absolute way. Therefore, an extra research in these parameters will possibly offer a better insight in this subject. Moreover, the influence of the vertical load to the lateral capacity of the monopile is a topic that should be also investigated as contradictory results exist in the current literature for this matter.

The last objective is about the evaluation of the p-y curves and its suitability in being applied to rigid piles. More specifically, the p-y curves have been developed for many years, and are now part of the API regulations, which have been followed in many offshore projects. However, it is suggested in the literature that p-y curves method is not accurate for modelling rigid piles. Therefore, its applicability should be further investigated and possibly provide recommendations on p-y curves approach for rigid piles.

1.3 Research Question

The main research question that is derived by the problem statements and objectives can be expressed as follows:

"What is the effect of scour formation & scour protection layer in the behavior of a typical rigid monopile embedded in sand in offshore conditions?"

The scouring process is the main component of this thesis, followed by the load conditions that prevail in a typical windfarm. This topic is quite complicated to be investigated as a whole, therefore, a valid approach dictates to divide the main question to sub-questions which will focus only on a certain aspect of the main topic. Specifically, three main sub-questions have been chosen to investigate the topic of the current thesis, which are presented below.

"What is the effect of the scour depth and type in the lateral capacity of the monopile? Which of the two parameters is more critical?"

Scour holes are generally characterized by their geometry and more specifically their depth and type. The second parameter is mostly dependent on the width of the hole. These two parameters have a certain correlation to each other, yet they can be studied separately, in order to isolate and understand each one's importance. Such an approach will allow to understand whether they have a similar influence in the scour formation's effect of diminishing the lateral soil capacity or determine which one is more critical. In addition, a new distinction will be attempted to be made for the different scour types, instead of the two established local and global.

"Can the scour protection layer offer considerable increase in the lateral capacity of the monopile? Which parameters need to be investigated?"

Up to now, the research on the scour protection layers is focused on its properties in order to be able to withstand the actions of the waves and the currents. However, this extra layer that is placed around the monopile could have the exactly opposite effect of the scour hole formation, by increasing the overburden pressures. Two parameters need to be investigated, namely the thickness of the layer, which corresponds to a distributed load, and the width of the protection, which differs in each project as it is case sensitive.

"What is the effect of the lateral loading scheme in the lateral capacity of the monopile? Which components of the cyclic loading needs to be investigated? Does the vertical load have any influence?"

A typical windfarm has to withstand a high number of cycling loading during its lifetime. However, this loading scheme can differ, based mostly on the amplitude of the load and the ratio between the maximum and minimum load. These two parameters are of great importance that need to be investigated, in order to better understand the load effect and have a better insight for the worst cyclic loading scenario. On the same context, the investigation of vertical load influence in the lateral capacity has produced contradictory results, thus experiments for this topic can offer meaningful conclusions.

1.4 Thesis Outline

The current thesis consists of five main chapters and an appendix in the end of the report. This section, chapter 1, is an introductory one, in which the motivation and the problem statement is presented, followed by the research question that is intended to be answered by this thesis.

Chapter 2 includes the background of the topic investigated in the current thesis. Initially, the scouring process is analyzed, explaining the formation of the phenomenon and its characteristics (geometry, range etc.). Then, the scour effects on the soil-pile system's response is presented based on the current research. The last part of the scour section contains information about the scour protection methods and its characteristics, based on field projects. The loading effect in the soil capacity and stiffness follows, in which the focus is given to the cyclic loading, as it is a crucial factor for the lifetime of a typical offshore monopile. Chapter 2 ends with the state-of-art in the investigated topic, by presenting the basic points of the p-y curves proposed by API method and the current recommendations by the relevant global organizations (DNV GL etc.).

The methodology that has been followed in this thesis for answering the research question is presented in chapter 3. The physical and the numerical modelling performed in the TU Delft's centrifuge and PLAXIS 3D respectively are analyzed. Specifically, both models are described with detail, including the material properties, the samples preparation, the constitutive model choice etc., along with the standard procedure followed in both of them. The plan of the series of centrifuge experiments and numerical analyses is also presented, and the concept behind it, is explained.

Chapter 4 contains the outcome of both the centrifuge and the numerical tests. It is distinguished in three main sections, the centrifuge monotonic experiments, the centrifuge cyclic experiments and the numerical cyclic analyses. Finally, the last main chapter follows, the fifth one, in which the conclusions drawn in chapter 4, are briefly discussed.

In the Appendix of this thesis, certain auxiliary numerical analyses are presented, along with assumptions made during the implementation of the results, which have not been evaluated as necessary to be presented in the main body of this report.

Chapter 2

Background

In the current chapter the technical and scientific knowledge for the topic investigated is presented. For a better overview, the whole literature review is divided into three main components, one relevant to the scouring process, one to the load effect, followed by the state-of-the-art for the monopile design and response during its lifetime.

2.1 Scouring Process

The scouring process occurs in general around objects in the seabed due to the actions of the waves and currents, leading to soil erosion. In this thesis, the focus is on the monopiles, both for the scour formation around them and for the preventive measures that can be deployed. These two states are separately described below in the following sections.

2.1.1 Scour Formation

Scour is defined as the erosion of the soil in the surrounding area of an object (such as a monopile) due to water flow caused by waves and mainly currents. Two cases of scour formation can be formed, the global scour, meaning that the elevation of the seabed is getting deeper in a relatively large area around the pile, and the local scour, in which soil is removed around a single pile in an inverted conical shape, forming a hole (Mostafa, 2012).

Figure 2.1 Local scour is observed in the hole that has been formed in each pile, while the global scour can be observed around the whole pile structure. (Whitehouse, 1997)

In general, local scour is most frequently formed around a single monopile, while global scour is common in large windfarms or in cases where strong currents prevail. The main difference between the two types of scour lies in the width of the hole, as the depth has a smaller variance, yet is slightly larger in the local scour holes (Whitehouse, 1997). In Figure 2.1 the distinction between local and global scour can be observed, as two different types of scour holes appear, one developed around each pile (local) and one larger developed in the whole area around the offshore structure (global).

In this thesis, the research is focused on the scour effect around a single typical monopile, both global and narrow. In Figure 2.2, three types of scouring are presented, that are all have been investigated in the literature (Mostafa 2012, F. Li et al. 2013, W. Li et al. 2014). The first two cases, the wide and the narrow one, are characterized as the local scour type while the last shape is the global scour formation. Local type scour formations are most frequent, as they may be caused by moderate waves, currents and the action induced by functionality of the wind turbine, while, as already mentioned, global type of scour implies extreme currents. Robertson et al. (2007), studying the effects of Katrina hurricane, reached the conclusions that global scour formation up to 1.0D may be formed due to sudden storms. In the literature, there is interest for both cases with respect to their influence in the soil-monopile system response.

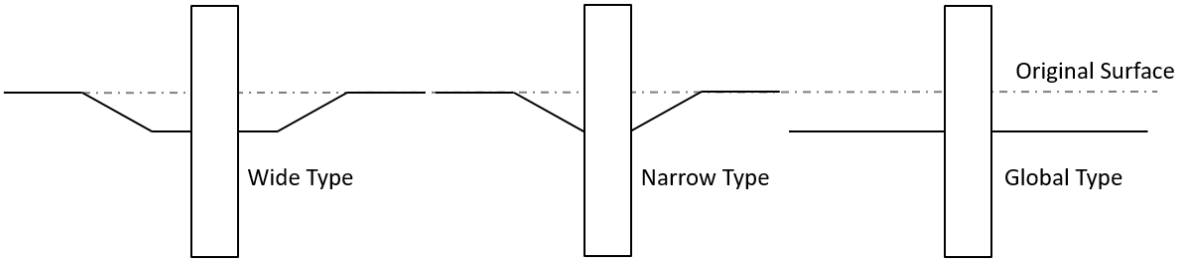

Figure 2.2 Different types of scour holes that may be formed around a typical monopile.

The prediction of the geometry of the scour hole that may be formed is yet not reliable. Based on monitoring of real cases though, the design guidelines of the OWEC suggest that the range of the scour depth is from 1.3 to 2.5 times the pile diameter, based on the work of many researchers (Hjorth 1975, J. S. Jones et al. 1992, Hosny 1995, Whitehouse 1997, Whitehouse 2006, Sumer & Fredsøe 2002, Soulsby 2004, Annandale 2006). On the same context, the research of B. M. Sumer et al. (1992) in scouring around vertical piles concluded that 1.3 times the diameter is a realistic scour depth value, combined with a standard deviation of 0.7D. However, Kuo & Achmus, (2008) state that in real case projects, less conservative values are adopted, since the scour is ranged from 1.0 to 1.5 times the pile diameter, in a vast number of windfarms.

In essence scour formation has two main components that may significantly reduce the offered soil lateral capacity. As the soil erodes in the upper part of the seabed, the free cantilevered length of the monopile is increased, meaning that there is smaller interface between soil and pile, and thus less soil resistance can be mobilized during lateral loading (J. S. Jones et al. 1992). Simultaneously, the stiffness of the soil around the monopile is considerably decreased, as lower overburden pressure occurs due to the erosion of the upper part of the seabed, especially in global scour cases, jeopardizing the stability and functionality of the monopile (Hoffmans & Verheij 1997; B. M. Sumer & Fredsøe 2012).

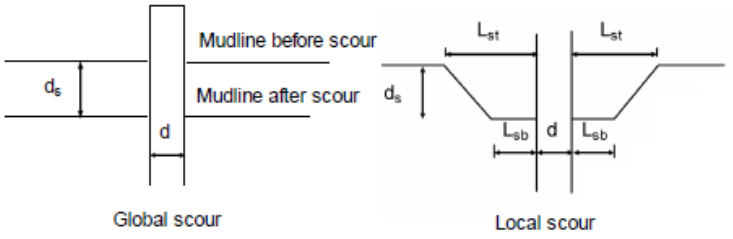

Figure 2.3 Design of the global and the local scour type that have been used in the numerical analyses. (Mostafa 2012)

Mostafa (2012) investigated both the effect of the scour depth and type (Figure 2.3) by numerical analyses in PLAXIS and LPILE. In the set of analyses, it was shown that global scour may diminish the lateral capacity, even for more than 50%, comparing to the no scour case. Moreover, global case was way more critical than the local ones, as it offered about 30 to 50% less soil resistance comparing to

the one offered βu the local scour cases. The comparison between the two local cases, narrow (L_{sb}=0) and wide (L_{sb}=D), proved to have less influence in the results, as the response of the monopile was slightly larger in the narrow case. The bending moment profiles and the pile displacements have also presented the same trend, being in accordance with the aforementioned observations. In total, the findings of Mostafa (2012) stated the high influence of the scour type and the negative effect of the increase of the scour depth in the lateral capacity and pile deflection. These effects were even greater as the pile displacements increased, which were attributed to the non-linear response of the soil and its plastification, leading to decrease of the mobilized soil resistance due to local soil failure.

Qi et al. (2016) investigated the scour effect in the p-y curves by centrifuge experiments for rigid embedded piles in sandy soil. In this research, scour depth and scour type have been both studied, along with the over-consolidation ratio. The final outcome of the experiments was the construction of the p-y curves at different depths, based on the bending moment profiles, acquired by strain gauges along the pile. Then the experimental curves were compared with the ones proposed by the API regulations. The API method proposed a much stiffer response than the actual one, highly overestimating the initial soil resistance. On the same context, the ultimate lateral capacity of the p-y curves was way larger by the API extracted curves. The OCR ratio did not seem to have any considerable effect, as the p-y curves have been mainly affected by the soil surface, after the soil erosion due to scour. However, this effect was limited in the upper part of the soil, as below a certain point the p-y curves of the no-scour case and the scour ones presented close convergence. This was attributed to the higher mobilized soil resistance for the no scour cases comparing to no scour one in the same depth, since the embedded pile length is smaller in scour case, and hence the same load is transferred in smaller area. This phenomenon though is more intense in the upper part of the pile, which was also shown in the bending profiles.

The scour formation may lead to diminishing of the lateral soil capacity of a typical rigid monopile. Many researchers have therefore approached this topic, studying the effect of scouring in the lateral soil capacity, either under constant or cyclic load (L. C. Reese et al. 1989, B.M. Sumer et al., 1992; J. S. Jones et al. 1992, Annandale 2006, B. M. Sumer et al., 2007, Bennett et al. 2009, Kishore et al. 2009, Y. Li et al. 2009, Lin et al. 2010, Mostafa 2012, F. Li et al. 2013, Peder Hyldal Sørensen & Bo Ibsen 2013, L. J. Prendergast & Gavin 2014, L. Prendergast et al. 2015, Qi et al. 2016, L. J. Prendergast et al. 2018). However, the scour phenomenon is not yet fully investigated, as it is not incorporated in the industrial design of relevant constructions, allowing space for extra research.

2.1.2 Scour Protection Layer

Excessive scouring around a monopile can cause serious instability of the structure and consequently its collapse. However, limited scour holes may also lead to certain loss of the lateral capacity of the pile, leading to inability to capture the serviceability limit state. More specifically, the wind turbine can cope with limited displacements in order to be functional and rotate its blades properly, without causing damage to the structure. Knowing already that predicting the scour formation and its geometry is not yet reliable, preventive measures have been developed against scour, by adding special layers in a certain area around the monopile, not allowing the soil to erode, at least not in an excessive quantity. In certain cases, though, large scour holes have already been developed, usually in fields without any protection, requiring mitigation measures to save the structure, which in essence propose the filling of the hole with material of certain specifications.

There is a wide variety of materials that can be used for developing a scour protection layer. Rock armor and filters are a common solution, but more complicated techniques that include rubber derivatives, geo-synthetics and eco-friendly materials have been investigated (Heibaum 2006, Hill 2015, Lengkeek et al. 2017). In the current thesis, the focus is given in the effects of the scour protection to the soil strength properties and therefore the nature of the protection layer is not crucial. As a result, the simplest solution, that included rock dumping is adopted for the experiments and the numerical analyses. The standard procedure for the rocky protection layers, as described by Harris & Whitehouse

(2017) includes two different steps. A first preparatory layer is installed, which consists of small rocks and gravel, at the designated area in the seabed around the pile. In the top of this filter layer, the main armor is placed, which contains large rocks or concrete blocks. This top layer composes the actual resistance against the scour and its properties are defined by the waves and currents that prevail in an area, meaning that scour protection is generally case sensitive. Figure 2.4a offers an visualization of a scour protection system. It needs to be stated though, that despite the guidelines and criteria that dictate the deposition method of the rocks, in reality it is quite difficult to create smooth layers with constant thickness. In certain cases, the scour effects are more severe than expected, requiring immediate mitigation measures to avoid the collapse of the construction. Filling the scour hole that has been formed by dumping rocks and aggregates is a common practice (Figure 2.4b), yet quite expensive procedure, which cannot always guarantee that the scour effects translating in loss of lateral capacity and stiffness will be adequately compensated.

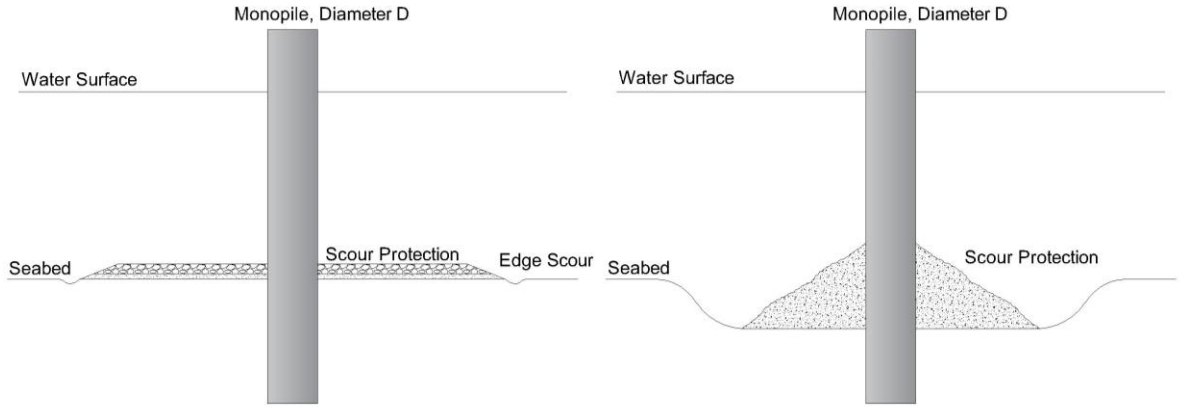

Figure 2.4 (a) Scour protection layer that is installed before scour formation, (b) Scour protection or mitigation measure that is installed after the formation of the scour hole.

Edge scour is an important phenomenon when a scour protection layer is installed. Specifically, the placement of the rock armor, supposing that is functional according to design, leads to no scour in the area that protects, yet it does not prevent scour from happening at its edges. Hence, in a way the scour protection layers are transferring the formation of scour holes away from the center of the monopile. If that distance is large enough, then consequently the scour edge does not pose any danger to the pile. However, it is possible to cause instability issues in the soil around the pile, as scour edge may lead to steep slopes that could dynamically cause soil sliding and collapse.

A series of typical cases in which scour protection layers have been installed or mitigation measures have been employed are presented, for a better overview of the characteristics of protection layers, which have been presented by Whitehouse et al. (2011). The first example is the Horns Rev OWF (Danish North Sea, Denmark), in which a windfarm has been constructed, including monopiles with diameter of 4.25 m in coarse, medium-dense sand. In this field, two protective layers have been installed before the pile driving. The first one was composed by small rocks with particle size d_{50}=0.10 m and had a total thickness of 0.50 m, and the second one, which was the rock armor and the main sour resistance, contained rock material with particle size d_{50}=0.40 m and was 1.5 m thick. The radius of the scour protection around the monopile from its center was 2.2D. It is interesting to state that scour edge has been observed, which was about 0.15D or one third of the total scour protection layer (including filter and armor), without though causing any stability issues. The second case that is briefly described is the Egmond aan Zee OWF (Dutch North Sea, Netherlands), in which monopiles of diameter 4.60 m have been used. In this windfarm, firstly the filter layer has been installed, with a thickness of 0.4 m and nominal rock size of 0.05 m, and has a radius of 2.6D from the center of monopile. On the other hand, the body armor, consisting of a nominal rock size of 0.40 m, 1.40 m thick, has been placed in a radius of 2.0 times the diameter from the center of the monopile, differing in this case from the previous windfarm. However, in both cases, similar configuration has been applied in the design.

The third and last case that is briefly described is about the Arklow Bank OWF (Irish Sea, Ireland). According to Whitehouse et al. (2011), monopiles of 5.0 m diameter have been installed in the seabed without any protection. However, scour holes around 1.0D deep have been formed, creating stability issues to the monopile. Therefore, it was decided to fill the holes with dumbed material, consisting of graded rock and gravel, compensating for the lateral soil capacity loss and increasing the stiffness of the system. After the dumping of the material, a secondary scour took place, yet was limited in the edges of the dumbed material. At a long enough period of time, the scour hole stabilized, being even 1.5D deep at the edges of the rocks, while close to the monopile the phenomenon was limited efficiently, allowing the proper functionality of the wind turbines.

The first offshore windfarms in the 90s have been constructed without any scour protection, as at the time the industry preferred to prolong the piles in order to compensate for possible loss of the lateral capacity due to scour formation. This philosophy, however, has changed in the recent years, as scour protection has become more reliable and thus more attractive from an economic point of view, as prolonging the pile means extra steel for each pile and more action to drive or hammer the pile into the seabed. As already mentioned, the most typical scour protection that is used in the current windfarms consists of rock and concrete blocks, depending on the availability in the region of the OWFs. The rock material used in each layer of the scour protection is characterized by rock's size d_{50}, unit weight and the thickness of the layer (Matutano et al. 2013). One of the biggest challenges in installing the scour protection layer is the dumbing method, as it can be quite difficult to create layers with the desired thickness. The available information for rocky scour protection layers, that have been installed in different regions of OWFs, are presented in the Tables 2.1 and 2.2. Note that the diameter of the scour protection layer and the added effective stress (dictated by the thickness and the unit weight) are the two relevant parameters investigated in this thesis.

Table 2.1 Characteristics of the fields and of the scour protection layers in different OWFs.

Name	**Location**	**Diameter [m]**	**Water Depth [m]**	**d_{50} [m]**	**Thickness [m]**	**Average Unit Weight [kN/m^3]**	**Added Effective Stress [kPa]**
North Hoyle	Liverpool Bay, *Wales*	4.00	10-16	0.3	Unknown	Unknown	Unknown
Egmond aan Zee	Dutch North Sea, *Netherlands*	4.60	15-21	0.4	1.4(armor)	20	14
Thornton Bank	Belgian coast, *Belgium*	5.20	12-27	0.35	0.7	25	17.5
Horn Rev	Danish North Sea, *Denmark*	4.25	6-15	0.2 (filter) & 0.4 (armor)	0.5 (filter) & 0.1 (armor)	25	15
Scroby Sands	North Sea, *UK*	4.20	5-10	0.15	Unknown	Unknown	Unknown
Arklow Bank	Irish Sea, *Ireland*	4.75	3-7	0.425	Unknown	Unknown	Unknown

Table 2.2 Recommendations in literature for the extension of scour protection.

Author	**Extension of Scour Protection**
Bonasoundas (1973)	2.5D-4.5D
Hjorth (1975)	2.5D
Breusers & Raudkivi (1991)	3.0D-4.0D
Hoffmans & Verheij (1997)	2.5D-4.0D
Melville & Coleman (2000)	3.0D-4.0D
May (2002)	2.0D

The data in the abovementioned tables indicate that is generally a high scatter in all the parameters characterizing the scour protection. This can be attributed to the fact that the scour protection in each offshore windfarm is case sensitive, dependent on the local prevailing condition of the waves and currents, affecting the median weight rock size and the thickness of the layers. On the same context, the extension of the scour protection is ranged from 2.0D to 4.5D, meaning there is quite a large scatter. However, the possible effect of the protection layers to the mechanical behavior of the soil-pile system could not be really dependent on its length, as the pile is mainly influenced by the soil in the close proximity of the its installation point.

2.2 Loading Effect

A typical offshore wind turbine is subjected to a constant vertical dead load due to its own weight, and a horizontal cyclic loading by several actions (wind, waves, currents, rotors functionality). Their effect on the monopile response and its lateral capacity are presented in this current section, based on the literature review in these topics.

2.2.1 Cyclic Loading

The cyclic loading, that a typical monopile is subjected to, is characterized by three main components, its frequency, its amplitude and the ratio between maximum and minimum value. The first component, frequency, is dictated by the combination of all actions that load the structure and usually has a small range of values, around f=0.1 Hz (Harris & Whitehouse 2017). Since this value is quite constant and determined by the nature of the actions (mostly due to the currents), the researchers have focused to the two other components (amplitude and the ratio between maximum and minimum value), which are present in a wide range in real-case scenarios. Current research generally recommends the introduction of coefficients for taking into account the effect of cycling loading (Verdure et al. 2003). Site experiments have been widely performed by many researchers (Lymon C Reese et al. 1974, Chang & Whitman 1988, Kramer & Heavey 1988, Little & Briaud 1988, Mezazigh & Levacher 1998, Remaud 1999) close to prototype scale, but they were often conducted for a small number of cycles and with low repeatability. Centrifuge tests have therefore widely used as they provide the possibility for parametrical analyses, and experiments can be duplicated easily (Verdure et al. 2003, Z. Li et al. 2010, W. Li et al. 2014). However, the number of cycles in a typical centrifuge test is relatively small, usually up to 50 cycles, and not really thorough investigation has been conducted for the load types ("one-way", "two-way", etc.).

$$R_H = \frac{H_{min}}{H_{max}} \qquad \textit{Eq. (1)}$$

Eq. 1, proposed by Verdure et al. (2003), is used to distinguish the type of cyclic load, based on its maximum and minimum value. The essence of this distinction is to determine whether the cyclic load changes direction during each cycle or if it keeps pushing the pile towards the same direction with a fluctuating magnitude. Therefore, for values larger than zero, the coefficient R_H corresponds to a cyclic load with constant direction, often called in the literature as "one-way" cyclic loading, while for negative values of the coefficient R_H, the load changes direction and is mentioned as "two-way" cyclic loading. For the special case of the "two-way" loading that the coefficient is equal to -1.0, the load is symmetrical, while for all other cases, it is asymmetrical, which is the most realistic scenario (Harris & Whitehouse 2017). An illustration of the different types of load is given in Figure 2.5, where blue line corresponds to "one-way" loading, the red line to asymmetrical "two-way" loading and the black one to asymmetrical "two-way" loading.

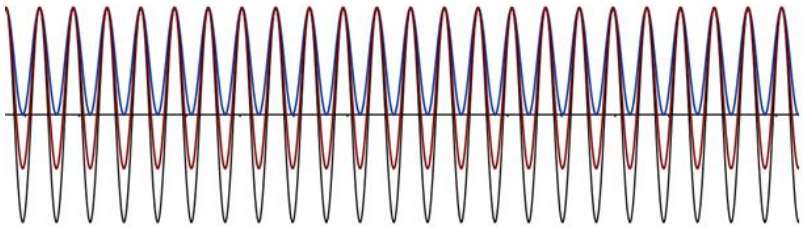

Figure 2.5 "One-way", "two-way" asymmetrical and "two-way" symmetrical cyclic load

According to LeBlanc et al. (2010), the "two-way" cyclic load is more critical than the "one-way" symmetrical one. In their research conducted, they observed that the measured displacements due to cyclic loading in a rigid monopile were up to 4 times larger for the "two-way" case comparing to the "one-way" case. The most unfavorable results in their experiments have occurred for cases simulating unsymmetrical "two-way" cyclic loading, as it caused the highest deformations of the pile. LeBlanc et al. (2010) stated that multidirectional cyclic loading (which is usually more realistic in the field) is a more favorable condition in terms of accumulated deformations, although they have not conducted tests for this scenario. Verdure et al. (2003) investigated different R_H scenarios, all for "one-way" cyclic loading. More specifically, 4 different scenarios were run, with ratios R_H=20%, 40%, 60% and 80%. As this ratio is getting larger, the load tends to simulate a static load, as the fluctuation of the load is minimizing. The aim of their research was the investigation of the effect of the fluctuation of the cyclic "one-way" loading in the lateral deformation and the stiffness of the soil-pile system. All the other parameters in their tests, meaning maximum load, soil's density, installation method, frequency of the load have been kept constant. Eq. (2), used to define the stiffness in each cycle of the tests. Note that the number of cycles conducted was 50, which is quite a small number comparing to the number of cycles that an object in the field will come up against in each lifetime.

$$K_i = \frac{\Delta load}{\Delta displacement} \qquad \textit{Eq. (2)}$$

During the interpretation of the results, Verdure et al. (2003) compared the stiffness in each current cycle with the second cycle, since in the first cycle a jump was observed in the stiffness of the system. This was attributed to the non-linearity caused by the loading and unloading due to the cyclic load. They observed that for large fluctuations (R_H=20%) the relative stiffness (K_i/K_1) was getting larger, as in the last cycle the ratio K_{50}/K_1 was about 1.25. This means that the deformation in each new cycle was getting smaller and smaller, as the load was kept constant throughout each experiment. On the other hand, when the fluctuation was small (R_H=80%) the relative stiffness has been observed to be almost constant as in the end of the 50th cycle there was an increase in the relative stiffness of about 3%. Therefore, the deformation has been kept in almost the same value during the experiment, as the load was constant. Similar observations were made by LeBlanc et al. (2010), in their small-scale 1g cyclic tests on loose and medium dense sand. The number of cycles in their experiments was ranged between 8000 and 60000 cycles, to simulate the real response of an offshore pile. They have found out that the stiffness was getting increased as the number of cycles was increasing, for all relative densities tested, as the main trend was observed both for loose and medium dense sand samples. This behavior is in contrast with the API method, which proposes the degradation of the soil stiffness during the cyclic loading, therefore the API regulations seem to fail to capture properly the cyclic behavior of the sandy soils.

Verdure et al. (2003) also investigated the cyclic load effect on bending moments and the p-y curves. Regarding the bending moments, they observed that as the number of cycles increased, the maximum bending moment was also increased, which can be attributed to the degradation of the soil due to the cyclic loading and therefore the loss of the lateral resistance that may offer. The second observation they made was about the depth of the maximum bending moment, which was getting deeper as the number of cycles increasing, up until it reached a depth of about z=5.0D, while in the monotonic loading the maximum moment was at a depth of about z=4.2D, where D stands for the pile diameter.

The evolution of the p-y curves with respect to the cyclic loading was also studied. More specifically, the peak load H_{max} at each cycle and the corresponding displacement at the same cycle for different depths have been used to plot the evolution of the p-y curves. They have observed that based on the trend of the p-y curves, the soil could be distinguished in two areas with different behavior. At depths ranging from 0 to 3.3D, the soil reaction was getting decreased as the number of cycles was increasing, while the displacement of the pile was increasing with the number of cycles. According to the authors, this can be attributed to the degradation of the soil strength caused by the cyclic loading, as in these depths, the yield limit of the soil has probably been exceeded. On the other hand, though, at depths larger than 3.3D, they observed that each new cycle led to a small only increase of the pile displacement and the soil reaction. Therefore, in larger depths the soil resistance is not considerably affected by the cyclic loading. However, the small increase of the soil reaction is attributed to the fact that in the small depths the soil resistance is reduced and to balance it, more soil resistance needs to be mobilized in larger depths, where there is no excess of the yield limit. These results are in agreement with the API regulations, as they propose to degrade the p-y curves up to a depth z/D=2.63 for taking into account the cyclic load effects, while in case of Verdure et al. (2003) the recommendation is in a depth of z/D=3.3.

Z. Li et al. (2010) have investigated the effect of the lateral cyclic load in pile's response in both axial and lateral direction. In their experiments, the cyclic load ratio (R_H) was kept constant ("one-way"), while the number of cycles ranged from 100 to 1000 in the four experiments performed. They used a dry sand, as the phenomenon is expected to be fully drained, therefore no excess pore pressures occur. This assumption is made in order to execute a relatively simple centrifuge test, since in case of wet sand, a specific viscous fluid should be used instead of water to be in accordance with the scaling laws. Their main object was to study the accumulated lateral deformations caused during the cyclic load, as well as the evolution of the pile lateral secant stiffness during the same load. They observed that even in the case of 1000 cycles, no obvious pile head settlement has been induced, although a certain axial displacement has been caused by the lateral deformation of the pile. However, this axial displacement was limited and attributed to the geometric relationship between lateral and horizontal displacement and not in some other phenomenon caused by the cyclic loading. Regarding the lateral deformation of the pile, they observed that both the maximum displacement and the minimum one (that is the permanent deformation) increase both with the increase of the number of cycles and the increase of the amplitude of the load. The mechanism that causes this behavior is attributed to local densification according to authors. More specifically, the "one-way" cyclic loading that was used in the experiments, lead to high mobilized soil stresses at the maximum load and low mobilized soil stresses at the minimum load. As a result, there is a lack of symmetry and the soil is getting densified mainly in front of the pile, causing the permanent deformations. In the same way, the higher the amplitude, the higher the induced soil stress and therefore a larger area is densified leading to higher permanent lateral displacements. It needs to be noted that in the higher amplitude that was used, the lateral displacements did not converge in a critical value, as they did in the lower amplitudes, implying that if the cyclic loading continued, failure would occur as excessive lateral displacements would occur. The secant cyclic stiffness was measured for each cycle as the ratio of the lateral load to the pile lateral displacement. They observed that in the first cycle there was an extreme increase in the stiffness as expected (similar to the monotonic load). Then when the cyclic loading begins, the stiffness is increasing with the number of cycles, in a reducing rate though. This behavior can be attributed to the densification of the soil, as described before, which will increase the stiffness. However, the densification is more intense in the first cycles, since after a number of cycles the relative density of the sand tends to the maximum one, not allowing for extra densification or at least extra densification occurs in a very slow rate.

Britta et al. (2012) studied the response of a monopile to monotonic and cyclic load, that has been equipped with wings. More specifically, they performed experiments in a centrifuge in two pile, a standard one that is used as reference and one with rectangular wings that have been placed in the sides of the piles. The aim of their study was to obtain a load-deformation relation and compare the results for the standard pile and the winged one. Two kind of piles have been used, short and long ones, subjected to one-way lateral cyclic loading with a frequency of 25 Hz. The amplitude was higher

in the long piles (4.0 MN) than the short ones (0.16, 0.48 & 0.80 MN). After performing a series of tests, they have reached the conclusion that the rate of the accumulation of pile head deflection was pretty much the same in both the standard and the winged pile. The only difference was the fact that the winged pile had a much larger starting stiffness, therefore, the deflection in absolute number was much lower in this case. The conclusion that can be drawn therefore is that the wings in the pile cannot really offer any extra resistance against the cyclic loading, as this type of load will affect in any case the soil. However, in case of limiting the total deflection, or reducing the cost to a minimum by the reducing the pile length, wings may offer a really good solution in marine environments in which cyclic loading prevails.

W. Li et al. (2014) have investigated the lateral response of a monopile in sand under cycling loading by conducting an experiment in a research site in Ireland. More specifically, they placed two piles of 3.0 m long and 34 cm diameter in a dense sand site, which has a relatively density close to 100% and a really high OCR profile in the first 3 meters, ranging from 10 to 40. This site has similar soil conditions to the North Sea, where lots of wind farms have been founded or are designed to get founded in this area. They first defined the ultimate lateral load in static conditions of the aforementioned piles, by performing static load in two identical piles in the same field. Then, having acquired the ultimate load, they could perform the cyclic loading in the two new piles with respect to it. In both piles, during the cyclic loading, the load was ranging from zero to the ultimate load for a certain number of cycles. More specifically, the first pile has been subjected to "one-way" cyclic load with maximum load of 0.2 and 0.5 of the ultimate load, while the last cycle was a monotonic push. In the second pile, the maximum load applied was 0.3, 0.4 and 0.7 of the ultimate load. Similarly, in the end of the experiment, a monotonic push has been applied. The total number of cycles in pile one was 4977 and in pile two was 3173.

The deformations were normalized to the initial value of the first cycle (Y_N /Y_1) for all the different amplitudes that have been performed. They observed that all the graphs (normalized deformation to number of cycles) tend between 1.75 to 2.00 in the axis of Y_N /Y_1 apart from one test, which might have affected from the previous tests. That means that the accumulated deformation due to the cyclic loading could lead up to two times the initial deformation of the soil in the first cycle. An interesting point they have observed was that the rate of accumulation was rapid when the piles have experienced for the first time the cyclic loading. However, in the subsequent cyclic loading (with larger amplitude) the rate of accumulation was much lower, which is possibly due to the previous loading. Therefore, the load history seems to affect the problem. A rather interesting fact though is that in the low amplitudes (about 20 to 30% of the maximum lateral capacity), the displacements tend to get steady after a few cycles (about 100), despite their quick rate of growth, while in higher amplitudes, ranging from 50 to 70% of the maximum lateral capacity the deformations continued to increased even after 1000 cycles in a slow rate though. This phenomenon seems rather important as in a typical offshore wind farm, the extreme weather conditions, that cause cyclic loading through currents, waves and air, will not prevail in the whole lifetime of the structure, but for a relatively small portion of time. Therefore, it is important to know if the deformations in the extreme conditions will accumulate in a sufficiently low rate for the stability and the serviceability of the wind farm.

2.2.2 Vertical Load

The effect of the vertical load in the lateral capacity of a monopile founded in sandy soil and subjected to lateral loading has been widely investigated in the past, yet there is no apparent conclusion as the results are quite contradictory. After conducting analytical investigations, a series of researchers (Davisson & Robinson 1965, Shakhirev & Yanyshev 1969, Shakhirev & Yanyshev 1969, Reddy & Ramasamy 1973, Wentian 1986, Han & Frost 2000) reached the conclusion that vertical load has a negative influence in the lateral soil capacity. However, numerical investigations in the same subject indicated that the soil lateral capacity would increase for an increase in the vertical pile load (Karthigeyan et al. 2006, K. Rajagopal & S. Karthigeyan 2008, Taheri et al. 2015). On the same context, Meyerhof & Sastry (1985) have observed both a positive and a negative influence of the vertical load in their work, while Trochanis et al. (1991), Anagnostopoulos & Georgiadis (1993), Abdel-Rahman & Achmus (2006)

and Achmus & Thieken (2010) have stated that the effect of the vertical load is negligible in the lateral capacity in sandy soils. Therefore, the results are contradictory, which may though be attributed to different approaches by the researchers. For instance, the vertical load may have a different effect when it reaches the ultimate vertical capacity comparing to be far away of this value. In Table 2.3, a summary of the conducted research on the effect of vertical load on the lateral response of piles is presented, which shows that there is not yet a clear conclusion on the topic.

Table 2.3 Summary of the investigation on the effect of vertical load on the lateral response of piles

Method	Author	Effect of vertical load on lateral response	Soil type	Pile material	Pile type (& L/D ratio)
Analytical Research	Davisson & Robinson (1965)	Negative	Sand/Clay	Reinforced concrete	Long flexible
	Shakhirev & Yanyshev (1969)	Negative	N/A	N/A	N/A
	Goryunov (1973)	Negative	Sand	Steel pipe	Long flexible L/D = 48
	Reddy & Ramasamy (1973)	Negative	Sand	Tapering circular	N/A
	Klein & Karavaev (1979)	Positive	Dense soil	Reinforced concrete	Short rigid L/D ≈ 7
	Wentian (1986)	Negative	N/A	Reinforced concrete	Long flexible
	Han & Frost (2000)	Negative	Dense & loose soil	Various materials	Long flexible L/D = 20~80
Numerical Research	Madhav & Sarma (1982)	Negative	Clay	N/A	Long flexible
	Trochanis et al. (1991)	Negligible	Soft clay	Reinforced concrete	Long flexible L/D = 20
	Abdel-Rahman & Achmus (2006)	Negligible	Dense sand	Steel pipe	Short rigid L/D ≈ 7~10
	Karthigeyan et al. (2006)	Positive	Dense & loose sand	Reinforced concrete	Short rigid L/D ≈ 8
	K. Rajagopal & S. Karthigeyan (2008)	Positive	Dense sand	Reinforced concrete	Short rigid L/D ≈ 8
	Achmus & Thieken (2010)	Negligible	Medium dense sand	Reinforced concrete	Long flexible L/D = 20
	Taheri et al. (2015)	Positive	Silty sand	Reinforced concrete	Long flexible
1-g Model Pile Tests	Meyerhof & Sastry (1985)	Depend on vertical load magnitude	Loose sand & soft clay	Steel closed-ended pipe	Short rigid L/D ≈ 13
	Kumar Jain et al. (1987)	Negative	Dense sand	Aluminium open-ended pipe	Long flexible L/D = 30
	Anagnostopoulos & Georgiadis (1993)	Negligible	Soft clay	Aluminium closed-ended pipe	Long flexible L/D ≈ 25
	Lee et al. (2011)	Negative	Various sand density	Steel open-ended pipe	Long flexible L/D ≈ 40

2.3 State-of-the-Art

The design of the offshore construction in general has been based on the regulations and recommendations by API (American Petroleum Institute). Rigid monopiles, that have been used as the foundation of wind turbines, followed the same regulations during their early period. However, the actual response of the field proved to be more critical, than the API method was predicting, leading to stability issues and the overcoming of the SLS (serviceability limit state), as stated by Achmus et al. (2009). Despite certain drawbacks that the application of the API method in rigid monopiles has, it still remains an important tool for offshore constructions, as it was the base of the design for many years. Therefore, it is analyzed in this section, along with the reasons why it fails to fully capture the behavior of a typical rigid monopile.

2.3.1 API Method

API regulations have been incorporated to the offshore piles design in the past years, during the rapid offshore constructions development. The main tool that they proposed and become part of the design is the p-y curves method. The concept of this tool is the simulation of the soil by a series of springs, based on the Winkler type approach. Specifically, the soil is divided into several zones and the response of each one is simulated by a single spring. Note that the springs are uncoupled, and complex sophisticated non-linear expressions can be used for relating the soil resistance (p) caused by lateral deflection (y) in any depth. As each spring is unique, it can have its own characteristics and hence different soil layers or soil heterogeneity can be simulated. The simplicity of applying this method along with the capability of simulating relatively complex soil profiles render the p-y curves tool rather popular among the researchers. The correlation between soil resistance (p) and pile deflection (y) is mathematically described by Eq. (3). Note that the terms E_p and I_p stand for the pile Young's modulus and the moment of inertia respectively.

$$E_p I_p \frac{d^4 y}{dz^4} - p(y) = 0 \qquad \textit{Eq. (3)}$$

Lymon C Reese & Matlock (1956) have initially developed the first version of the p-y curves in the 60s. However, the evolution of the p-y curves to their modern form has started mainly in the 70s and 80s due to the oil and gas industry development, that highly increased the demand for offshore construction and hence piles. A series of experiments have been conducted, many of which in full scale, that investigated the pile response under both static and cyclic conditions (Lymon C Reese et al. 1974, McClelland & Focht 1980, Murchison & O'Neill 1984). Based on the current research at this time, the API 1993 has been published, providing recommendations and standards for the design of offshore piles.

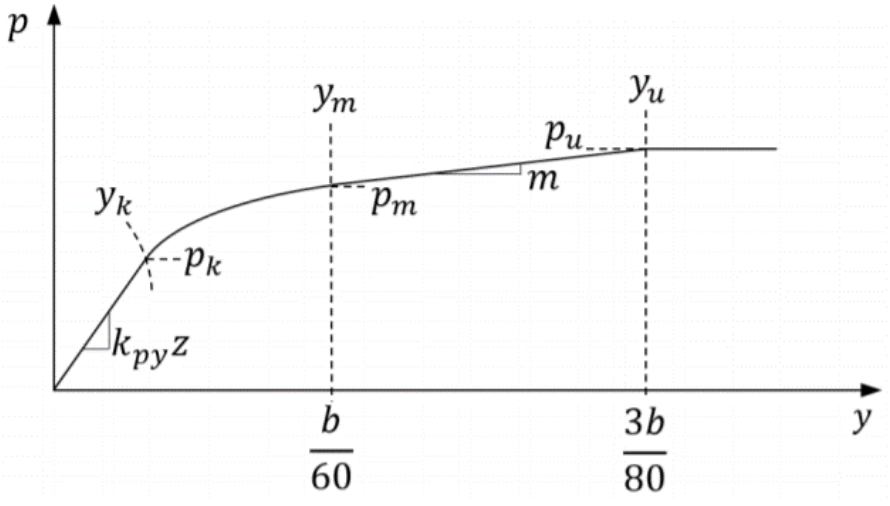

Figure 2.6 p-y curves for sandy soils as proposed by Lymon C Reese et al. (1974)

Figure 2.6 illustrates the shape of the p-y curves for sandy soils as proposed initially by Lymon C Reese et al. (1974). The modern approach of the API regulations as described in API (2007) uses this graph for the formation of the p-y curves. The shape of the curve can be distinguished in three different parts. The first component of the curve adopts an elastic behavior, the third component corresponds to the plastic branch where the soil has reached its maximum capacity, and between them, the second part contains the smooth connection between elastic and plastic area. Note, that the parameter b in Figure 2.6 stands for the pile diameter, meaning that the plastic branch is reached at a displacement of 0.0375 times the pile diameter.

The mathematical expression of the modern p-y curves that are proposed in the API (2007) are presented in Eq. (4). This equation is applied to both static and cyclic loading, by modifying the coefficient *A*, which is an expression of soil depth and pile diameter for static load conditions, and equal to 0.9 for all cyclic conditions, regardless of the problem geometry. The term *H* corresponds to the depth of the derived curve. The term p_u is the ultimate lateral capacity (which obviously differs at each depth) and is derived by empirical charts, correlated by the angle of internal friction and the desired depth. The term *k* stands for the subgrade modulus, that is also derived by empirical charts, in correlation with the angle of internal friction, the soil density and the water table's position with respect to the depth of each curve.

$$p = Ap_u \tanh\left(\frac{kH}{Ap_u} y\right) \qquad \textit{Eq. (4)}$$

The API regulations and recommendations proved to have a wide application in the design of the first offshore constructions. Initially, they have presented a remarkably low rate of failure (Achmus et al. 2009), rendering the method rather popular and well-known in the industry. However, this situation changed when these regulations and recommendations have been applied to the new generation of offshore monopiles, which were short and rigid in contrast to the initial long slender piles. In these cases, the API method tended to overestimated the response of the pile to the field, leading to stability issues and SLS problems. A series of numerical and experimental analyses on the response of a rigid monopile in offshore conditions has been conducted for both monotonic and cyclic loading (Verdure et al. 2003, LeBlanc et al. 2010, Qi et al. 2016). The general conclusion was that the API method highly overestimates the response of the monopile, both in terms of ultimate capacity and of the initial response. Specifically, the API predict a very stiff behavior for small displacements, which is way larger than the actual initial response measured in experiments. Therefore, there is a failure in capturing the actual response of the pile during the design, leading to excessive displacements. This has been attributed to certain aspects of rigid monopile's behavior that are not actually implemented in the API method development. The most obvious drawback of the API method is the fact that all the empirical charts have been derived by measurements of long slender piles, usually with small diameters. Specifically, the API regulations have been derived for small diameter piles up to 3.0 m, while the modern rigid monopiles have typically larger diameters, around 6.0 m. On the same context, the rigid piles, which are over 75% the method of foundation of the wind turbines, behave completely differently, as they do not deform in their axis, but instead they rotate as rigid bodies around a constant rotation point, which is located at a depth of around 3/4 of the embedded pile length. That means that "toe-kick" will appear (Achmus 2010) meaning that the bottom of the pile is moving to the opposite direction of the top, developing high stresses. On the contrary, a slender pile acts as a cantilever, in which the pile deforms in its axis and is deflected up to a point, from which no displacements occur up to the tip of the pile. Therefore, part of the embedded length is not fully activated as in the case of a rigid pile. Consequently, the equilibrium mechanisms for a rigid and a slender pile are quite different, meaning that the API should incorporate in its design possibly different approaches based on the pile stiffness.

The derivation of the ultimate lateral capacity of the soil by the API method seems to be also a point of discussion, as the only crucial soil parameter used is the angle of internal friction (Qi et al. 2016). However, the density of the soil, the stress state etc. also affects the ultimate capacity. On the same context, the initial response cannot only be dictated only by the friction angle, explaining partially the

overestimation that has been observed by the API method. Another point to be taken into account is the cyclic coefficient that the API method has incorporated in its regulations and recommendations. Specifically, the regulations have been derived for a relatively small number of cycles (200 cycles) comparing to the ones that an offshore structure will come up against in its lifetime, that exceed 10000 cycles. Therefore, the fatigue effect, leading to degradation of the soil has not actually been taken into account, meaning that a crucial effect of the cyclic loading has not been incorporated in the aforementioned regulations.

2.3.2 Current State-of-the-Art

The API issues in capturing reliably the behavior of the rigid monopiles have led to criticism over their applicability and in certain cases API regulations have been rendered outdated and old-fashioned. Certain aspects, though, and recommendations of the API method are still considered by many firms and they are consulted during the design phase. However, new regulations and norms have been proposed by International Electrotechnical Commission (IEC), Det Norske Veritas (DNV) and Germanischer Lloyd (GL). These organizations propose recommendations for offshore constructions and hence for modern rigid monopiles. IEC is an international organization focusing on the electrical and electronic technologies around constructions in marine environments. The industry of the wind energy is a sector that IEC is interested in, proposing guidelines and norms towards that matter. IEC 61400-1 (Wind turbines: Part 1: Design requirements) and IEC61400-3 (Wind turbines: Part3: Design requirements for offshore wind turbines;2009) are the two more relevant guidelines to the topic of the current thesis. They focus generally on the foundations of the wind turbines and gives recommendations for the soil-pile interaction, in case a monopile is qualified as the most appropriate type of foundation.

Det Norske Veritas (DNV) and Germanischer Lloyd (GL) are now emerged into a single international organization known was DNV GL. DNV was originally an organization for classifications in Norway, while the GL had the same role in Germany. The new organization, DNV GL, is now the largest classification organization in the field, and provided guidelines and recommendations for maritime contractions, for the renewable energy sector and the oil-gas industry. The monopile design is covered by the "Technical Report, DNV; 2014 (DNV-OS-J101)" and "Guideline for the Certification of Offshore Wind Turbines; 2012, GL" provided by the DNV GL. In these guidelines, the ultimate limit state (ULS), serviceability limit state (SLS) and fatigue limit state (FLS) are discussed and certain factors for the actions acting in the monopiles are provided, along with recommendations relevant to monopiles' design.

Note that the ULS, according to the current state of art, is considered to occur at a horizontal displacement of 0.1D at the soil surface. This value is actually a conventional failure, as it does not correspond necessarily to actual failure, such as excessive deformations or even collapse of the monopile. However, it stands for an indication that the monopile is reaching a no-return situation, meaning that the wind turbine is way non-functional and the integrity of the monopile is under question. Scour formation, which is an important part of investigation in this thesis, is incorporated in these regulations, as they offer predictions for the possible scour geometry. However, it is clearly stated that scour is a case sensitive phenomenon and yet there is not enough knowledge on this matter. Consequently, all the formulas proposed, mainly for scour prediction, are recommended to be used cautiously. The p-y curves are also evaluated by these recommendations. There are certain rules that are proposed, that recommend the reduction of the ultimate lateral capacity at each depth, but the final conclusion given is that the p-y curves tool has been derived for slender piles, and despite being reliable for such cases, it should not be trusted completely for cases of rigid piles, but instead used with caution and as a supportive tool.

Chapter 3

Methodology

The investigation of the topic of the current thesis has been performed both by physical and numerical modelling. Specifically, experiments have been conducted in TU Delft centrifuge facility and additional numerical analyses were performed in the finite element code of PLAXIS 3D (Brinkgreve et al. 2016). The methodology that has been followed for the laboratory tests and the numerical modelling are analytically described in the following sections.

3.1 Centrifuge Experiments

3.1.1 Facilities & Equipment

TU Delft facilitates a beam centrifuge that is used for a wide variety of problems, including slope stability, dikes and embankments, soil structure interactions etc. In Figure 3.1 the centrifuge and a schematic illustration of it are presented, showing the basic standard equipment of the beam centrifuge operating in the university.

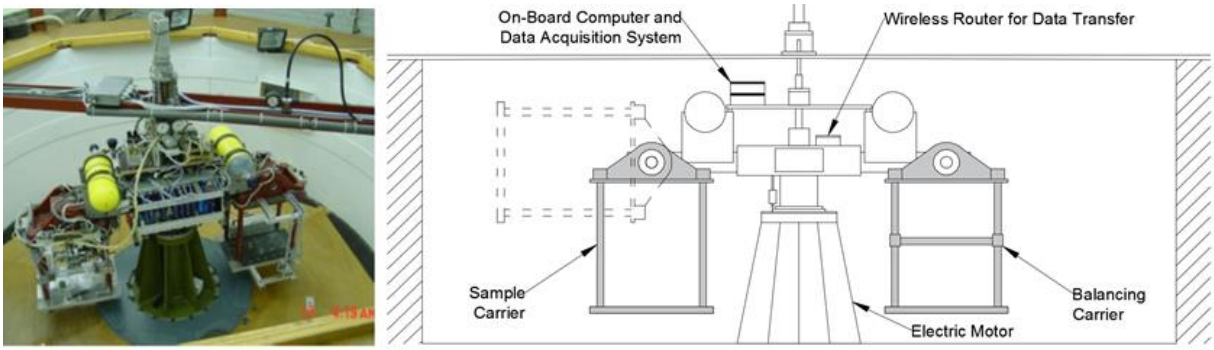

Figure 3.1 TU Delft beam centrifuge and a schematic illustration of its main components (modified after Alderlieste 2011)

The main centrifuge characteristics are presented in Table 3.1 (Allersma 1994). The maximum payload of the centrifuge is 40 kg at its maximum acceleration of 300g (rotation velocity of 450 RPM), while in this thesis a payload of about 23 kg was applied at an acceleration of 100g. The maximum carrier dimensions are also presented in the Table 3.1 and in combination with the strongboxes used, define the size limitations of the model that will be inserted in the centrifuge. The strongboxes that have been used in the current project have dimensions of 410x150x165 mm^3.

Table 3.1 TU Delft Centrifuge Characteristics

TU Delft Centrifuge Characteristics		
Radius of the centrifuge arm *(mm)*		1195
Maximum design acceleration *(g)*		300
Maximum design payload (at 300g)		40
Carrier dimensions	Height *(mm)*	500
	Width *(mm)*	240
	Length *(mm)*	380

3.1.2 Soil Properties

All the experiments have been performed, using the Geba sand. This sand is a uniform silica one, composed of rounded and sub-angular particles. This type of sand is characterized by a mean grain size of d_{50}=0.11 mm, meaning that is a very fine sand, with considerable liquefaction susceptibility in a range of small to medium relative densities (de Jager et al. 2017). Azua Gonzalez (2017) has defined the Geba sand properties with Dr. David Mašín, through experimental tests in the laboratory (triaxial, simple shear and oedometer tests). The three characteristic values of the void ratio have been extracted, the maximum one (e_i), the critical one (e_c) and the minimum one (e_d), which are respectively 1.28, 1.07 and 0.64. Note that the critical void ratio (e_c) corresponds to the void ratio e_{max}, and the minimum void ratio (e_d) to the e_{min}. The tests have been performed for a dense sand, of relative density equal to 80%, which means that the void ratio of the samples that have been placed to the centrifuge carrier was 0.726. The specific gravity Gs was also defined as equal to 2.67, giving a dry unit weight of 15.2 kN/m^3 and a saturated one of 19.3 kN/m^3.

Table 3.2 Basic soil properties of Geba sand

Geba Sand Properties	
Group Symbol Based on USCS[1]	SP
Median Particle Size, D_{50} *(mm)*	0.11
Curvature Coefficient, C_C	1.24
Uniformity Coefficient, C_U	1.55
Specific Gravity, G_S	2.67
Plasticity Index, *PI*	NP
Maximum Void Ratio, e_{max}	1.07
Minimum Void Ratio, e_{min}	0.64

Grain scale effect is a typical problem that occurs in centrifuge experiments. More specifically, through the scaling laws, the geometry of the physical model is converted to prototype dimensions. In that case, if the ratio between the grains and the model (e.g. the pile) is below a certain limit (based on the phenomenon modelled), then the sand does not behave as a continuum medium, affecting considerably the output. In this thesis, the ratio of the pile diameter (D) to the average grain size (D_{50}) is about 164. This value is way larger than 60 which is proposed by Remaud (1999) and Garnier et al. (2007), as the limit value, above which the grain scale effects become negligible for lateral loaded piles. On the same context, the ratio D/D_{50} in this set of tests is higher than the value 20 suggested by Gui et al. (1998), above which the sand behaves as a continuum medium.

All the experiments that have been performed in the centrifuge, have been executed with dry Geba sand, with a relative density of 80%. The reason for using dry sand is due to the scaling law of the centrifuge. More specifically, when the centrifuge rotates at a certain g level, in order to extract the results from the model to prototype, certain factors are used. However, in extracting water flow's results, this factor is different when the correlation between model and prototype is defined from a microscopic and a macroscopic point of view. To deal with this problem, it is possible to use instead of water, a fluid with different viscosity of the water and extract the results accurately. Using such a fluid, though, is relatively hard. As a result, it is quite common, as found in literature (Verdure et al. 2003, Z. Li et al. 2010, Britta et al. 2012), to use a dry sand instead of saturated one in the centrifuge, as sand indicates drained behavior. Therefore, excess pore pressure cannot occur (except for certain cases of cyclic loading), so using drained sand is considered valid.

[1] Unified Soil Classification System (USCS) (ASTM D2487)

3.1.3 Pile Model

An open-ended aluminum pile has been used in the centrifuge experiments (Figure 3.2). Aluminum material was preferred instead of steel as it allows the development of a better model. More specifically, the model needs to simulate a prototype pile, based on the centrifuge scaling laws and the "g-level" performed. Therefore, if steel was used, to have a valid correspondence between the model's and the prototype's stiffness, an extremely small thickness should be applied, less than 1.0 mm. Obviously, such a model would be quite difficult to be constructed, therefore the aluminum pile solution has been chosen. Ten pairs of strain gauges are distributed along the pile shaft (Figure 3.2), for deriving the bending moment profile of the pile during its lateral loading. The type of these strain gauges is FLA-3-11 and have been fabricated by Tokyo Sokki Kenkyujo (Tokyo Sokki Kenkyujo, 2018). It needs to be noted that due to channels limitation of the centrifuge, only 7 out of 10 strain gauges can be used for data acquisition in each experiment. Based on the geometry of each experiment, the most suitable set of pairs of strain gauges was chosen for each case. This choice, and the concept behind it, is analytically described in another section, in which the method of deriving the p-y curves is explained. In the top of the pile two dead loads of 150g have been attached, having in total 300 gr of weight. This dead load is equivalent to 3.0 MN vertical load in prototype scale, which is the typical load that an offshore monopile carries due to the wind turbine.

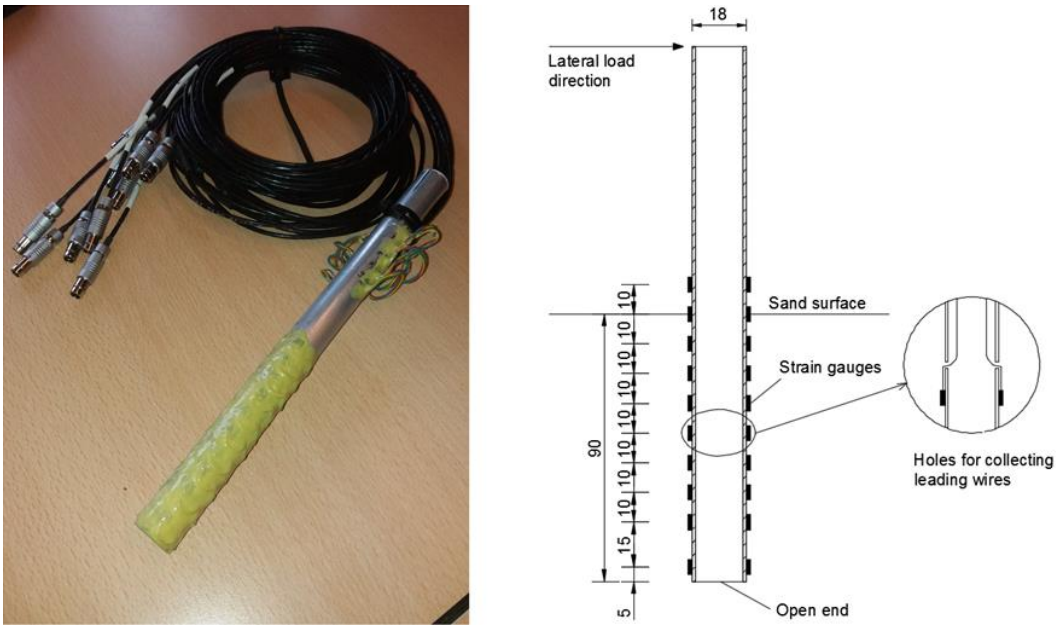

Figure 3.2 Model pile used in the experiments and a schematic illustration of this pile

The pile characteristics are presented in the Table 3.3. The outer diameter of the pile is equal to 18 mm, with a thickness of 1 mm. The total length of the pile is 24.0 cm, while the maximum embedded pile length in the soil is 9.0 cm. It was determined beforehand that at least one pair of strain gauges should be above the current soil surface, for reasons that are discussed analytical in another section. The aluminum Young modulus is 70 GPa, which is about one third of the steel Young modulus.

Table 3.3 Model Pile Characteristics

Model Pile Characteristics					
Outer Diameter	**Thickness**	**Inner Diameter**	**Length**	**Elasticity Modulus**	**Moment of Inertia**
(mm)	*(mm)*	*(mm)*	*(cm)*	*(GPa)*	*(cm4)*
18	1	16	24	70	0.194

By the scaling laws, the model dimensions as well as the experimental results can be extracted into the prototype. The correlation between each parameter for the model and the prototype are located in the Appendix A. From now on, in this project all the dimensions and the results that have occurred by the experiments will be mentioned for the prototype. In Table 3.4, the extracted pile dimensions for the prototype are presented for an acceleration of 100g in the centrifuge.

Table 3.4 Model Pile Characteristics

Equivalent Prototype Pile Characteristics for 100g					
Outer Diameter	**Thickness**	**Inner Diameter**	**Length**	**Elasticity Modulus**	**Moment of Inertia**
(m)	*(m)*	*(m)*	*(m)*	*(GPa)*	*(m4)*
1.8	0.1	1.6	24	70	0.194

Note that in prototype dimensions, the 1.8 m diameter of the pile is not representative of an offshore monopile, as a typical diameter is about 5.0 to 6.0 m. However, the ratio of the embedded pile length to the diameter (L_{emb}/D) is equal to 5, which is a characteristic value that is observed in most offshore windfarms. Therefore, it is valid to assume that the model is in accordance with a typical offshore rigid monopile.

3.1.4 Procedure of Performing the Experiments

In Figure 3.3, the actuator and the sample with the pile in the centrifuge carrier along with a schematic illustration of the whole system are presented. The equipment that was used enables the vertical and the horizontal displacements by the two actuators that it contains (vertical and horizontal). Both actuators are displacement-controlled, meaning that they apply a certain displacement and through load cells the equivalent stress is measured.

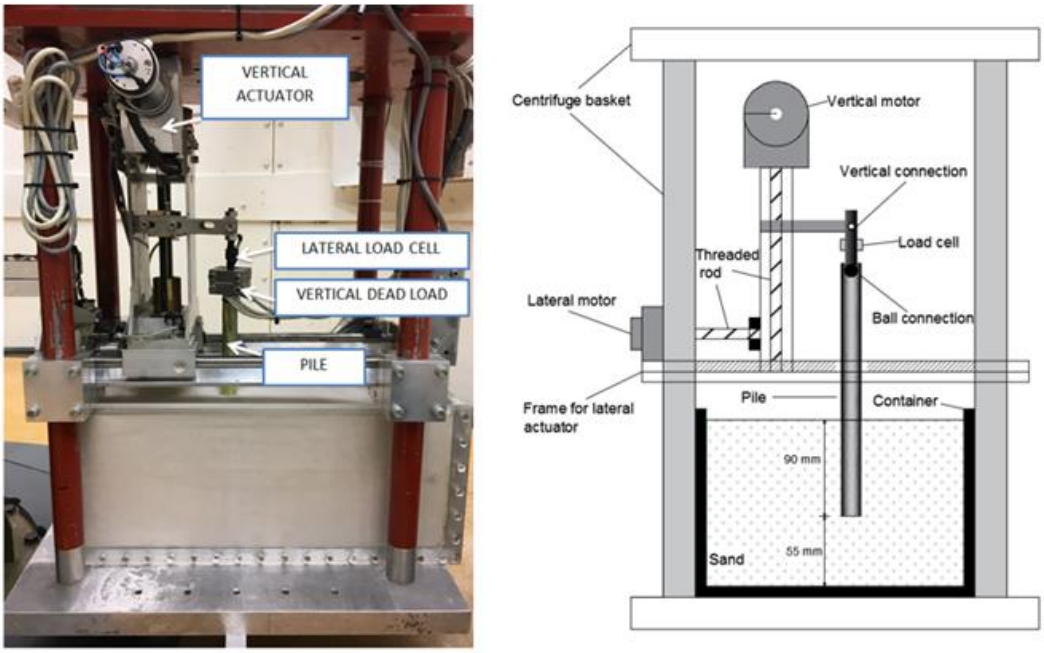

Figure 3.3 The actuator and the sample with the pile in the centrifuge carrier and a schematic illustration of the whole system.

The initial idea was to use the vertical actuator for installing the pile at an acceleration of 100g. However, it was observed that the vertical load has limited functionality at 100g as it is not strong enough to push the pile into the soil. Therefore, it was decided to install the pile at 1g conditions and the execute the

lateral displacement at 100 times the field gravity. The connection of the pile and the actuator is succeeded through a metal ball inserted in the pile. In the upper part of the pile, Teflon has been placed in the inner sides of the pile to create a very smooth surface with the minimum friction possible. This connection is quite innovative, as it allows the ball to slide into the pile's inner surface during the lateral pile deflection, maintaining a constant point of loading. On the contrary, if the connection was not a ball but a beam instead, after a minimum displacement bending moment and torsion would develop, reducing the quality of the results. A special load cell has been created for the set of experiments conducted, which was placed in the rod of the ball connection. This load cell consists of strain gauges which convert the bending moment of the rod to horizontal load. It needs to be stated that the rod is quite rigid, hence it deforms in this axis almost negligibly compared to the pile deflection. Therefore, the displacement sent from the computer room to the actuator and the one that is imposed to the pile are practically the same. In the case, that the rod was not rigid enough, the actual deflection of the pile would be smaller than the one sent by the computer room, due to the high deformation of the pile.

All the samples have been created with a certain procedure to ensure that the same conditions have been applied to all of them. In this way the human error should not affect the results, as the samples were almost identical to each other. They were filled with Geba sand by adopting the "rainy method". This method dictates that sand is falling into the strongbox by using a bucket with small diameter holes form a constant distance. The size of the holes and the distance that needs to be kept is chosen with respect to the desired relative density. As the strongbox is getting filled by the sand, the person applying the "rainy method" should gradually lift the bucket, keeping in this way the necessary distance between bucket and soil surface. The filling should be done smoothly, meaning that no elevation should be observed during the filling of the strongbox. Obviously, at the end of the procedure, the surface cannot be completely flat, but if it is almost there, it can be flattened by using certain tools. It needs to be stated that reaching a relative density of 80%, meaning a high-dense sand, cannot be succeeded only by the gravity energy of the grains as they fall from the bucket to the strongbox. Therefore, extra densification is needed which is often performed by hammering of the sample. However, in this thesis, the strongbox used are relatively large, especially in the long direction, hence hammering would densify the soil more, close to the walls than in the center of the sample. Ultimately, after some tryouts with the hammering, it was decided to use another method for the densification, which dictates raising the strongbox and let it fall in a steady surface from a small distance (around 5 to 10 cm) successively, up until the desired density is captured.

Figure 3.4 Samples prepared for the centrifuge tests, with scour formation (left) and with scour protection (right).

Figure 3.5 presents two typical samples used in the centrifuge experiments, one with a wide type of scour (left), and one with a scour protection layer (right). The scour formation has been succeeded by very softly removing the soil needed to reach the desired scour type and depth. Obviously, removing soil is impossible without distracting the sample. However, if this part of the procedure, is carefully executed, the possible local densification of the soil will be limited in a very shallow area close to the surface. Therefore, the experiment will not be really affected as the main resistance to the pile deflection is offered to higher depths which have remain undistracted in the initial relative density of the 80%. On the same context, the scour protection layer has been installed by adding softly a carton ring in the sample. Then, this ring is filled with sand, and by applying small pressure to the added sand it gets densified. Then the ring is removed, causing obviously the slopes observed above, as sand is a cohesionless material.

It needs to be noted that both the removal and the installation of soil (simulating the scour formation and the scour protection respectively) have been performed at 1g conditions. However, if the same procedure was executed in the centrifuge when accelerated at 100g, it could lead to a different evolution of the experiment. Specifically, forming a scour hole at 1g conditions means that a much smaller overburden pressure is removed from the remaining soil around the mono-pile comparing to the same hole, excavated at 100g. An auxiliary series of numerical analyses (based on the model presented in section 3.2) have been conducted to investigate the possible influence of excavating the scour hole in 1.0g instead of 100g conditions. The results (Appendix B) indicated that the difference between the two approaches is limited in a range of 10% and even less, around 6%, in the ULS area (with the 1g case leading to smaller soil capacity compared to the 100g case). Therefore, it was considered valid to form scour holes at 1.0g, knowing that the potential error is in satisfactory limits, as this procedure enabled to perform the centrifuge experiments time-efficiently.

The geometry of the different scour scenarios investigated is illustrated in Figure 3.5. Specifically, three different scour cases have been investigated, the local that is divided to narrow and wide, and the global one. The difference between local narrow and local wide is observed in the location of the starting point of the slope. Specifically, in narrow case, the starting point is at the pile wall (W_b=0), while in the wide case, the starting point is in a distance of 1.0D from the edge of the pile (W_b=1.0D). In both cases, the slope angle α is equal to 30°, which is in accordance with previous research (Hoffmans & Verheij 1997, Mostafa 2012). For the global case, the geometry is very simple, as the whole soil surface is getting deeper up to the required scour depth. For all three scour cases, three different scour depths (D_s) have been investigated, 1.0D, 1.5D and 2.0D. Note, that the initial embedded length (L) in all cases before the scour formation was equal to 5.0D.

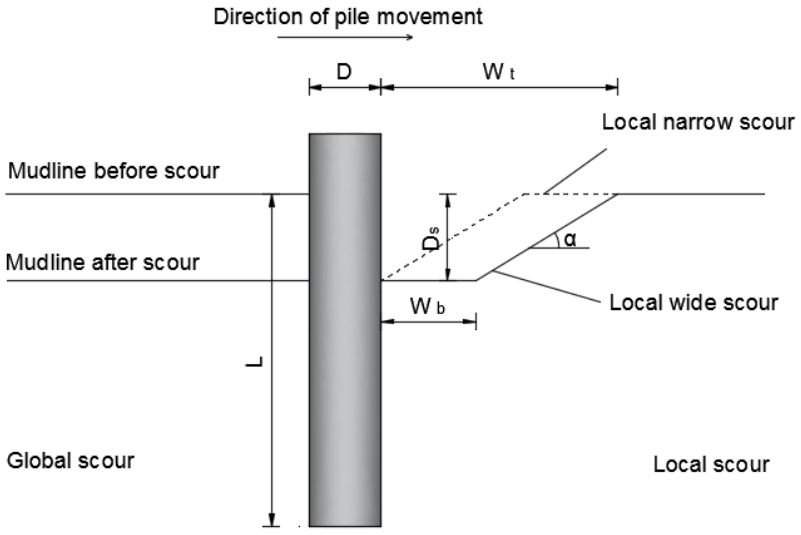

Figure 3.5 Wide type of scour formations as it was modelled in the centrifuge experiments

The scour protection tests aimed to investigate the possible contribution of the extra layer to the soil-pile stiffness, due to the overburden pressure to the soil around the monopile. According to the literature review in previous chapter, scour protection consists of rocky layers of unit weight of around 25 kN/m^3 and a thickness of 1.0 m. Taking into account the buoyancy in the field, that corresponds to an effective load of 15 kPa in the soil around the pile. In the experiments performed, it was decided to simulate the load, and not necessarily the material used. Specifically, adding gravels to simulate the rocks would cause large difficulties in the centrifuge tests without offering considerable advantages, since the mechanism needed to be investigated was the overburden pressure. Consequently, it was crucial to simulate the load and not the material in the centrifuge model. Therefore, a layer of Geba sand was used, with a thickness of 1.0 cm, as it has a dry unit weight of 15.2 kN/m^3, which correspond to a load of 15.2 kPa in prototype dimensions.

After the preparation of the samples, the strongboxes were placed in the centrifuge carriers. The pile was installed manually into the sample at 1g, as the vertical motor was not strong enough to do the installation at 100g. After the installation of the pile and its connection with the actuator through the special ball connection described above, the 7 out of 10 strain gauges were connected to the 7 available channels and the final check of the model and the equipment was performed. Then, the centrifuge room was getting locked and the experiment could start by the computer room, where full control of the actuator and the rest equipment was available. The sample in the carrier was accelerated up to 100g, which was equivalent with 286RPM, and was kept constant at this acceleration for one minute. Depending on the type of experiment (monotonic push or cyclic loading), two different scenarios were following. In the monotonic push case, a lateral displacement with a rate of 0.1 mm/s was applied, until a deflection of 3.0 mm was achieved at the top of the pile (equivalent to 3.0 m in prototype), unless failure has already occurred. In case of cyclic loading, 100 cycles were performed with a rate of 0.01 mm/s. The cyclic experiments were load controlled, although the actuator is displacement-controlled machine. More specifically, the computer had set two load values, as maximum and minimum limits, and the actuator was imposing small displacement towards one direction, while the load was getting measured, up to the load limit value and then immediately was changing direction. Obviously, if the rate was too fast, the actuator would change direction in considerably higher loads than the desired maximum one and respectively lower than the desired minimum one. Therefore, the very low rate of displacement was crucial to coordinate the actuator and the load cell measurements in order to stay within the load limits.

During the whole duration of the experiment, the data measured are transferred to the main computer, allowing for data implementation afterwards. More specifically, the displacement at the ball connection between actuator and pile is given. Note that this is the only know displacement of the pile, as there is no other point where pile deflection or rotation is measured. The measurements of the 7 pairs of strain gauges that have been connected for each experiment are also transferred to the main computer. Each pair gives a single value that corresponds to the strain of the pile wall with respect to the neutral line of the pile. The last values that are sent to the computer room are the load cells' measurements, both for the vertical and the horizontal one. For this set of experiments though, only the horizontal load cell is of interest, as no vertical displacement is imposed to the pile during the experiment.

3.1.5 Series of Experiments

Eighteen experiments have been conducted in total in the TU Delft centrifuge. They can be divided to two main categories, the monotonic loading, consisting of 14 tests, and the cyclic tests, consisting of 4 tests. In the monotonic tests, three sets of analyses have been conducted. The first one's aim was the investigation of the vertical load effect on the lateral capacity of the soil. Three different scenarios of vertical load have been chosen (0.0, 1.5 & 3.0 MN), which has been simulated through dead load attached to the pile. Then the pile was subjected to a prescribed lateral displacement, measuring the equivalent lateral load. The main body of experiments was about the scour formation's effect in the soil lateral capacity and stiffness. Nine experiments have been conducted, for all combinations between scour type (narrow, wide, global) and desired scour depth (1.0, 1.5, 2.0D), all with a dead vertical load

of 3.0 MN (prototype scale), which corresponds to the actual load transferred from a wind turbine to a monopile. The last set of analyses included two tests for the scour protection effect in the lateral soil capacity. The different parameter investigated in the two tests was the length of the scour protection, as the other characteristics of the scour protection (thickness and unit weight) are usually similar in all field projects. The series of monotonic experiments that have been performed are concisely depicted in Table 3.5.

Table 3.5 Series of monotonic experiments performed in the centrifuge.

Vertical Load Set of Experiments				
	Scour Type	**Scour Depth**	**Dead Load(MN)**	**Loading**
1	-	-	0.0	Monotonic
2	-	-	1.5	Monotonic
3	-	-	3.0	Monotonic
Scour Formation Set of Experiments				
	Scour Type	**Scour Depth**	**Dead Load(MN)**	**Loading**
1	Narrow	1.0D	3.0	Monotonic
2	Narrow	1.5D	3.0	Monotonic
3	Narrow	2.0D	3.0	Monotonic
4	Wide	1.0D	3.0	Monotonic
5	Wide	1.5D	3.0	Monotonic
6	Wide	2.0D	3.0	Monotonic
7	Global	1.0D	3.0	Monotonic
8	Global	1.5D	3.0	Monotonic
9	Global	2.0D	3.0	Monotonic
Scour Protection Set of Experiments				
	Scour Protection Length (D)		**Dead Load(MN)**	**Loading**
1	5.0		3.0	Monotonic
2	7.0		3.0	Monotonic

Table 3.6 illustrates the cyclic set of experiments that have been conducted in the centrifuge. All the tests have been run for 100 cycles. It was considered to increase the number of cycles, but it was rejected due to time and data limitation. The first three tests aim to investigate the effect of the type of the load in the pile response, as they include an "one-way" test, a "two-way" asymmetrical and a "two-way" symmetrical. The last test simulates a storm event, as the amplitude increases three times for a limited number of 20 cycles. The concept of this test is to observe how the pile will respond to normal loading conditions, after an extreme loading for limited time.

Table 3.6 Series of cyclic experiments performed in the centrifuge

Cyclic Set of Experiments				
	Loading	**Type of Load**	**Load Amplitude (kN)**	**Cycles**
1	Cyclic	One-Way	0 to 100	100
2	Cyclic	Two-Way	-50 to 100	100
3	Cyclic	Two-Way	-50 to 50	100
4	Cyclic	Storm	0 to 100, 0 to 300, 0 to 100	40, 20, 40

3.2 Numerical Modelling

The numerical analyses have been performed in the finite element code of PLAXIS 3D (Brinkgreve et al. 2016). The numerical model has been mainly developed to conduct extra cyclic analyses, further from the ones performed in the centrifuge. In addition, some assumptions needed to be made during the implementation of the centrifuge tests. It was considered best to use the PLAXIS model to acquire them, as in this way, the assumptions will be based on a scientific background. The model developed with respect to the physical one, meaning that it should be almost identical to it. The characteristics of the model, including geometry, properties etc. are presented in the following sections.

3.2.1 Model Geometry

In Figure 3.6 the numerical model used in PLAXIS analyses is presented. It is a fully drained 3-D plane-symmetric model with respect to xz-plane, as a laterally loaded pile is a typical example of symmetrical problems in geotechnical engineering. The dimensions of the model have been determined to be exactly the same with the samples used in the centrifuge experiments, meaning that the model geometry is 41x7.5x14.5 m. Obviously, the dimensions in the y-axis are divided by two, due to the symmetry of the model. Both the width and the height of the model are not large enough to eliminate possible boundary effects. However, the same conditions existed in the centrifuge samples, where also some boundary effects are expected to occur. Therefore, it was considered valid to keep the same dimensions also in the numerical modelling, to have identical physical and numerical models, at least to a satisfactory level. On the same context, the characteristics of the dry Geba sand were given as input, as the model should be dry to be in accordance with the centrifuge. Geba sand is in general susceptible to liquefaction for low to medium relative densities. In such a sample, excess pore pressures could develop during the cyclic loading, meaning that using a dry sand model may not be a valid approach. However, in this thesis, dense sand is used, with relative density of 80%, while the frequency of the cyclic load applied is generally low. Therefore, conditions are not favorable for excess pore pressures development, hence, using dry sand is a valid assumption.

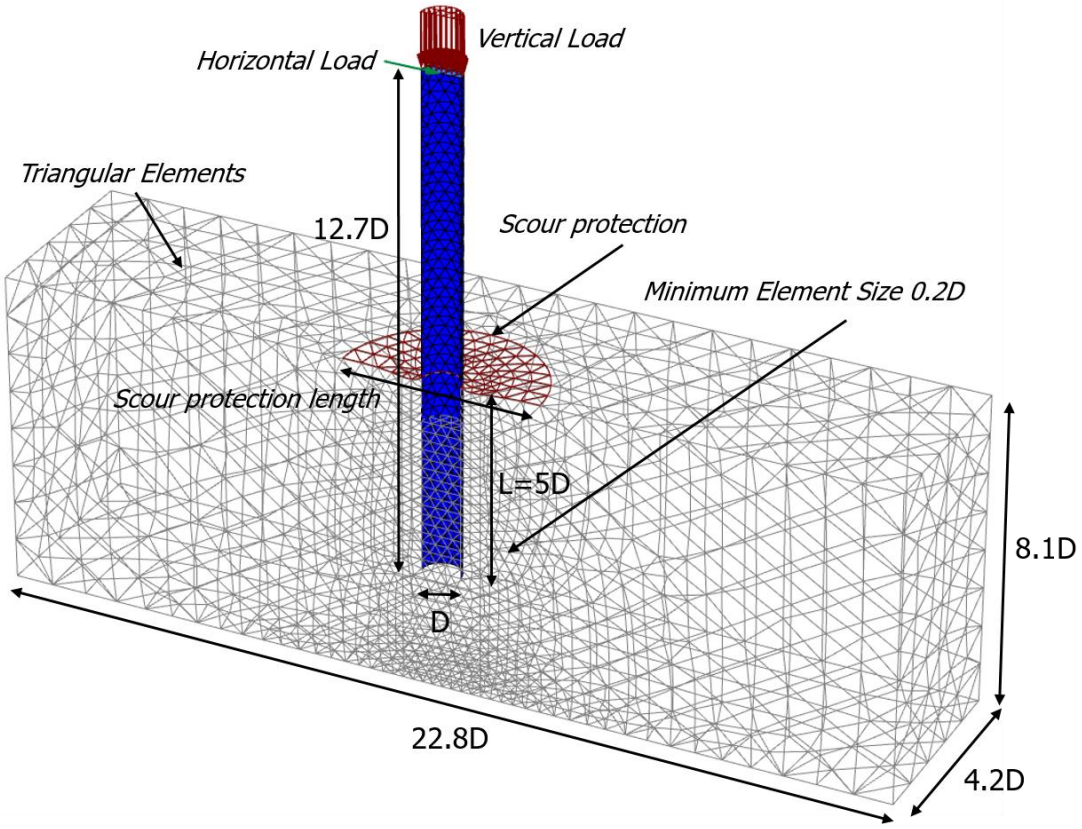

Figure 3.6 PLAXIS model simulating the centrifuge set-up.

The pile has a diameter of 1.8 m and it is embedded 9.0 m deep into the soil. The ratio L_{emb}/D is equal to 5.0, which is a typical value of a monopile in an offshore wind farm. In the centrifuge tests, the pile was loaded vertically with 3.0 MN (in prototype dimension), by attaching special weights. In the numerical model, a very stiff plate was created at the top of the pile (with a thickness of 0.5 m and a Young's modulus of 200 GPa) and was used as the surface where vertical distributed load was applied to. Such a stiff plate was chosen in order not to deform and hence transfer the whole load to the pile walls and mainly to the soil layer, as in the centrifuge. The unit weight of this plate was set equal to 0.0, as otherwise due to its own weight would impose an extra load to the pile. During the analyses, a horizontal load or a horizontal prescribed displacement was applied in the aforementioned plate, for the same reasons as with the vertical load. Figure 3.7 illustrates the distributed vertical load and the horizontal point load applied to the head plate.

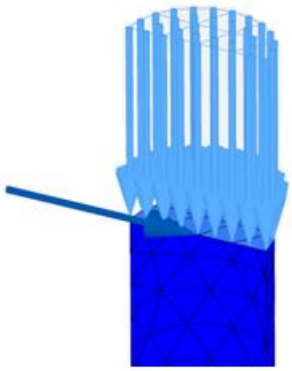

Figure 3.7 Top of the pile, where the dead vertical load and the prescribed displacements are applied.

Based on the constitutive model chosen and the nature of the problem modelled it was decided not to use interface between soil and pile. Specifically, the hypoplastic constitutive model has been implemented in this model, which is presented analytically in the next section. Note this model is a user-defined model and not one of the standard models offered in PLAXIS 3D. Mašín (2011) stated that the use of interface in combination with the hypoplastic model may cause convergence error in certain simulations, as the one in the current thesis. It was then decided to create in the meshing a small soil zone outside the pile with reduced properties to act as an interface. However, the pile used in the centrifuge model, due to the strain gauges and the special sealing glue in its exterior part, is quite rough, meaning that the friction angle between the pile and the soil could be higher than φ. Therefore, applying a friction angle $\delta=2/3\varphi$ seems not to be a valid assumption, hence it was chosen to use an interface friction of $\delta=\varphi$. On the same context, using the small zone created mesh problems, as the quality of the mesh has reduced significantly. A preliminary analysis has been conducted though (Appendix E) with the two scenarios described above ($\delta=2/3\varphi$ & $\delta=\varphi$). No considerable effect has been observed in the lateral capacity of the monopile for these two cases, which can be attributed to the mechanisms affecting the lateral response of a monopile. More specifically, the interface affects mainly the shear stresses which are crucial for the axial loading of the pile, while the lateral loading normal stresses have the larger contribution in the soil resistance. After all, no interface or "interface-zones" have been implemented in the model.

The incremental filling ratio (Figure 3.8) is a term to define the plugging that has occurred in the pile during its driving in the soil. Defining this ratio is practically impossible in the centrifuge, as there is no way to observe or measure up to which length the pile is filled with soil. Therefore, a set of preliminary analyses had been conducted to indicate the effect of this parameter to laterally loaded piles (Appendix E). It was observed that only of really small values of the IFR, the lateral capacity is affected, as for values above 50%, the difference in the system's lateral response was negligible. Consequently, an IFR ratio of 80% was applied, meaning that the interior of the pile was filled up to 1.0D from the initial soil surface.

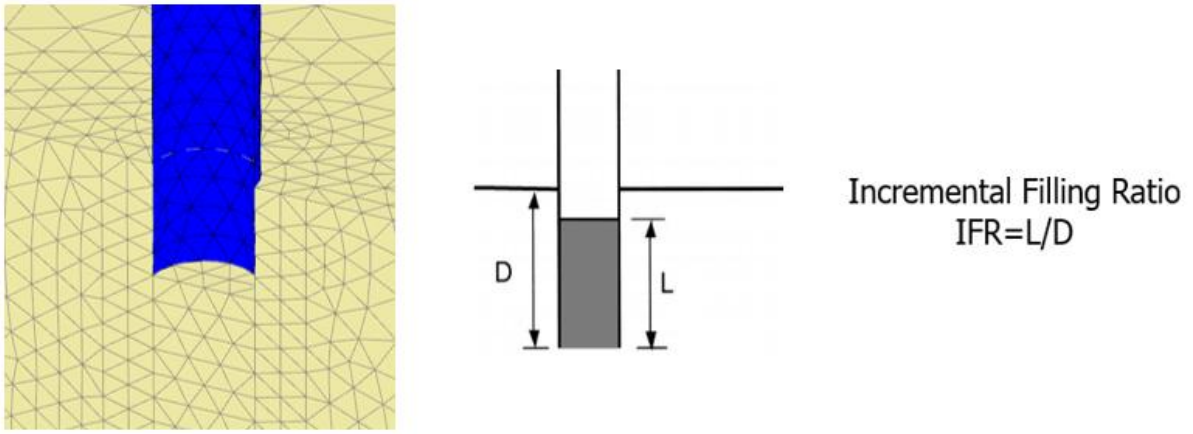

Figure 3.8 Incremental filling ratio of the model pile.

In Figure 3.9, the meshing of the numerical model is depicted. The area of the model in which the pile is installed is densely meshed in an area of about 2.5D, and gradually becoming wider to the boundaries. Note that in PLAXIS 3D a fine mesh has been chosen for the aforementioned area. Having an even more dense mesh was tried in preliminary test analyses, but running the cyclic analyses in a denser mesh was not feasible due to the extreme computational time needed. As a matter of fact, the mesh presented below required roughly 17 hours for a 100-cycles analysis. Having checked though the denser mesh with the one presented below in monotonic analysis, the difference at the load-displacement curve was no more than 10%, meaning that the accuracy of the final mesh is considered to be satisfactory.

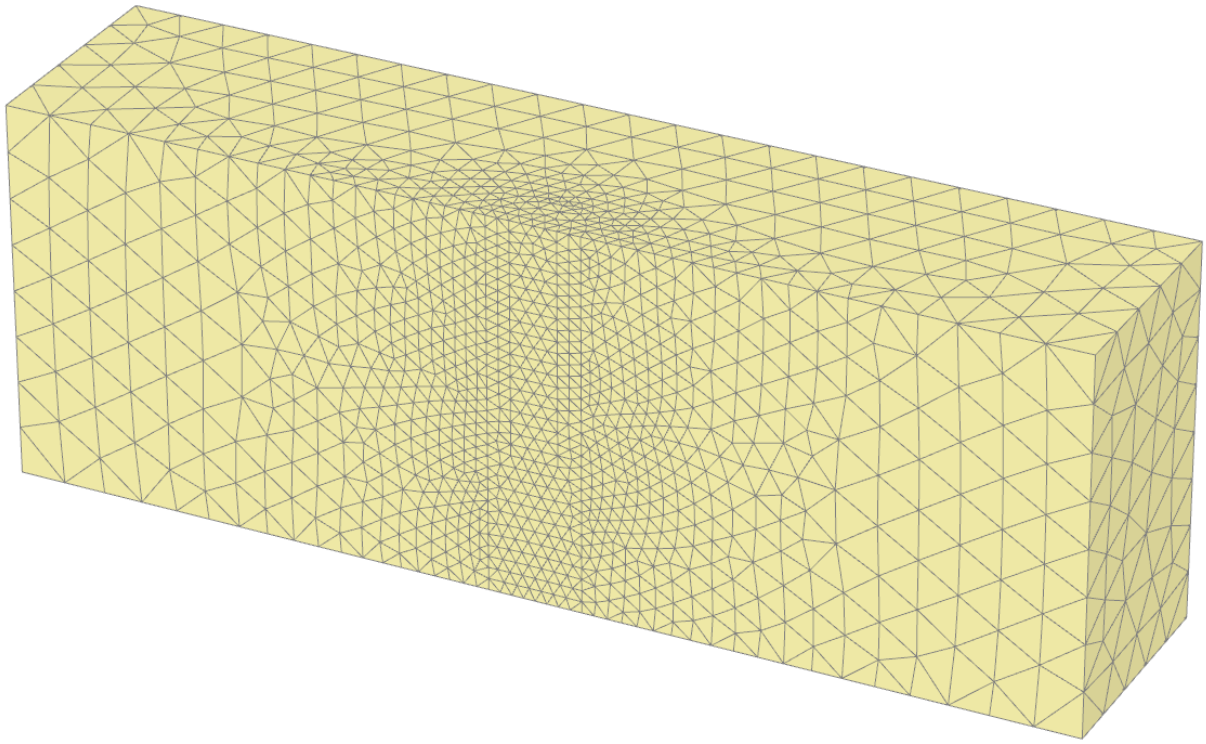

Figure 3.9 Meshing of the PLAXIS model, which includes the pile and the soil.

The goal of the scour protection is to stop the formation of holes around a monopile. The material used for this case are usually dumped rocky blocks, but they can also be rubber derivatives or packed small rocks. Therefore, its possible contribution will not be the one of a homogenous layer, like a very short "embankment". On the contrary, it may affect the soil-pile stiffness due to the overburden pressure in the soil around the monopile. Consequently, the proper way to simulate its effect in the numerical model

is by adding a distributed load around the monopile, instead of adding an extra layer. A typical scour protection layer installed in the numerical model is illustrated in Figure 3.10. It is about a scour protection layer of 5.0D length, which is simulated as a half cycle (the pile area is removed) due to the symmetry of the problem.

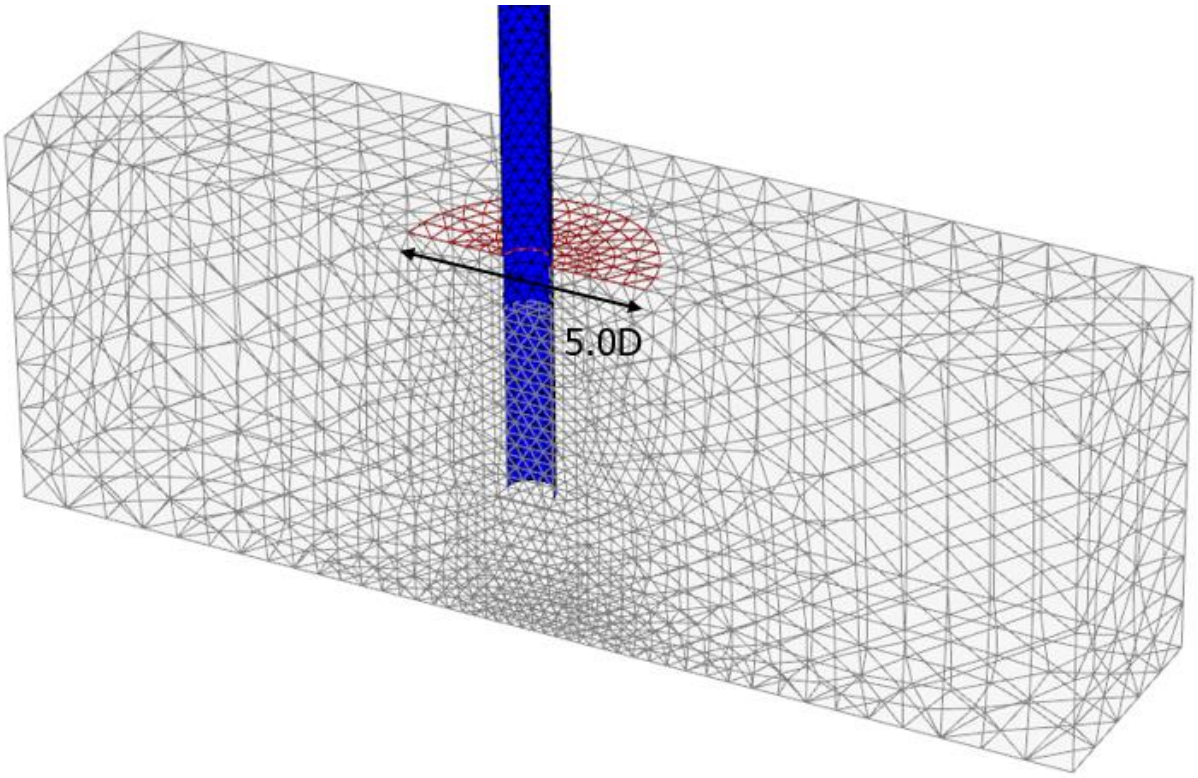

Figure 3.10 Simulation of scour protection of 5.0D length in PLAXIS 3D with (red surface)

3.2.2 Constitutive Model

The constitutive model chosen for this current thesis is the hypoplastic model. It is a sophisticated model, with its main characteristic being the correlation of stress and deformation with a single equation, without distinction between elastic and plastic region. It is considered an expansion of the critical state theory, and it is applied for hardening and softening soil behavior simulation, which was the reason for being used in this thesis. Capturing the undrained behavior of soils is its main disadvantage, as there is a poor accordance between numerical and laboratory results. However, in dry sand (as in this thesis report) undrained behavior cannot occur, therefore, there is no issue. The hypoplastic model contains a lot of parameters, which do not always have a clear physical meaning, rendering its calibration quite difficult. It has been introduced by Kolymbas (1985), with the original idea being the formulation of the inelastic behavior of a granular material by only using a single nonlinear tensor, with a tensorial function of the rate type. Initially, a single state variable was used, the Cauchy granulate stress tensor. Due to its single tensorial equation, no distinction mas made between elastic and plastic area, meaning that principles such as the yield surface, the flow and the hardening rule are non-applicable in the current model. Bauer (1996), added a second state variable, the void ratio e. The version that is used today for the hypoplasticity was developed by von Wolffersdorff (1996), which was based on the previous research, by improving the implementation of the two states variables. The model by von Wolffersdorff (1996) was valid in a wide range of stresses and densities, but certain defects have been revealed in cyclic loading. The most important ones can be described by the term ratcheting, which implies an excessive accumulation of deformations caused by a cyclic loading of small amplitude. For that reason, Niemunis & Herle (1997) introduced the concept of intergranular strain which could predict more accurately the small-strain stiffness and also took adequately into account the recent stress history.

3.2.2.1 Von Wolffersdorff's Version of Hypoplasticity

Von Wolffersdorff's version of the hypoplastic model has been established, with the addition of the intergranular strain concept. Its main advantages are firstly the loading programs that are used, which are not the conventional triaxial tests but instead deviatoric loading paths. In this way, the friction angles acquired are more realistic for both the critical and the limit states of the material. Another improvement comparing to the previous models is that the upper limit of the void ratio is defined by the isotropic compression curve which is the most appropriate one, in contrast to the oedometer one. Note, that the Von Wolffersdorff's version is functional both with and without the intergranular strain concept.

The general form of the hypoplastic constitutive equation is expressed in Eq. (5), in which $\dot{T}$ is the stress rate and depends on the state variables T that is the current Cauchy stress and e that states the void ratio. The term D is the stretching tensor. The rate of the second state variable, which is the void ratio is expressed in Eq. (6).

$$\dot{T} = F(T, e, D) \qquad \textit{Eq. (5)}$$

$$\dot{e} = (1 + e)trD \qquad \textit{Eq. (6)}$$

The parameters e and D in the equation 6 are the same ones described above. The modified hypoplastic constitutive equation as expressed by von Wolffersdorff (1996) is presented in the following equation (Eq. 7). The term F is a function of the deviatoric stress ratio tensor, while the terms $(\hat{T}^*)$ and f_s are described in Eq. (8) and Eq. (9).

$$\dot{T} = \frac{f_s}{tr(\hat{T} \cdot \hat{T})}[F^2 D + a^2 \hat{T} tr(\hat{T} \cdot D) + f_d a F(\hat{T} + \hat{T}^*)\|D\|] \qquad \textit{Eq. (7)}$$

$$f_s = f_e f_b = \frac{h_s}{n}\left(\frac{1 + e_i}{e_i}\right)\left(\frac{e_i}{e}\right)^{\beta}\left(\frac{-tr(T)}{h_s}\right)^{1-n}\left[3 + a^2 - \sqrt{3a}\left(\frac{e_{i0} - e_{d0}}{e_{c0} - e_{d0}}\right)^{\alpha}\right]^{-1} \qquad \textit{Eq. (8)}$$

$$\hat{T}^* = \hat{T} - \frac{1}{3}I \qquad \textit{Eq. (9)}$$

In the equation 8, the factors f_b, f_d and f_e are used to describe the density dependence (pycnotropy) and the pressure dependence (barotropy) as proposed by Kolymbas (1985). The basic concept of using this factors is to separate the density and pressure dependence from the tensorial part of the response function F. In order to improve the previous versions of the hypoplasticity models, Kolymbas (1985) developed functions that have been based to the Drucker/Prager model and the Matsuoka/Nakai yield criterion. The term α describes the failure according to the aforementioned yield criterion, which is expressed in Eq. (10).

$$a = \sqrt{\frac{3}{8}}\frac{(3 - sin\varphi_c)}{sin\varphi_c} \qquad \textit{Eq. (10)}$$

Regarding the void ratio, three characteristic values are implemented in the model, the maximum void ratio (e_i), the minimum void ratio (e_d) and the critical void ratio (e_c). According to Bauer (1996), all the state values of the void ratio are reducing with the mean pressure which is defined in Eq. (11).

$$p_s = -tr(T/3) \qquad \textit{Eq. (11)}$$

The void ratio will reach the values of e_{i0}, e_{d0} and e_{c0} when the mean skeleton pressure is almost vanished, while for really great values of p_s will approach a zero value. Of course this conditions are

considered to be transitional, as the extreme values of p_s can be connected to grain crushing and suppression of dilation, hence the model is consistent for a high range of values between these two extreme conditions. Eq. (12) expresses the relationship between void ratio states and mean skeleton pressure.

$$\frac{e_i}{e_{i0}} = \frac{e_d}{e_{d0}} = \frac{e_c}{e_{c0}} = \exp\left[-\left(\frac{3p_s}{h_s}\right)^n\right] \qquad \textit{Eq. (12)}$$

The hypoplastic model as proposed by von Wolffersdorff (1996) requires eight parameters as an input. These parameters are briefly described in Table 3.7.

Table 3.7 Parameters required in the hypoplastic model proposed by von Wolffersdorff (1996)

Parameters	Physical Meaning
φ'_{cv}	Critical state friction angle. It is obtained by the angle of repose.
e_{i0}, e_{d0}, e_{c0}	Maximum, critical and minimum void ratio at vanishing mean skeleton pressure. They are obtained by index tests.
h_s	Granular hardness, expressed in units of stress. It is used as a reference pressure and does not represent the strength of single soil grains. It is obtained by oedometer compression test.
n	Dimensionless exponent which correlates to sensitivity of granular skeleton to changes of pressure. It is determined by oedometer compression tests.
α	Dimensionless exponent related to the transition between peak and critical stress. Determined by monotonic triaxial test.
β	Dimensionless exponent representing the change in stiffness at current density. Determined by oedometer compression test.

3.2.2.2 Intergranular Strain Concept

The original hypoplastic models that have been developed (Gudehus 1996 & Bauer 1996), even the von Wolffersdorff's version, presented defects during loading in small stress cycles, as excessive accumulation of deformations has been observed leading to unrealistic large displacements. According to research conducted by Atkinson et al. (1990) and later by Puzrin & Burland (1998) which including experimental measurements, the soil response in the small strain region is highly inelastic and is affected mainly by the stress path history and the strain direction. Niemunis & Herle (1997) introduced a new state parameter, the intergranular strain (h). This tensorial state variable takes into account the deformation of the granular interfaces along with the re-arrangement of the soil grains in the small strain region to solve the aforementioned weakness of the von Wolffersdorff's version.

The integration of the intergranular strain in the hypoplastic model mainly affects the stiffness calculation. More specifically, the intergranular strain tensor is driven by the difference in the direction of the actual strain rate $\dot{\varepsilon}$ and the intergranular strain rate $\hat{h}$ along with the value of the tensor h. This is depicted in the equations 13 and 14 below.

$$\dot{h} = \begin{cases} \left(\Im - \hat{h} \times \hat{h}\rho^{\beta_r}\right) : \dot{\varepsilon} & for \;\; \hat{h} : \dot{\varepsilon} > 0 \\ \dot{\varepsilon} & for \;\; \hat{h} : \dot{\varepsilon} \leq 0 \end{cases} \qquad \textit{Eq. (13)}$$

$$\hat{h} = \begin{cases} h/\|h\| & for \;\; h \neq 0 \\ 0 & for \;\; h = 0 \end{cases} \qquad \textit{Eq. (14)}$$

The magnitude of the intergranular strain tensor h is calculated as $\rho = \|h\|/R$, with R being the intergranular strain radius. The maximum value that the tensor can acquire cannot exceed the value of the parameter R, which is in a range of 10^{-7} to 10^{-3} for large and small grains respectively. The general interpolation of the stiffness M is performed for the relative angle θ between the current strain rate $\dot{\varepsilon}$ and the recent strain history (Eq. (15)).

$$M = [\rho^x m_T + (1-\rho^x)m_R]\mathcal{L} + \begin{cases} \rho^x(1-m_T)\mathcal{L}:\hat{h}\times\hat{h} + \rho^x N\times\hat{h} & for \quad \hat{h}:\ \dot{\varepsilon} > 0 \\ \rho^x(m_R - m_T)\mathcal{L}:\hat{h}\times\hat{h} & for \quad \hat{h}:\ \dot{\varepsilon} \le 0 \end{cases} \qquad \textit{Eq. (15)}$$

The intergranular strain concept (ISC) as proposed by Niemunis & Herle (1997) requires five parameters as an input. These parameters are briefly described in Table 3.8. As already stated, the addition of the ICS in the von Wolffersdorff's version allows the model to simulate small strain behavior, meaning that it can capture sufficiently the soil response when subjected to cyclic loading. An overview of the ICS effect in the performance of the hypoplastic constitutive model is given in Appendix C.

Table 3.8 Parameters required in the hypoplastic model proposed by Niemunis & Herle (1997)

Parameters	Physical Meaning
R	Radius of elastic range, that indicates the maximum strain at which no longer linear elastic response of the soil is expected. Obtained by cyclic triaxial test.
m_R	Stiffness increase after full load reversal (180°). Obtained by biaxial test.
m_T	Stiffness increase after a 90° change in the direction of the strain path. Determined by cyclic shear test.
β_r	Dimensionless constant that controls the rate of the intergranular strain. Obtained by cyclic triaxial test.
χ	Dimensionless material constant that represents the degradation of the soil stiffness. Determined by cyclic triaxial test.

3.2.3 Material Properties

The hypoplastic model requires a certain number of parameters in order to be defined. The ones that are directly related to the sand properties, such as the three void ratios states (minimum, critical and maximum) and the unit weights (dry and saturated) are already known as presented in the previous chapter 3.1.2. The rest have been calibrated initially based on the work of Dr. David Mašín, who has performed laboratory tests for the Royal IHC (Mašín 2017). Note that Dr. Mašín has highly contributed to the evolution of the hypoplastic model, hence he is considered among the researchers' society an expert in the hypoplasticity. However, his report regarding the calibration cannot be presented in this thesis due to confidentiality issues. After the initial validation, there was not a satisfactory match between numerical and experimental analyses. Therefore, a second validation was conducted by the author, based both on monotonic and cyclic tests, which are presented in (Appendix D).

3.2.3.1 Soil

The parameters for the hypoplastic model that have occurred by the calibration of the model are presented concisely in the Table 3.9. They are distinguished into two parts, the von Wolffersdorff (1996) version' parameters and the intergranular strain concept's ones. Specifically, the calibration of the Von Wolffersdorff's parameters has been mainly based on the monotonic tests, while the intergranular strain concept's ones have been extracted based on the cyclic tests. These parameters have been given as input for the constitutive model to the PLAXIS 3D model. Note that the hypoplastic model (known as UDSM in PLAXIS 3D) is a user-defined model and not yet incorporated in the software as standard model for the 3D version.

Table 3.9 Hypoplastic model parameters after the calibration of the PLAXIS 3D model

von Wolffersdorff's hypoplastic model parameters							
φ_c	h_s	n	e_{d0}	e_{c0}	e_{i0}	α	β
34	4200MPa	0.15	0.640	1.070	1.280	0.07	0.75
Intergranular Strain Concept							
m_R		m_T	R_{max}		β_r		χ
6.9		5.0	0.0001		0.3		1.0

3.2.3.2 Pile

The pile has been modelled in the PLAXIS 3D by plate elements, having the same characteristics as the centrifuge pile, after been extracted to the prototype dimensions. The aluminum elasticity modulus was adopted again, while the rest of the pile's characteristics are presented in the Table 3.10. The behavior of the pile is modelled by an elastic isotropic model, where the elasticity modulus and the poisson ratio are 70 GPa and 0.3 respectively. The unit weight of the aluminum is γ=27 kN/m^3, which is one of the parameters that are required by the PLAXIS 3D for the plates.

Table 3.10 Model Pile Characteristics

Outer Diameter	**Thickness**	**Inner Diameter**	**Length**	**Elasticity Modulus**	**Moment of Inertia**
(m)	*(m)*	*(m)*	*(m)*	*(GPa)*	*(m4)*
1.8	0.1	1.6	24	70	0.194

3.2.3.3 Soil-Pile Interaction

As already discussed in the section 3.2.1 (Model Geometry), the PLAXIS model should identical to the maximum level possible to the prototype model extracted by the centrifuge one. Therefore, a soil-pile interface that corresponds to the actual model of the centrifuge should be used. The ordinary choice is to have an interface with a friction angle δ equal to 2/3 of the internal friction angle φ, but in this certain case it was considered more valid to choose an interface with an external friction angle equal to the internal friction one, hence δ=φ. This choice was based on the pile roughness and the nature of the problem (Appendix E). Note that all the numerical analyses conducted for this thesis included laterally loaded piles, while the friction between pile and soil is more crucial in cases of axial loading. Therefore, this parameter is not considered crucial for the nature of the problem investigated.

3.2.4 Series of Analyses

The numerical analyses conducted in PLAXIS 3D can be divided into two categories. The first one, the basic cyclic set of analyses, investigates the effect of load properties in the monopile response. It repeats two of the centrifuge tests, the most likely to occur in offshore conditions, meaning the "one-way" loading the "two-way" asymmetrical. In addition to them, two more tests have been decided, with their amplitude changing every 25 cycles. In the first one, the maximum load is gradually increases from 25 kN to 100 kN with a step of 25 kN. The other test consists of rapid changes between the load, as the maximum load goes from 100 to 300 kN, then reduces to 100 kN and after 25 cycles it reaches again a value of 300kN. The second set of analyses is focused on the scour protection layers. More specifically, it contains five tests in total in which the scour protection length and load (which is equivalent to their material density and thickness) are investigated. The cyclic parameters are constant (100 cycles of "one-way" loading from 0 to 100 kN), as the aim is to investigate the response of the monopile under different scour protection scenarios. The cyclic tests are concisely presented in Table 3.11. It needs to be noted that extra numerical analyses have been conducted, mainly for monotonic loading, either to check the

efficiency of the model or to reach valid assumptions needed for the "p-y curves" derivation, as described in the next chapter. These analyses, if they are of importance, are presented and discussed in the Appendix.

Cyclic analyses in PLAXIS 3D can be performed either as a dynamic analyses or as a pseudo-static one. The general equation of motion for a structure subjected to a load *F(t)* causing a displacement *x* is expressed in Eq. (16), in which *m* stands for the system's mass, *c* for dumping and *k* for stiffness (Chopra 2006). The term $\dot{x}$ is the velocity of the system (derivative of displacement) and term $\ddot{x}$ is the system's acceleration (double derivative of displacement). This equation can be applied to any system, for any kind of loading. However, the first two terms ($m\ddot{x} + c\dot{x}$) have a considerable magnitude compared to the third one (kx) only when the structure is subjected to a cyclic load with relatively high frequency (as in an earthquake). On the contrary, if the load is applied with a slow or zero rate (cyclic loading with low frequency or monotonic load) the acceleration $(\ddot{x})$ and the velocity ($\dot{x}$) of the system tend to zero. In these cases, a simplified version of Eq. (16) can be applied, as expressed in Eq. (17). This equation (Eq. 17) corresponds to a pseudo-static analysis and can describe the displacement of a system subjected to even a cyclic loading, with a low frequency, having an acceptable small error as dynamic effects are not taken into account ($m\ddot{x} + c\dot{x}$).

$$\mathrm{m} \cdot \ddot{\boldsymbol{x}}(t) + c \cdot \dot{\boldsymbol{x}}(t) + k \cdot \boldsymbol{x}(t) = \boldsymbol{F}(t) \qquad \textit{Eq. (16)}$$

$$k \cdot \boldsymbol{x}(t) = \boldsymbol{F}(t) \qquad \textit{Eq. (17)}$$

PLAXIS 3D can execute both dynamic analysis (Eq. 16) and pseudo-static one (Eq. 17). The first one though is generally more time consuming, which can make a considerable difference in tests containing 100 cycles. The cyclic experiments performed in the centrifuge have been conducted with a low frequency, due to motor limitations, in dry sand, meaning that no undrained behavior is expected and consequently dissipation effects etc. As in PLAXIS, the same conditions needed to be applied, it was considered valid to perform pseudo-static analyses, as the centrifuge conditions indicated negligible dynamic effects.

Table 3.11 Series of numerical analyses performed in PLAXIS 3D

Basic Cyclic Set of Analyses

	Loading	Type of Load	Load Amplitude (kN)	Cycles
1	Cyclic	One-Way	0 to 100	100
2	Cyclic	Two-Way	-50 to 100	100
3	Cyclic	One-Way	0 to 25, 0 to 50, 0 to 75, 0 to 100	25, 25, 25, 25
4	Cyclic	One-Way	0 to 100, 0 to 300, 0 to 100, 0 to 300	25, 25, 25, 25

Scour Protection Cyclic Set of Analyses

	Loading	Load Amplitude (kN)	Scour Protection Length (D)	Scour Protection Load (kPa)	Cycles
1	Cyclic One-Way	0 to 100	3.0	15.0	100
2	Cyclic One-Way	0 to 100	5.0	15.0	100
3	Cyclic One-Way	0 to 100	7.0	15.0	100
4	Cyclic One-Way	0 to 100	5.0	20.0	100
5	Cyclic One-Way	0 to 100	5.0	25.0	100

Chapter 4

Results & Discussion

In this chapter the results of the current thesis are analytically presented. For a better overview, they are distinguished in three sections, the centrifuge monotonic results, the centrifuge cyclic ones and the PLAXIS cyclic ones.

4.1 Centrifuge Monotonic Experiments

The outcome of the monotonic tests executed in the centrifuge is presented in this section. More specifically, it includes data regarding the vertical load effect, the scour formation and the scour protection effect in the stiffness and the lateral capacity of the monopile. Then, the derived p-y curves by the centrifuge experiments are presented, along with the method followed for the curves' extraction, based on the bending moment profiles.

Note that the conventional failure of an offshore monopile is considered to occur at a displacement of 0.1D at the original soil surface by the current state of art, regardless of the possible scour formation or protection layers (Section 2.3.2). In the centrifuge set-up however, the displacement at the soil surface is not known, as the only available measurement of the pile deflection is close to the pile head (Section 3.1.4). However, due to the high rigidity of the monopile (L/D=5), it can be assumed that the pile rotates as a rigid body around the rotation point, allowing almost negligible deformation in its axis. It is then shown by the model geometry that when the pile head reaches a displacement of 0.3D, the pile deflection at the soil surface is 0.1D and hence the conditions for the conventional failure have been met (Figure 4.1). Therefore, for the centrifuge results presented below, the ULS is considered to be reached at a pile displacement of 0.3D at the point of measurement (pile head). It needs to be stated that the rotation point's depth depends on the scour hole's geometry, as it gets deeper from 1.0D to 2.0D case. However, this increase of the depth is negligible compared to the whole length of the pile and the experimental set-up, meaning that the 0.3D value at the pile head can be applied to all different scour depth cases.

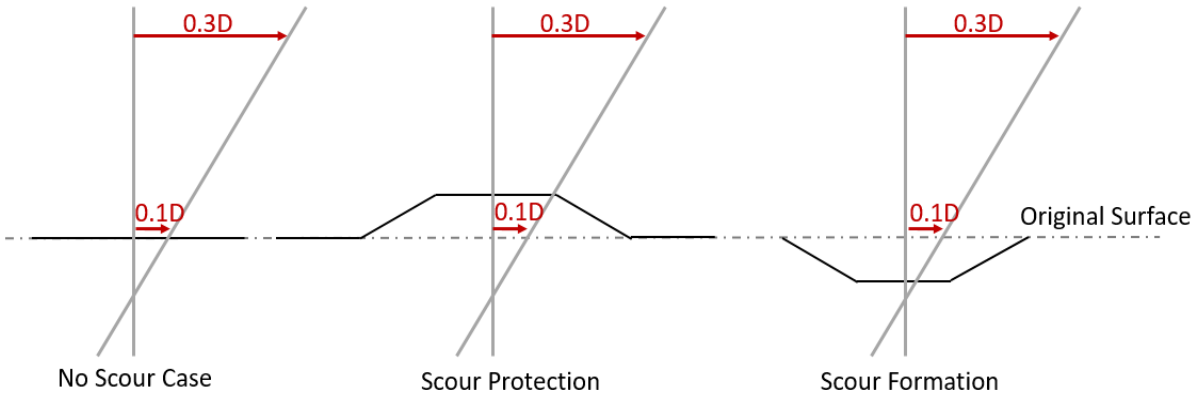

Figure 4.1 Soil surface displacement at which failure of the soil-pile system is considered to occur.

4.1.1 Load-Displacement Curves & Bending Moment Profiles

4.1.1.1 Vertical Load's Effect in Monopile's Response

The effect of the vertical load in the lateral soil capacity of the monopiles has been investigated by attaching dead loads to the pile head. Three different test scenarios have been performed, including 0.0, 1.5 and 3.0 MN dead load. It is observed in Figure 4.2 that the vertical load has a positive influence in the lateral capacity of the monopile for the 3.0 MN curve. The 0.0 MN and 1.5 MN curves follow almost the same path up to a displacement y/D=0.4, after which the 1.5 MN dead weight leads to higher soil resistance. It seems, therefore, that for dense sands the vertical load has a positive influence in the soil-pile system's lateral capacity, although, this influence is not always considerable, especially close to the ULS. Consequently, the increase of the dead load offers a positive, yet quite often negligible, increase in the soil lateral capacity. Note that the vertical loads applied to the pile by the dead weights, are way lower than the vertical soil capacity, meaning that they do not mobilize lot of the available soil resistance. This behavior could be different for considerable larger loads, close to the failure one, but in this case it was considered more valid to simulate realistic dead weights of a typical offshore wind turbine.

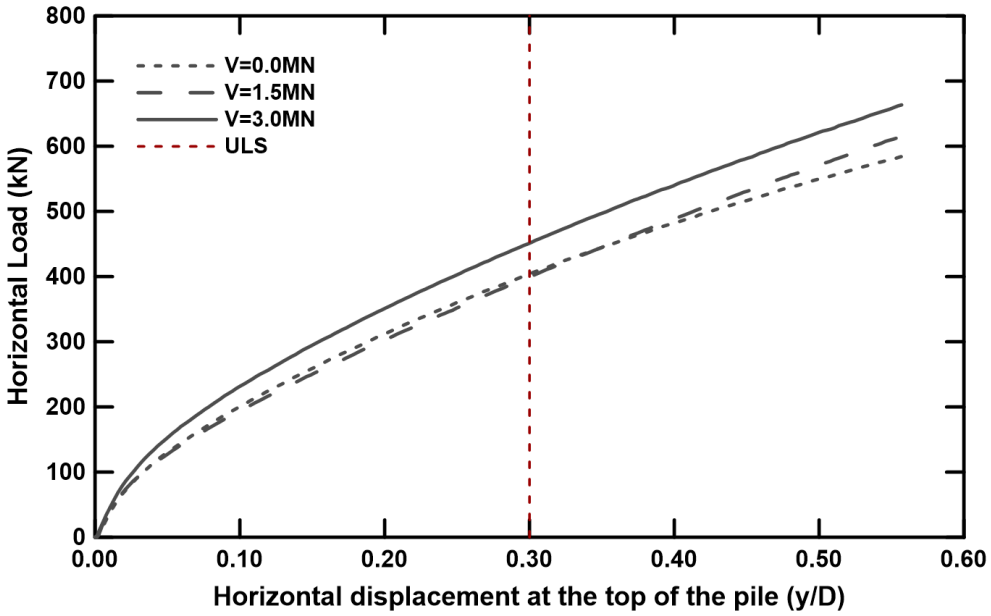

Figure 4.2 Load-displacement curve for three different lateral dead loads (0.0, 1.5 & 3.0 MN).

4.1.1.2 Scour Depth's Effect in Monopile's Response

The main body of analyses in the monotonic centrifuge experiments was about the scour formation. Nine combinations have been made, between three scour depths (1.0, 1.5 & 2.0D) and three scour depths (local narrow, local wide and global). The results are presented initially with respect to the scour depth and then with respect to the scour type. In Figure 4.3, three graphs are presented, each one containing the load-displacements curves for the no-scour case and three scour depths for a single scour type. The same trend is observed in all of them, as regardless of the scour type, the increase of the depth of the scour hole leads to considerable loss of the lateral capacity, which in the ULS can exceed 50%. More specifically, for 1.0D scour depth the reduction of the soil capacity is ranged between 10% and 25%, for the 1.5D scour depth from 25% to 30% and for the 2.0D case the same percentage is in a range of 35% to even 70% at the ULS. This behavior can be attributed to the reduction of the pile's embedded length due to the scour formation. Specifically, the no-scour case is founded 5.0D deep into the soil, while the same value is 4.0D, 3.5D and 3.0D for the 1.0D, 1.5D and 2.0D scour cases respectively. That means that the soil resistance is limited to a smaller length as the scour depth increases, therefore the total resistance is getting lower due to the scouring process. On the same context, the scour hole formation means that a certain soil volume is removed. This process despite the reduction of the embedded pile part (already discussed) leads also to lower overburden pressure to the

soil around the pile across its whole length. Consequently, the confining pressures of the soil are getting lower which corresponds to smaller strength, meaning that the soil in scour scenarios fails in lower stresses compared to the no scour case. Ultimately, the response of the monopile under the effect of scour formation is defined by two factors, the reduction of the embedded pile length and of the confining pressures applied to the remaining soil around it.

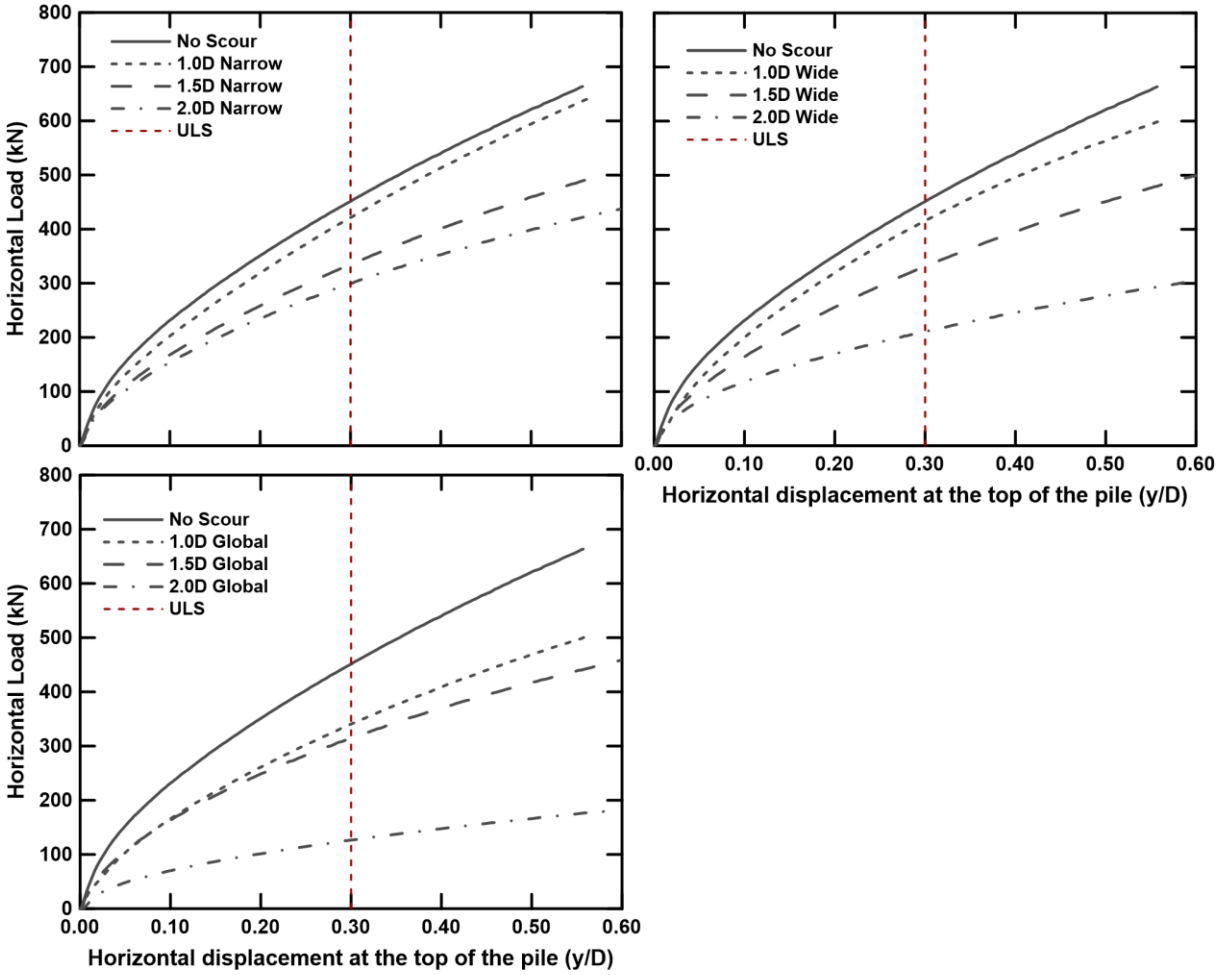

Figure 4.3 Load-displacement curves for the no scour case and three different scour depths (1.0, 1.5 & 2.0D) for the narrow, wide and global scouring types.

In Figure 4.4, three graphs are presented, each one containing the bending moment profiles for the no-scour case and the three scour depths for a single scour type. The profiles have been extracted at the ULS, which corresponds to a pile head displacement of 0.3D (as depicted in Figure 4.3). The general trend observed is that higher soil bending moments develop for the no scour case, which are gradually reduced from the narrow case, to the wide and ultimately the global for the same displacement. The higher moments mean that the soil offers larger resistance in order that the desired pile deflection is achieved, so stiffer behavior is expected as the scour depth is reduced. Note that the 1.0D narrow & 1.0D wide curves follow almost the same path with the no-scour one, and in some depths they present larger values. However, it needs to be considered that the no-scour case mobilizes 5.0D embedded pile length instead of 4.0D, meaning that it can present a stiffer behavior in total and simultaneously develop smaller moments in limited parts of the pile, due to the extra 1.0D embedded pile length that the no-scour experiment contains. The findings of Figures 4.3 & 4.4 are in agreement, as they show the negative effect of the scour depth in the lateral soil capacity. However, the data for the two graphs have been acquired by two different measurements systems, load cell actuator for the load-displacement curves and strain gauges for the bending moment profiles. These two systems are independent, therefore, reaching the same conclusions with both of them is a good indication that the experimental set-up works properly.

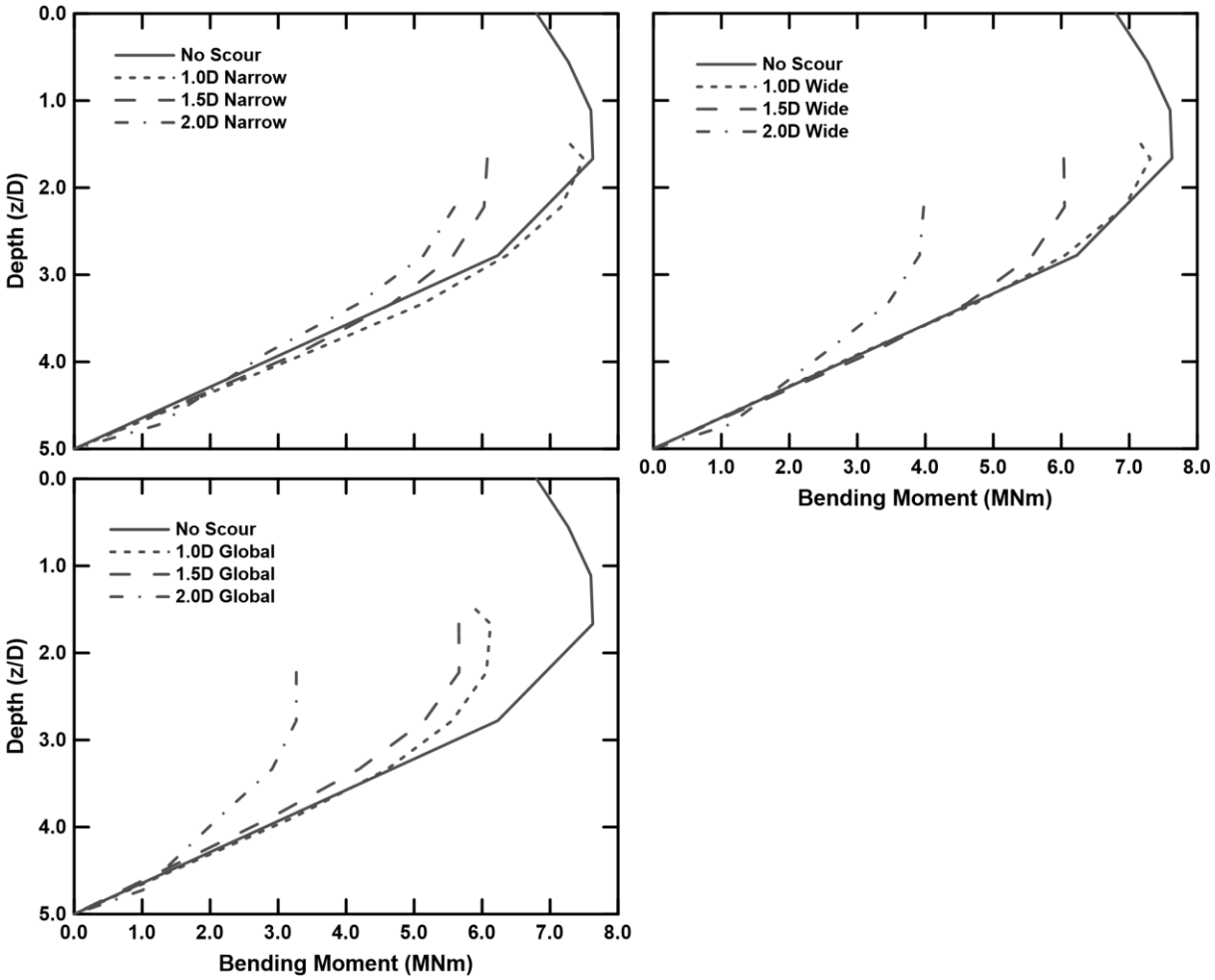

Figure 4.4 Bending moment profiles for the no scour case and three different scour depths (1.0, 1.5 & 2.0D) for the narrow, wide and global scouring types at ULS.

4.1.1.3 Scour Type's Effect in Monopile's Response

Figures 4.3 & 4.4 present the results with respect to the scour depth. However, it is more interesting to observe the scour type effect on the pile response, as it is not straightforward, at least not to the same extent as the scour depth. In Figure 4.5, three graphs are presented, each one containing the load-displacements curves for the no-scour case and the three scour types (narrow, wide and global) for a constant scour depth. Note that the curves for 1.5D narrow and 1.5D wide almost overlap each other, in contrast with the equivalent curves for 1.0D and 2.0D scour depth. For that reason, it is suspected that the response of one of these curves is unrealistic due to error occurred during the performance of the experiment. The general trend observed is that the narrow case is the most favorable in terms of soil lateral capacity, while the global one is the most critical. The wide scour hole is an intermediate state between the two extremes, which though may be characterized as the most possible to occur in real conditions. The effect of the scour type can be crucial in the pile response, as the difference between the two extremes, the local narrow case and the global one, for the same scour depth is ranged from 20% to 55%. Furthermore, even in the case of the local scour, the distinction between narrow and wide is important, as it may lead to difference responses at the ULS up to 20%, meaning that the term local scour should not be sufficient in the design, as the hole's geometry highly dictates its effects. Since the results have been plotted with respect to the scour type, the scour depth has no effect on the results, as in each graph of Figure 4.5, the same embedded pile length exists. Therefore, the different response is explained only by the hole's geometry. More specifically, in the narrow case, a small inversed conical shape of soil is removed, meaning the overburden pressures are not significantly reduced. On the contrary, in the global scour case the soil layer is uniformly deepened, meaning the overburden and hence the confining pressures are considerably lower, leading to a softer behavior compared to the

narrow case. The wide scour case is an intermediate state, as already mentioned, as a much wider volume is removed than in the narrow case, not reaching though the extreme of the global scour formation.

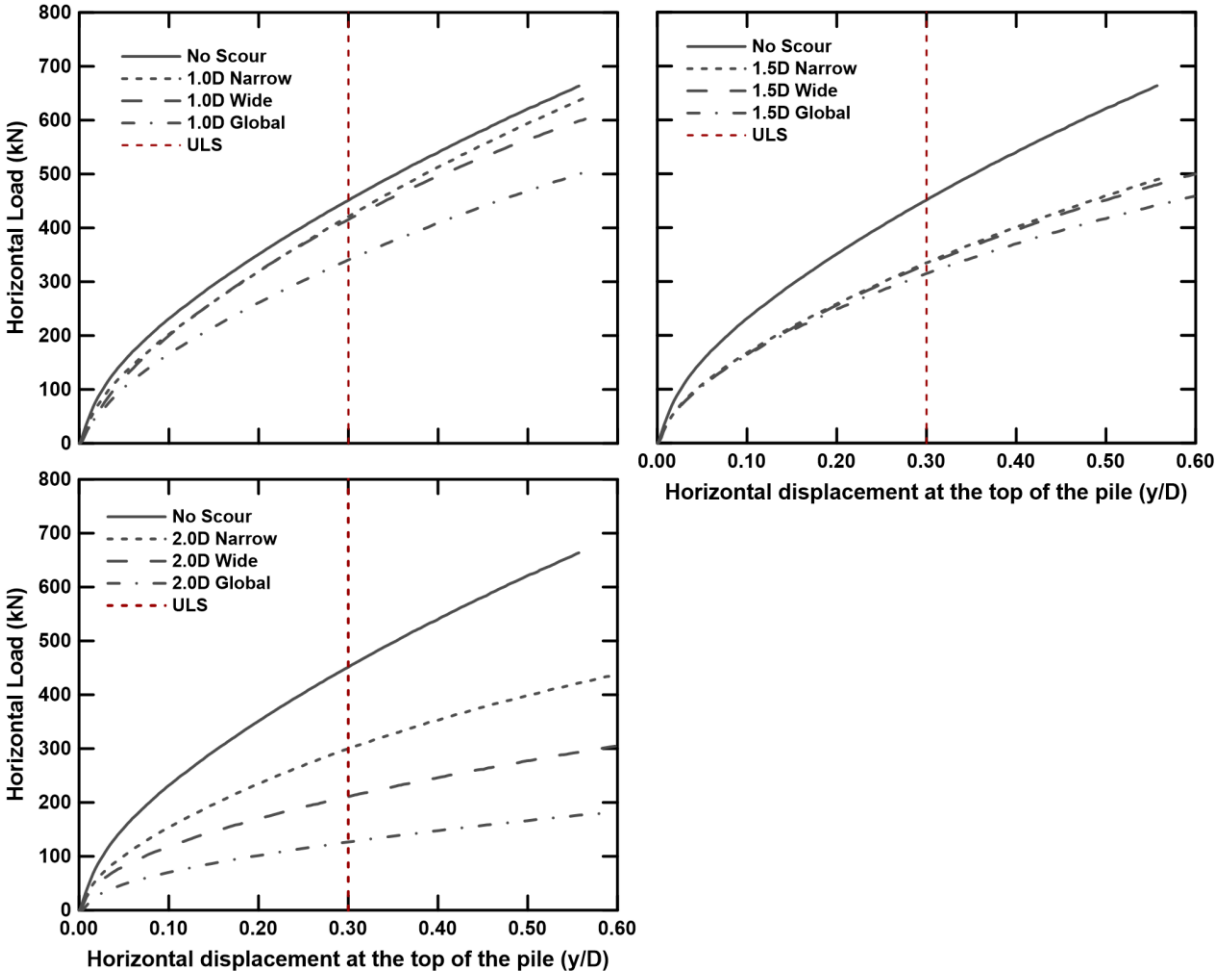

Figure 4.5 Load-displacement curves for the no scour case and the three different scour types (narrow, wide and global) for three different scour depths (1.0, 1.5 & 2.0D).

In Figure 4.6, three graphs are presented, each one containing the bending moment profiles for the no-scour case and the three scour types (narrow, wide and global) for a constant scour depth at the ULS displacement. As observed in the graphs of Figure 4.5 the curves for 1.5D narrow and 1.5D wide are almost identical, in contrast with the equivalent curves for 1.0D and 2.0D. It is already explained that the load-displacement curves and the bending moment profiles have been derived by different systems, so it is suspected that the 1.5D narrow and 1.5D wide experiments may not been executed properly due to the poor samples. However, all the other curves show that the narrow scour case is more favorable, followed by the wide case, while the global scour formation is the more critical, as the ULS displacement is reached with a relatively low resistance. The general conclusion drawn by Figures 4.5 & 4.6 is that the modern design should take into account the scour type, as the depth on its own is not enough to fully predict the monopile's response. In addition, the local scour type was often described as a unique state in the literature review, though its geometry can lead to different responses. Therefore, local scour should be incorporated into the monopiles' design as at least two scenarios, the narrow and the wide ones.

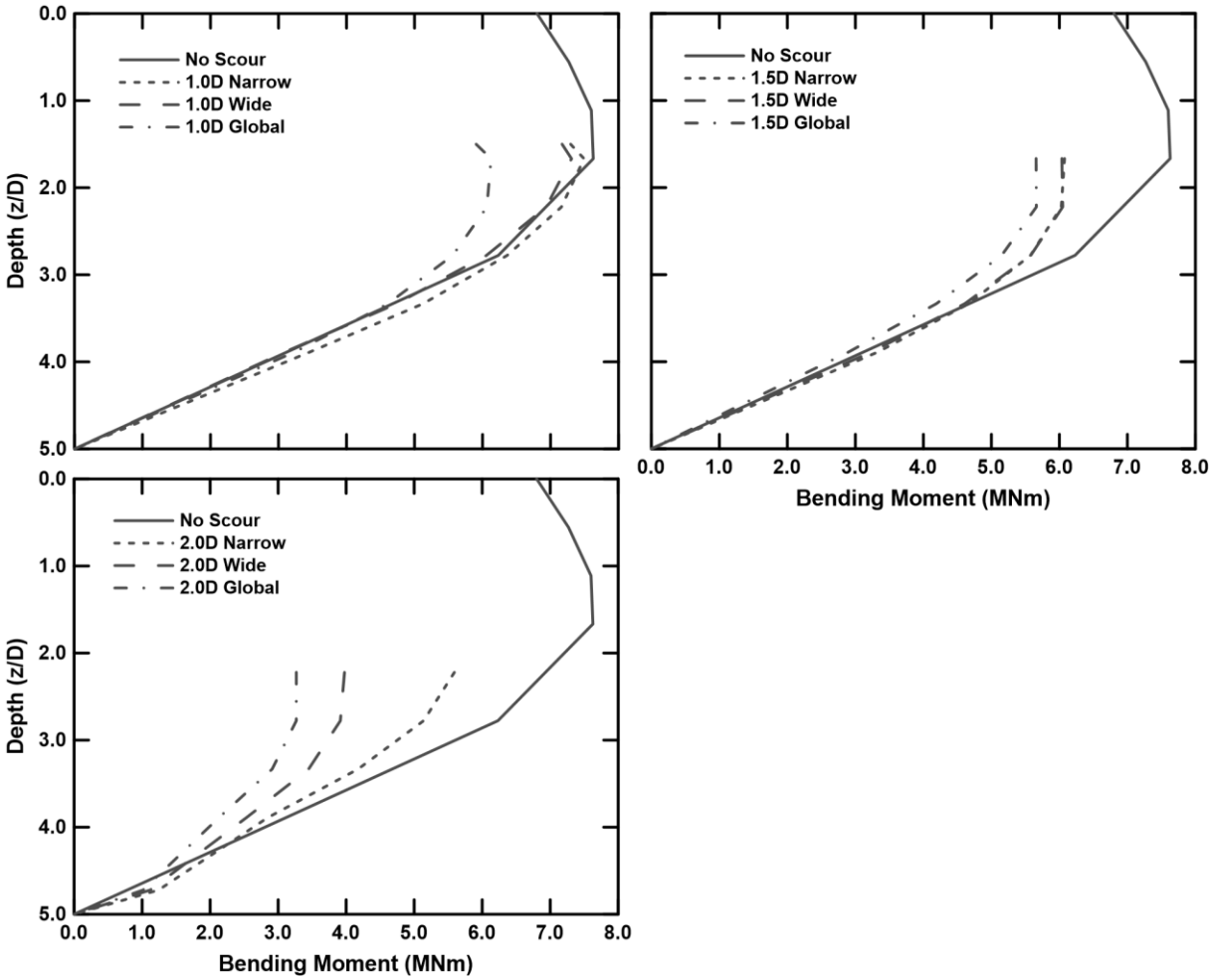

Figure 4.6 Bending moment profiles for the no scour case and the three different scour types (narrow, wide and global) for three different scour depths (1.0, 1.5 & 2.0D) at ULS.

4.1.1.4 Scour Protection's Effect in Monopile's Response

The effect of the scour protection layer in the lateral soil capacity of the monopiles has been investigated by performing two experiments with the same thickness layer but different lengths (5.0D & 7.0D). In Figure 4.7 the load-displacement curves for the two protection layer cases and the no scour case are presented. It is observed that the scour protection can offer a considerable increase in the lateral soil capacity, which is more than 30% in the ULS displacement. The larger protection layer (7.0D length) has led to an increase of the soil lateral capacity at ULS of about 5% comparing to the smaller one (5.0D length). Taking into account that in most cases the scour protection has a minimum length, it seems that this parameter is not crucial. On the contrary, the extra resistance offered can be attributed to the thickness of the protection layer which acts as a pre-load to the soil around the pile, increasing significantly the overburden pressures and hence the soil strength. The same mechanism is described in the previous sections, of the scour depth's and type's effect. In essence the scour protection layers are used to prevent scour from happening, and therefore their properties are dictated by the currents speed, the grains size etc. However, this same layer can offer a considerable increase in the stiffness of the soil-pile system, as shown in Figure 4.7, meaning that it would be plausible to reduce the original pile's embedded length (saving steel and hence lowering the cost of each wind turbine) by taking into account the scour protection layer's contribution. On the same context, the industry nowadays generally prefers to add protection layers in each pile, instead of predicting the scour formation (which is highly unlikely to be accurate). Therefore, it is recommended that the scour protection contribution to system's stiffness is incorporated in the modern design of the monopiles.

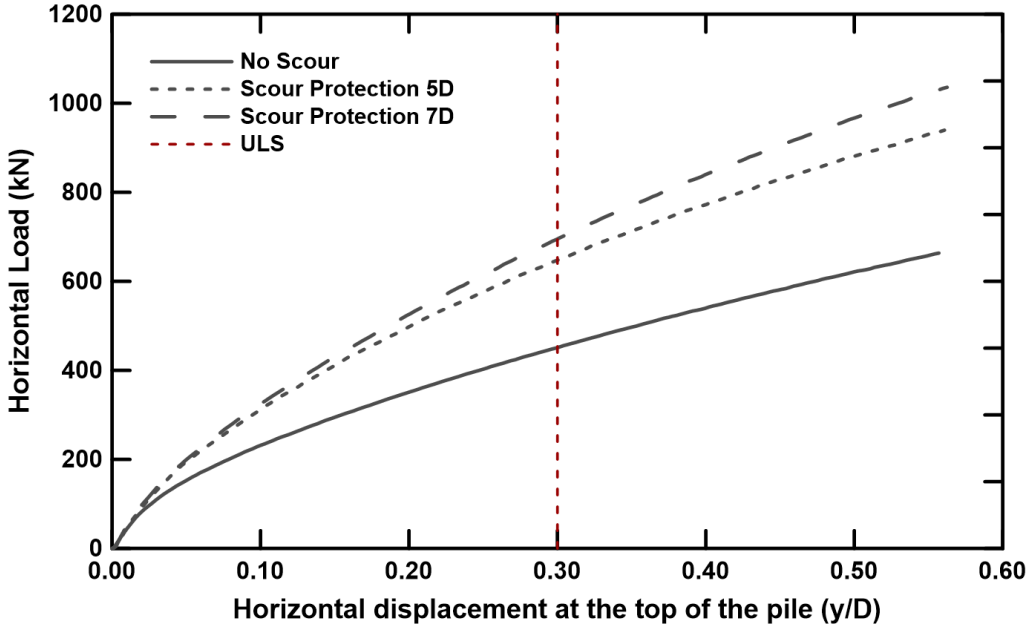

Figure 4.7 Load-displacement curves for the no scour case and for two scour protection cases with different length (5.0D & 7.0D).

4.1.2 p-y Curves

The p-y curves of the centrifuge monotonic experiments are presented in this section, along with an evaluation of the method used for the extraction and a comparison with the API method. Then, the scour effect on the p-y curves is discussed.

4.1.2.1 p-y Curves Presentation

The pairs of the strain gauges installed in the pile walls gave the bending moment profiles presented in the previous section. Based on them, the soil pressures across the length of the pile along with the pile deflection have been calculated. The procedure followed is analytically described in the section 4.1.2.2, as extracting p-y curves from bending moment profiles is a challenging process.

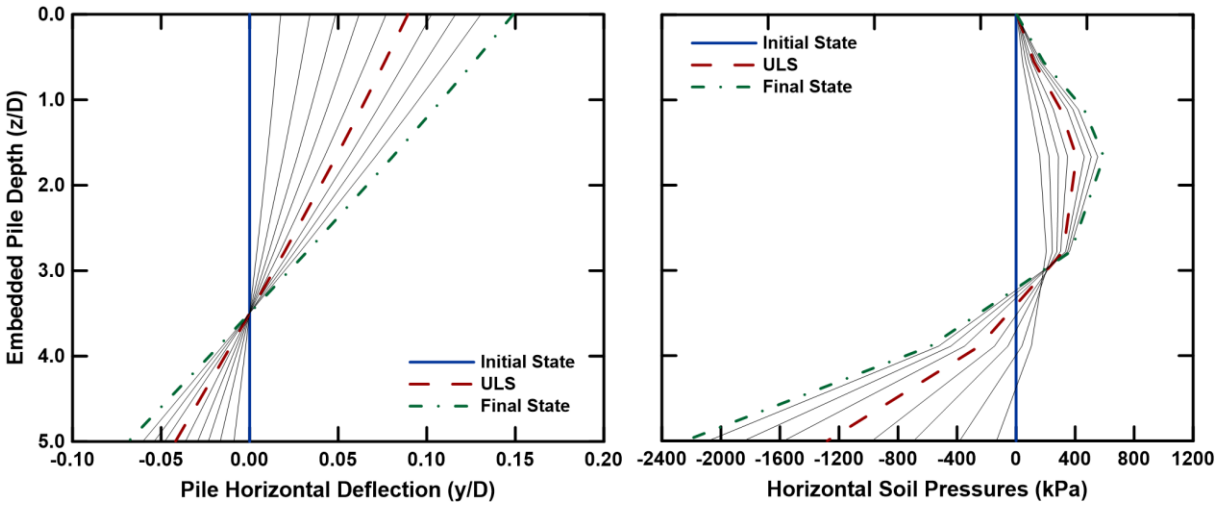

Figure 4.8 Evolution of the pile deflection and of the horizontal soil pressures across the pile for steps of 0.10 m pile head displacement for the no scour case.

In Figure 4.8 the evolution of the pile deflection and of the horizontal soil pressures across the pile for the no scour case is illustrated. More specifically, the curves presented have a constant step of pile head displacement equal to 0.10 m (0.06D) up to a total deflection of 1.0 m at the top of the pile. Through

the first graph illustrating the pile deflection, it is interesting to observe the rigid response of the monopile, as it deforms negligibly in its axis. On the contrary, it rotates as a rigid body from a constant rotation point, depicting a completely different response compared to a typical slender pile. In the second graph, the "toe-kick" developed in the tip of the pile is observed. Specifically, large soil pressures develop in the bottom of the pile, as the soil is stiffer and even a small displacement, mobilize high normal stresses. Note that the exact values on the bottom of the pile could not be calculated very accurately due to the small number of strain gauges available at the tip, and hence lack of data, for reasons explained below. In Figure 4.9 the p-y curves are depicted for the no-scour experiment. The depths chosen are the ones where the strain gauges have been placed as at these points the measurements are the most accurate, allowing for the higher possible quality. On the graph though 5 curves are depicted, despite the 7 activated pair of strain gauges in the test, as the upper two were place slightly above the soil surface (as it is explained below) and hence no soil pressures have been applied. As it is observed, the p-y curves are getting stiffer as the depth increases, while the maximum deflection is located at the shallower curve (z/D=0.55) due to the rigidity of the pile. The deeper curve (z/D=3.90) is quite close to the rotation point, meaning that it has experienced a relatively small displacement.

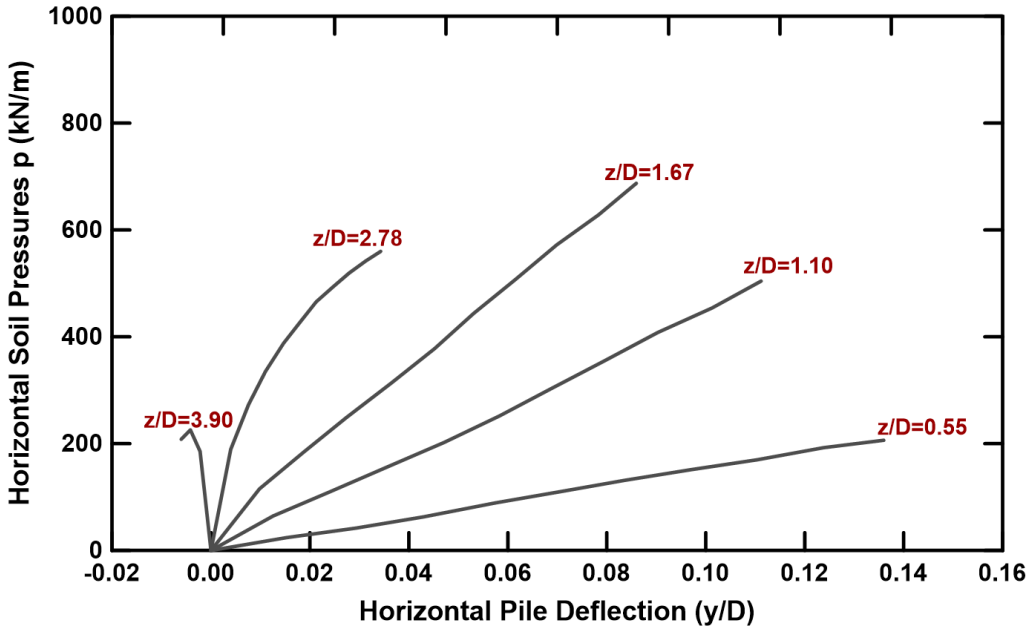

Figure 4.9 p-y Curves for the no scour case for the depths of the installed pairs of strain gauges.

4.1.2.2 Procedure of the p-y Curves Derivation

The p-y curves are derived by the bending moment distribution, which is obtained by the strain gauges. Through materials engineering, the moment (M) is correlated with the stress (σ) and the moment of inertia (I) in a position (z) from the neutral axis (Eq. 18).

$$\sigma = \frac{M}{I} \cdot z \qquad \textit{Eq. (18)}$$

The gauge pairs installed in the pile that has been used in the centrifuge experiments, give a single value which correspond to the pile's strain with respect to the neutral axis. Therefore, the distance z is equal to half the pile diameter (D/2). Based on the Eq. (18), the bending moments have been calculated though the formula in Eq. (19), where the term ε is the strain and E the Young modulus of the aluminum, that was the material of the pile.

$$\mathrm{M} = 2 \cdot \frac{E \cdot \varepsilon}{I} \cdot D \qquad \textit{Eq. (19)}$$

The bending moment profile derived by the strain gauges is discrete, while for the derivation of the p-y curves a continuous line is required. Therefore, a polynomial curve is fitted to the moment points by the strain gauges for producing a continuous moment profile. The choice of the fitting method, which is analyzed below, is based on minimizing the error during the fitting of the curve to the discrete bending moment points, as this error affects the quality of the produced p-y curves. Subsequently, the known distribution of bending moment (M), with depth (z), is differentiated two times to produce the soil reaction (p) and integrated twice to produce the pile deflection (y), according to the following equations, respectively:

$$p = \frac{d^2M}{dz^2} \qquad \textit{Eq. (20)}$$

$$y = \iint \frac{M}{E_p I_p} dzdz \qquad \textit{Eq. (21)}$$

The double integration of discrete data points is favorable in terms of minimizing the measurements errors by the strain gauges. Therefore, a negligible numerical error occurs when calculating the pile deflection y by the equation (21). Hajialilue-Bonab et al. (2014) stated that the odd-degree polynomials are usually more accurate than those of even-degree during the procedure of the double integration for the calculation of the pile deflection *y*. On the contrary, the double differentiation of the discrete data points (Eq. 20) tends to highly increase the existing measurement errors and thus produces inaccurate soil pressures p. Piecewise Polynomial Curve Fitting (Dunnavant 1986), High Order Global Polynomial Curve Fitting (L. Reese & Welch 1975, Wilson 1998), Weighted Residuals Method (Wilson 1998) and Cubic Spline Curve Fitting (Mezazigh & Levacher 1998) are all methods for deriving the soil pressures p with the minimum error possible. (Yang & Liang 2006) evaluated these methods based on full-scale tests in which they compared the curves by the instrumental measurements and the ones by computer programs (LPILE & COM624P). Their conclusion rendered the piecewise polynomial as the most efficient method, especially when the measurements are relatively sparse, which is the case in the majority of the tests performed in this study.

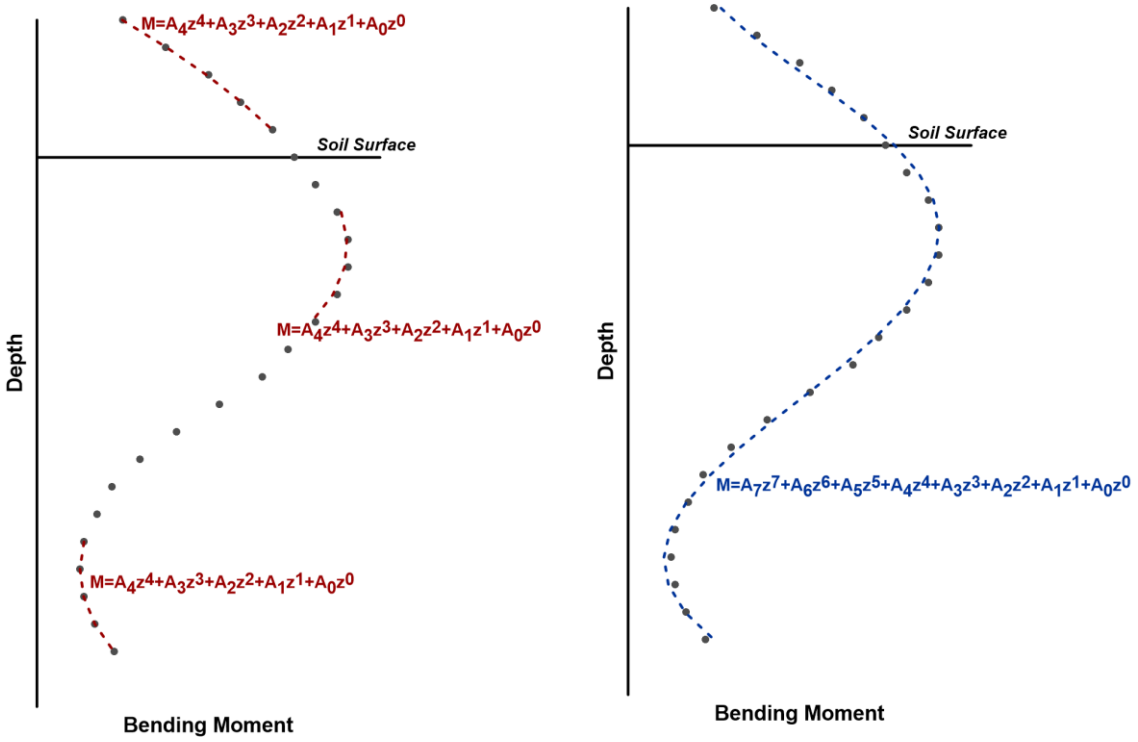

Figure 4.10 Schematic illustration of the procedure followed for extracting the soil pressures (left graph) and the pile deflection (right graph) from the bending moment profile.

The piecewise polynomial curve-fitting method (Dunnavant 1986, Yang & Liang 2006) was adopted for the calculation of the soil pressures, with a small modification, as a fourth-order polynomial was used instead of a third-order one that was suggested by (Yang & Liang 2006). This detail proved to be important on capturing the right soil response, at the top and the bottom of the pile. When using this method, five successive moment data points are fitted to a certain-order polynomial using a least-square method (Figure 4.10 left). The polynomial is then differentiated twice and the soil response p evaluated at the central data point. The soil response for the uppermost and lowermost three points are obtained from the polynomials fitted to the highest and lowest data points, respectively. Therefore, a third order polynomial when derived two times gives a straight line at the top and at the bottom of the pile, unless there are many strain gauges and hence measurement points. In this thesis, using a fourth-order polynomial proved to be more reliable, due to the small number of strain gauges, especially at the bottom of the pile.

The lateral deflection of pile y was calculated by integrating the bending moment twice as shown in equation (21), by using a seventh-order polynomial fitting for acquiring the bending moment profile (Figure 4.10 right). Two integration constants C1 and C2 needed to be determined during the double integration. The first one was calculated by the measured displacement at the loading position of the pile. The second one was determined by making the assumption of a zero deflection case at the point of zero lateral resistance. This assumption was based on extra numerical analyses run in the Finite Element software PLAXIS 3D (Brinkgreve et al. 2016), as the no-rotation point highly depends on the pile properties. Specifically, it can be at the embedded length of the pile, at its tip or even below the bottom of the pile. Based on the numerical analyses (Appendix F) the no-rotation point is assumed to occur at a depth of 70% of the current embedded pile length in each case, taking into account the scour formation hole. In similar studies in literature, the second integration constant is given by measuring the rotation at the top of the pile. Note that the deflection of the pile is vastly determined by the boundary conditions (integration constants C1 and C2), whereas, the effect of the other terms of the integrated polynomial is negligible (Wang & Qi 2008). The whole procedure described above has been performed by the software of MATLAB 2017b.

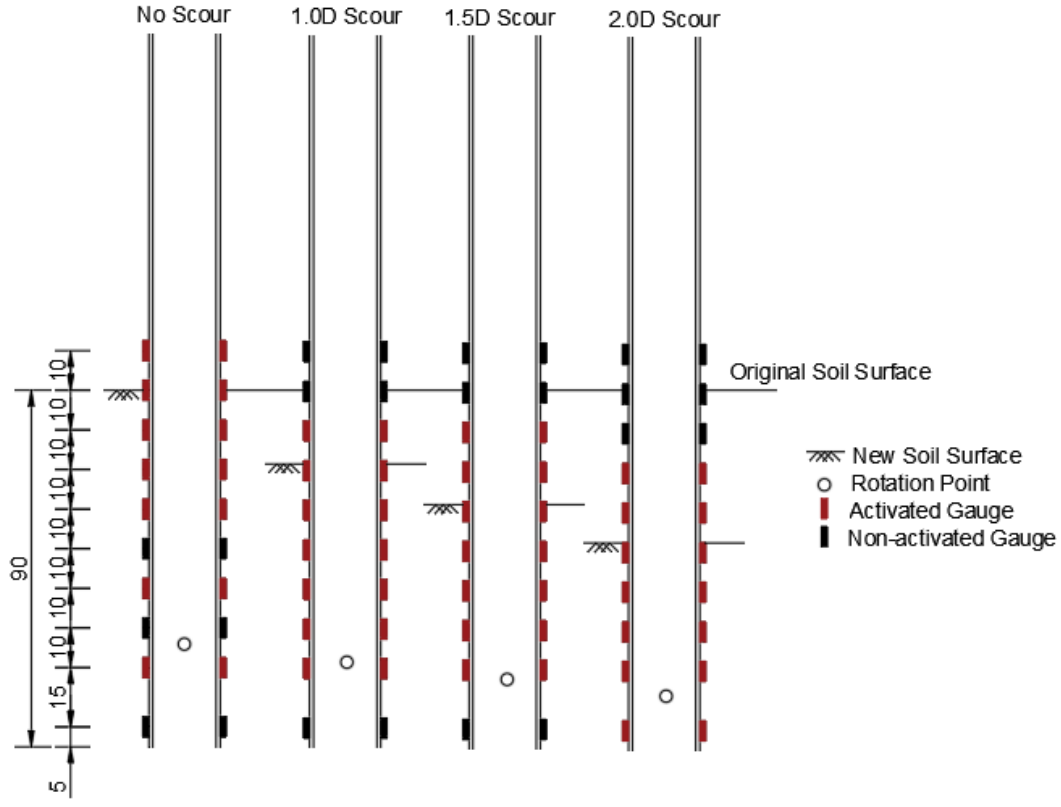

Figure 4.11 Distribution of activated strain gauges for all scour scenarios, along with the no rotation points.

As already stated, in each experiment in the centrifuge, 7 out of 10 strain gauges were activated due to limitations in the channels available for data acquisition. The choice of which pairs of gauges should be activated in each test was mainly based to the soil surface. Specifically, the distribution of the gauges need to be very dense close to the soil surface, including measurements above it, in order to extract the p-y curves accurately. On the contrary, the measurements close to the tip of the pile are not so crucial, although if all ten strain gauges could be activated in each test, higher quality would be expected, especially at the bottom. Therefore, the mesh of the gauges depended on the scour hole depth, as they were always concentrated around the surface of each scour case, as it is illustrated in Figure 4.11. In the same figure, the assumed rotation points are presented, which are in all cases, except of 2.0D, close to the last pair of strain gauges. Consequently, in no scour, 1.0D and 1.5D case, the p-y curves below the rotation point could not be developed sufficiently due to the lack of data, as in the only gauge's position below the rotation point, small displacement occurred.

4.1.2.3 p-y Curves Benchmarking by L-Pile Software

The p-y curves have been extracted by the procedure described in the section above. However, as certain assumptions have been made, including the fitting of polynomials to the discrete data by the strain gauges and the second integration constant, the quality of the derived curves needed to be investigated. L-Pile software has been qualified as ideal for this case. Specifically, this program simulate the lateral soil response based on the Winkler's approach by using non-linear springs, which can be described either by standard industry curves, such API curves, or by user defined curves. Therefore, the extracted p-y curves from the centrifuge experiments have been inputted in the L-Pile software, along with the boundary conditions at the soil surface, meaning the horizontal load and the bending moment. Then, the program gave as output the bending moment profiles which correspond to the inserted p-y curves. These L-Pile profiles were compared with the initial centrifuge measurements, containing the discrete bending moment points. Note that at least one curve below the rotation point was required by the L-Pile software, so it was decided to check the results for the derived p-y curves of all three experiments performed with a scour depth of 2.0D. This choice was based to the strain gauges' position in each experiment due to the channel limitation (Figure 4.11), as only in 2D scour depth enough data have been acquired for constructing p-y curves deep enough below the rotation point.

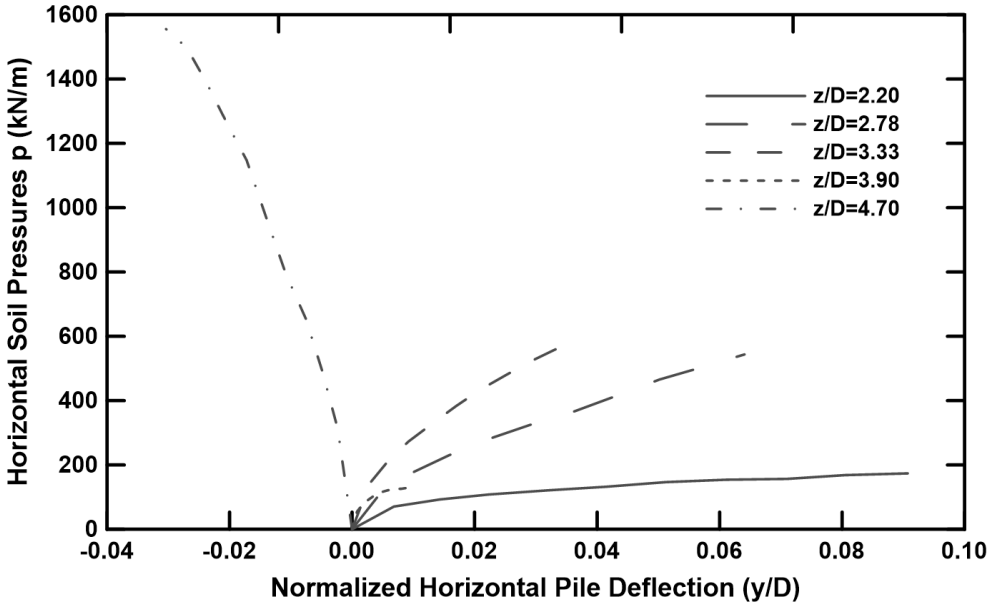

Figure 4.12 "p-y curves" for the 2D global scour case for the depths of the installed pairs of strain gauges.

Figure 4.12 illustrates the p-y curves for the 2D global scour experiment for the depths of the activated pairs of strain gauges. These curves have been inputted in the L-Pile software, as discussed above, for benchmarking. In Figure 4.13 the bending moment profiles produced by the L-Pile are depicted with a dashed line for three horizontal loads. In the same graph, the centrifuge bending moment profiles for

the same load are presented (discrete data points). It is observed that in the upper part of the pile (around 50% of the embedded pile length) there is a good convergence between the experimental data and the L-Pile software profiles, indicating that the p-y curves have been derived very accurately. At the tip of the pile though, considerably higher bending moments are depicted for the centrifuge data compared to the L-Pile software's values. This deviation is attributed to the laterally-loaded piles' behavior in their tip, as high passive soil pressures develop in the bottom of the pile ("toe-kick") and large shear stresses are mobilized in the tip, leading to high bending moment even just above the pile's base. L-Pile current version cannot simulate this pile's response, as it does not take into account the possible shear stress acting in the annular part of an open-ended pile and ultimately the extra moment observed in the centrifuge experiment is not calculated. Consequently, this magnitude difference in the bottom of the pile occurs between centrifuge and L-Pile. Overall, though, a relatively good match is observed in the curves of the L-Pile and the discrete data of the centrifuge, meaning that the extracted p-y curves are validated by the software, and hence they are accurate, especially in the upper part of the pile. It is highly recommended though a new version of p-y curves should be adopted for the rigid piles, which will take into account the potential shear force developed in the tip of the pile. Note that the current version of p-y curves incorporated in the L-Pile software is based on long slender piles.

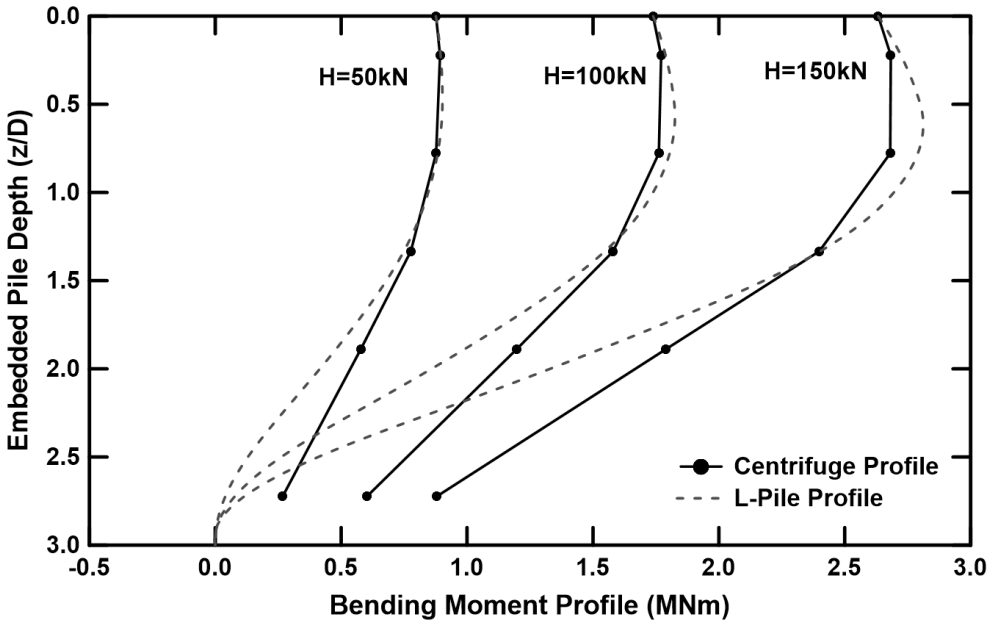

Figure 4.13 Bending moment profiles by the centrifuge experiments and the L-Pile simulations for three different horizontal loads (50, 100 & 150 kN) for the 2D global scour case.

4.1.2.4 API "p-y curves" evaluation

The API recommendations (API 2007) have been used to construct the p-y curves simulating the centrifuge experiments in prototype scale for comparison purposes. In Figure 4.14 the curves derived from the centrifuge no scour case experiment and from the API method are presented. The depths that have been chosen correspond to the strain gauges' positions, as already explained. It is observed that the API approach highly overestimates the initial stiffness of the soil-pile system as well as the ultimate lateral capacity especially for the curves of larger depths. It is indicative to state that even for very shallow curves (z/D=0.55 and z/D=1.10) where the divergence is smaller than the other curves, the API has twice as stiff response compared to the centrifuge extracted curves. The outcome of the comparison is in accordance with the literature review which states that the API overestimated the pile's behavior as the actual displacements in the field were way higher than predicted. Note that certain researchers (Zaaijer 2006, Hald et al. 2009, Kallehave et al. 2015) by comparing the actual response of monopiles in the field with the one predicted by the API method, have stated that the API curves underestimate the sand response. However, this behavior was limited only to a very upper part of the pile, as going deeper showed a profound overestimation by the API both of the initial stiffness and the

ultimate lateral capacity. This observation was also confirmed by numerical analyses conducted by McGann et al. (2011), who has stated that the initial stiffness predicted by API increased with depth in a considerably larger rate than the one determined by FE numerical methods.

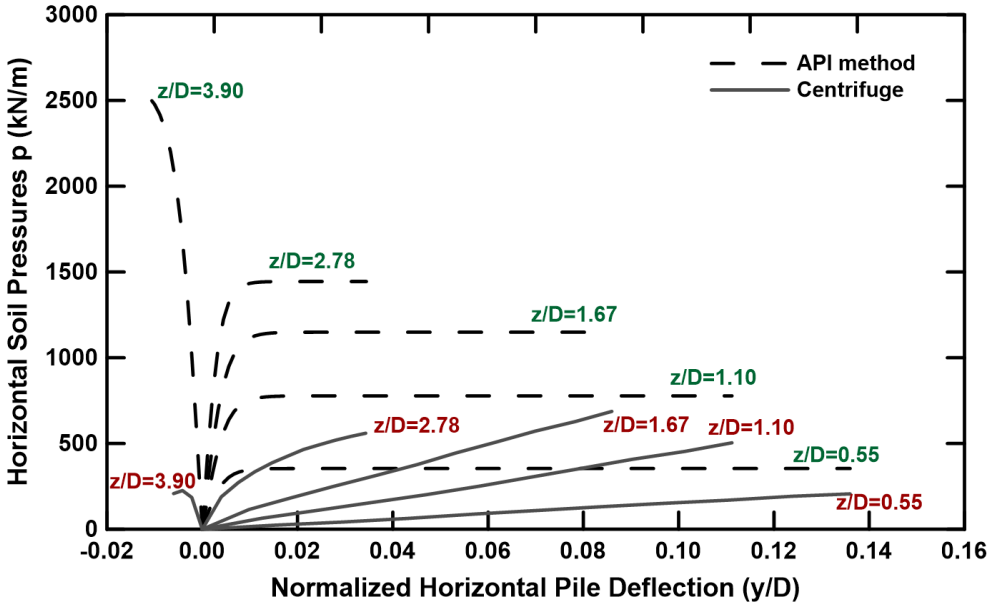

Figure 4.14 "p-y Curves" for the no scour case extracted by the centrifuge experiments and the API (2007) *for the depths of the activated pairs of strain gauges.*

The difference in the response between the API method and the centrifuge extracted curves is most likely due to the high rigidity of the model pile used (simulating a real-case offshore monopile), as the API regulations have been developed based on measurements in long slender piles, which present a completely different behavior. Specifically, a typical slender pile has an effective length that is activated when laterally-loaded. At the end of this length, the deflection tends to be rather small, tending to zero, while the vectors of the displacements across the pile have the same direction. On the contrary, a rigid pile activates its whole length and the displacement have different directions above and down of a constant rotation point, meaning that in the tip of the pile considerable deflection occurs, along with high pressures and possible shear stresses in its annular base. Overall, it seems that the current API regulations fail to capture the real response of a rigid monopile. It is therefore recommended to be modified in order to become applicable for the typical offshore monopiles used in most windfarms.

4.1.2.5 Scour Type's Effect on the "p-y Curves"

The scour type's effect on the derived p-y curves is investigated in this section. Specifically, the p-y curves have been constructed for nine different scour scenarios, which include three scour types (narrow, wide and global) and three scour depths (1.0, 1.5 and 2.0D). In Figures 4.15, 4.16 and 4.17 all these curves are illustrated with respect to the scour type. Specifically, each graph contains all the three scour types for a constant scour depth, as in this way each graph has the same soil surface after the scour formation. Note that the curves for the depths of z/D=1.7, 2.2, 2.8 & 3.3 are above the rotation point, while the curve at z/D=4.7 is located below it. The depth z/D=3.9 is located quite close to the rotation point, meaning that at this point low deformations occur, hence the shape of the curve is small, not allowing for very useful conclusions to be drawn.

The shallower p-y curves (z/D=1.7, z/D=2.2D) are highly affected by the scour type. Specifically, in the depth z/D=1.7 the same trend is observed in all depths, as the narrow case leads to the stiffer response, while the global corresponds to the softer one, reaching its ultimate capacity in quite small deformation. The wide scour case is an intermediate state between the two of them. The divergence of the aforementioned curves due to the scour type can be up to 30%, as the deflection is getting larger. In essence the difference in their response is attributed to the overburden pressure as in the local case

only a small volume of soil is removed, while in the global case the whole original mudline is deepened. The specific mechanism has been already analytically described in previous section. At the following depth of z/D=2.2 there is not clear trend, as in each depth a different scour type leads to stiffer behavior. It is suspected though that this occurs due to the different embedded pile length in each graph, meaning that different soil resistance needs to be mobilized in each layer in order to reach equilibrium. The divergence in the graphs though is quite smaller, around 15 to 20%.

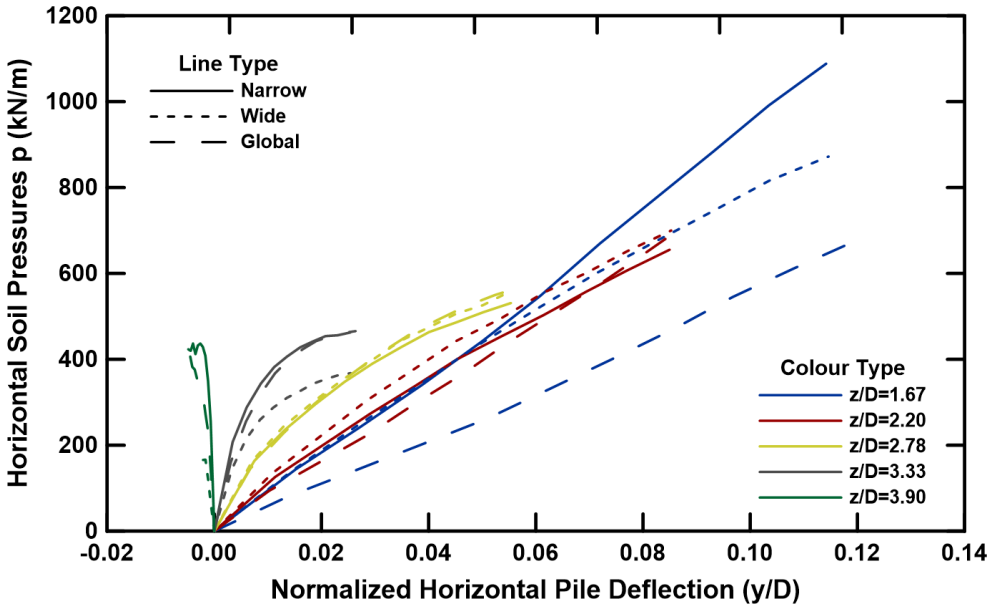

Figure 4.15 "p-y Curves" for the 1.0D scour depth case at the depths of the activated strain gauges' pairs for narrow, wide and global scour type.

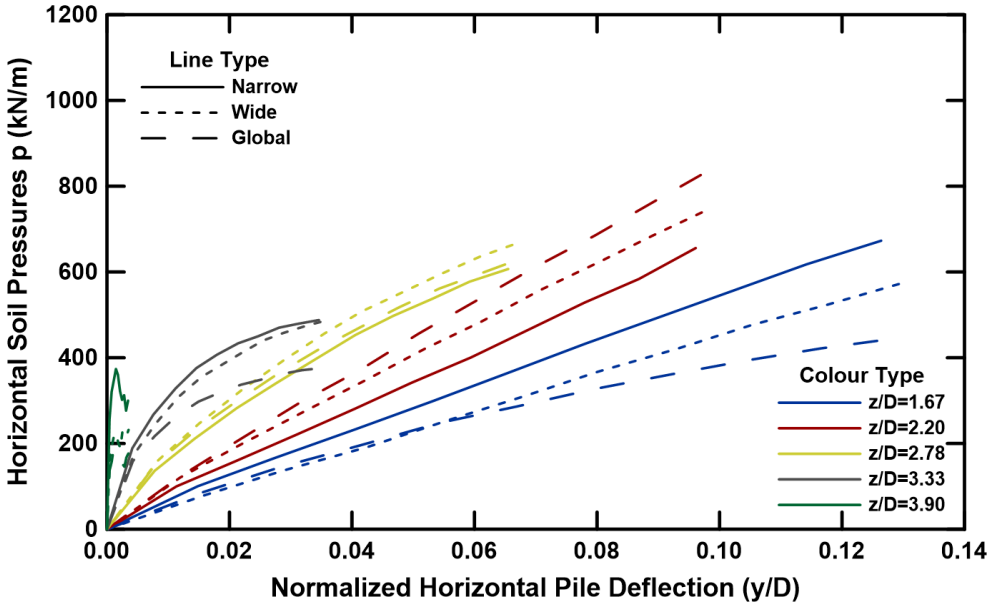

Figure 4.16 "p-y Curves" for the 1.5D scour depth case at the depths of the activated strain gauges' pairs for narrow, wide and global scour type.

As the depth of the curves increases (z/D=2.8, z/D=3.3), still though remaining above the rotation point, the curves seem to converge as they follow almost the same path. Note that the global z/D=3.3 in Figure 4.15 and the narrow z/D=3.3 in Figure 4.16 do not overlap the rest curves of the same depth, yet it seems that as the depth approached the rotation point, the scour type effect is reduced. Similar conclusion can be expressed for the depth z/D=3.9, but as it is quite close to the rotation point, the curves are not large enough to offer satisfactory results. Below the rotation point, at z/D=4.7D, there

are satisfactory data in Figure 4.17, in which the curves present a very stiff behavior. The very high soil pressures ("toe kick") are more likely due to the mechanism of reaching equilibrium, meaning that the upper and the bottom part of the pile are resisting the applied lateral load cumulatively. Below the rotation point, the lower part of the pile that deflects on the opposite direction of the applied load, is much smaller, as it is about 30% of the embedded pile length, leading to the development of relatively large passive soil stresses.

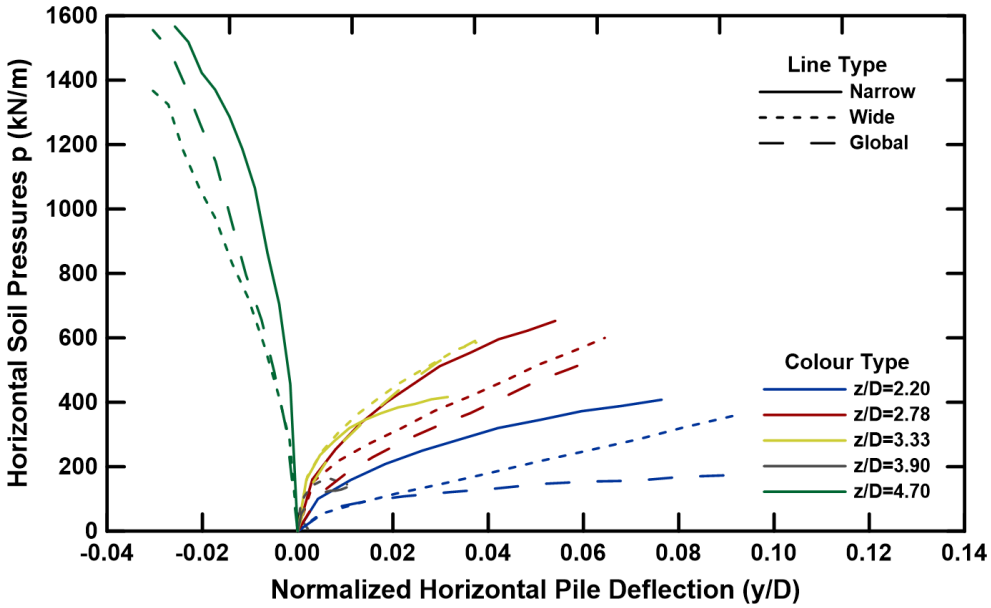

Figure 4.17 "p-y Curves" for the 2.0D scour depth case at the depths of the activated strain gauges' pairs for narrow, wide and global scour type.

The general conclusion drawn by Figures 4.15, 4.16 and 4.17 is that the scour type effect is limited to the shallower derived p-y curves, as the same effect become much smaller as the depth increases and could be characterized even as negligible close to the rotation point. As already stated, the term local scour seems to be outdated, as difference up to 20% may occur before narrow and wide type of scour, meaning that the geometry of the hole is crucial. The curves extracted for the global scour cases are generally softer than the local scour ones, as expected, leading to smaller ultimate capacity up to 40%.

4.2 Centrifuge Cyclic Experiments

In this section the centrifuge cyclic tests results are presented. More specifically, the load-displacement curves are depicted, along with the stiffness evolution with respect to the number of cycles. Expressions relating the maximum and residual displacements for the number of cycles have been extracted for each test. The last part of this section contains the p-y curves, derived with the method already described in 4.1.2.2.

4.2.1 Load-Displacement Curves

The four cyclic experiments performed in the centrifuge are depicted in Figure 4.18, in form of load-displacement curves. All the tests were load-controlled, with their frequency been dictated by the actuator, which was pushing the pile back and forward with a constant rate of 0.01 mm/s until the desired minimum and maximum loads were captured. Each test contained 100 cycles, with different R_H ratios ($R_H=H_{min}/H_{max}$) and amplitudes. An "one-way" has been performed from 0 to 100 kN ($R_H=0$), a "two-way" symmetrical from -50 to 50 kN ($R_H=-1.0$) and a "two-way" non-symmetrical from -50 to 100 kN ($R_H=-0.5$). The "storm" test simulates a scenario in which the pile is subjected to 40 cycles from 0 to 100kN, followed by a "storm event" with 20 cycles from 0 to 300 kN and returned to initial state with 40 cycles from 0 to 100 kN. The last 40 cycles are depicted in the graph with a yellow curve, as they coincide with the large cycles of the "storm". In all the experiments performed, it is observed that the

residual displacements (minimum ones at the end of each cycle) are increasing with the number of cycles, but in a reducing rate. It is characteristic that in the "one-way" experiment, the accumulated residual displacements in the first 10 cycles are larger than the ones accumulated in the following 90 cycles. The same trend is observed in both the "two-way" experiments, and the "storm" one, indicating possibly an increase in the soil-pile system, meaning that the sample could be densified. Note that the samples used had a relative density of 80%, yet it is possible that the Geba sand will experience a larger relative density, before dilation effects occur. The change in the stiffness with respect to the cycles is analytically discussed in a following section. It is interesting to observe the soil response in the "storm" experiment. Specifically, initially in the first 40 cycles, the trend already described above is depicted, with the residual displacement being accumulated with a reducing rate. When the maximum load increases, though, the soil behaves in the same way as in the 40 first cycles, as if the test was started again with a new sample, meaning that the previous load history with a smaller amplitude does not actually affect its response. However, when the maximum load drops again to 100 kN, the soil-pile system presents instantly a very stiff response, which can be easily detected by the yellow curve's angle. Therefore, it seems that the previous load history highly affects the pile's response, only if the current amplitude is lower than the maximum experienced by the soil.

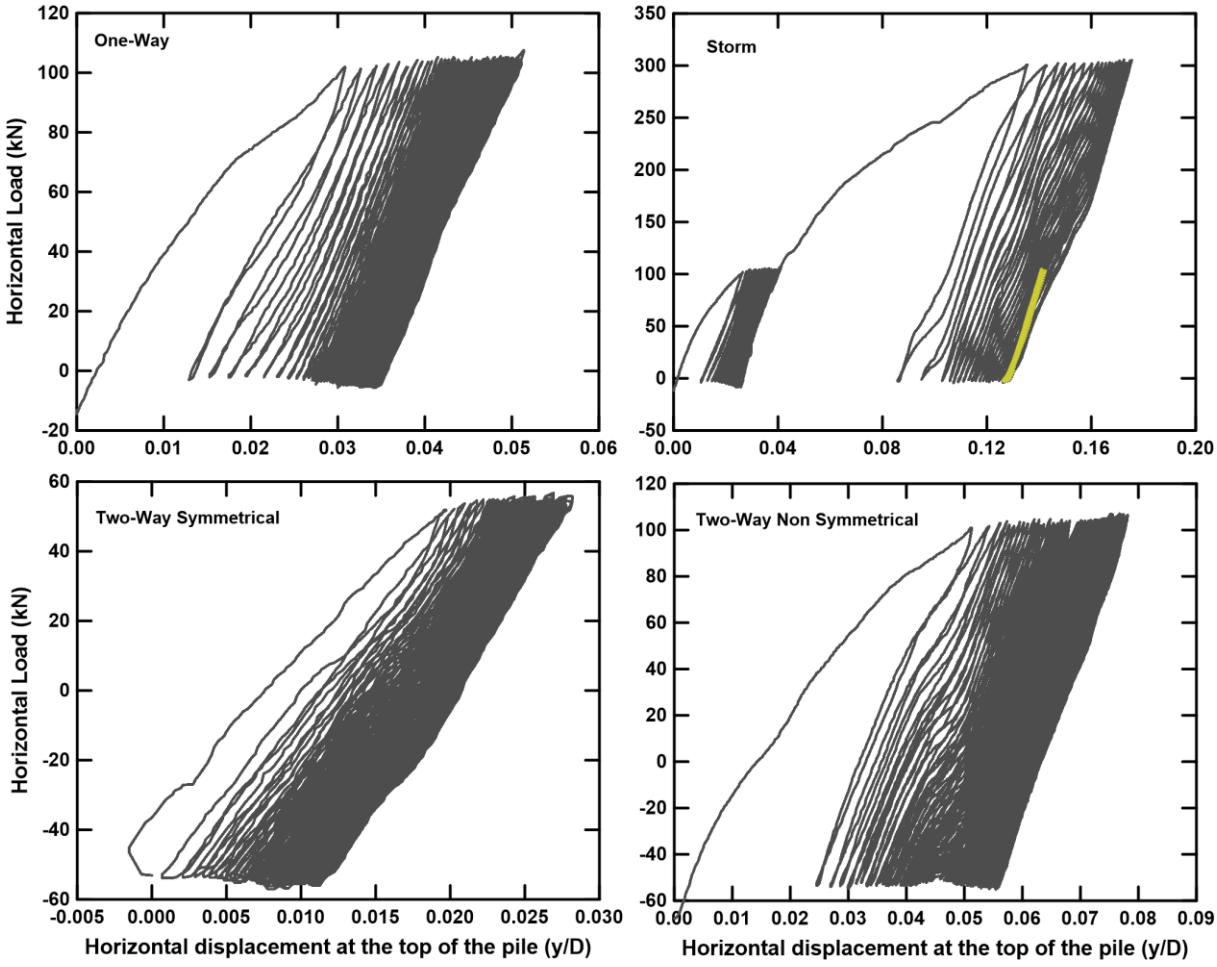

Figure 4.18 Load-displacement curves for the four cyclic tests performed in the centrifuge.

In Figure 4.18, it is observed that for each test the first actual cycle begins from a different displacement, mainly due to the different maximum load achieved in the initial loading. Therefore, for having a valid comparison between the "one-way" test and the "two-way" ones, the load-displacement curves for the three experiments have been plotted after the initial loading, from the second cycle of the system, starting from a zero displacement. In Figure 4.19 the updated curves are illustrated, with the "one-way" tests beginning from a zero load and the "two-way" experiments form a -50 kN load. It is interesting to compare the "one-way" test with the "two-way" symmetrical one, as they have the same amplitude

(100 kN) with different R_H ratios though (0.0 & -1.0 respectively). It is shown that the symmetrical load is more favorable with respect to the pile's deflection, as the accumulated residual displacements are considerably lower than in the "one-way" case. However, this trend is not confirmed when comparing the "one-way" experiment (R_H=0.0) with the "two-way" non-symmetrical one (R_H=-0.5). Specifically, the non-symmetrical case leads to excessive residual deformations, much larger than the ones measured in the "one-way" test. Note though that the total amplitude is equal to 150 kN in the "two-way" non-symmetrical experiment, instead of 100 kN in the cases of the "one-way" and "two-way" symmetrical tests. It seems, therefore, that the total amplitude is more crucial in this case, as it is likely to cause a larger soil degradation due to the exhaustion by the cyclic loading, leading ultimately to higher residual deformations. However, if the amplitude parameter is constant, the coefficient R_H can dictate the response of the monopile when subjected to cyclic loads.

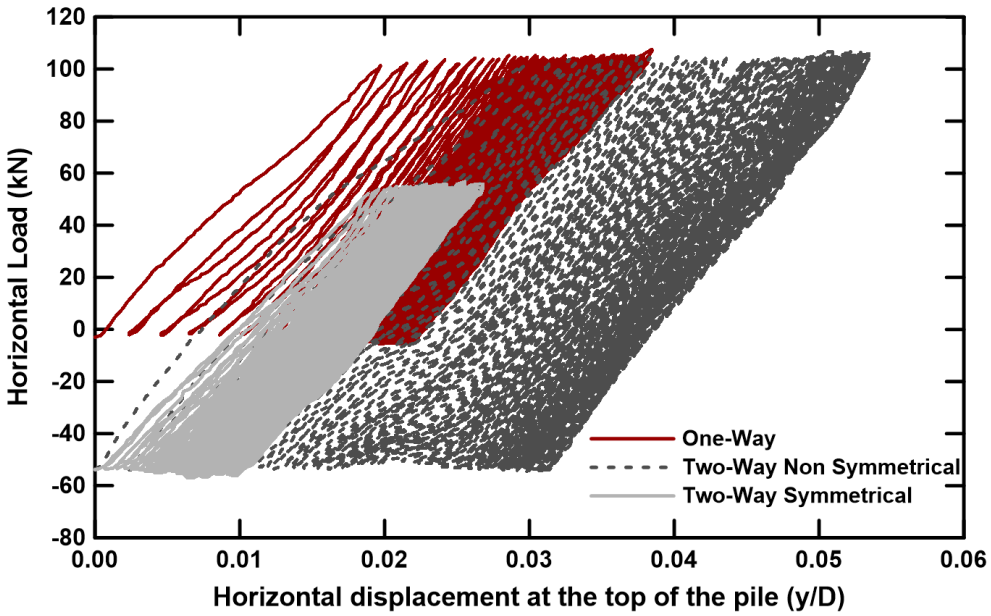

Figure 4.19 Load-displacement curves for the three centrifuge tests starting from the second cycle with initial displacement set equal to zero.

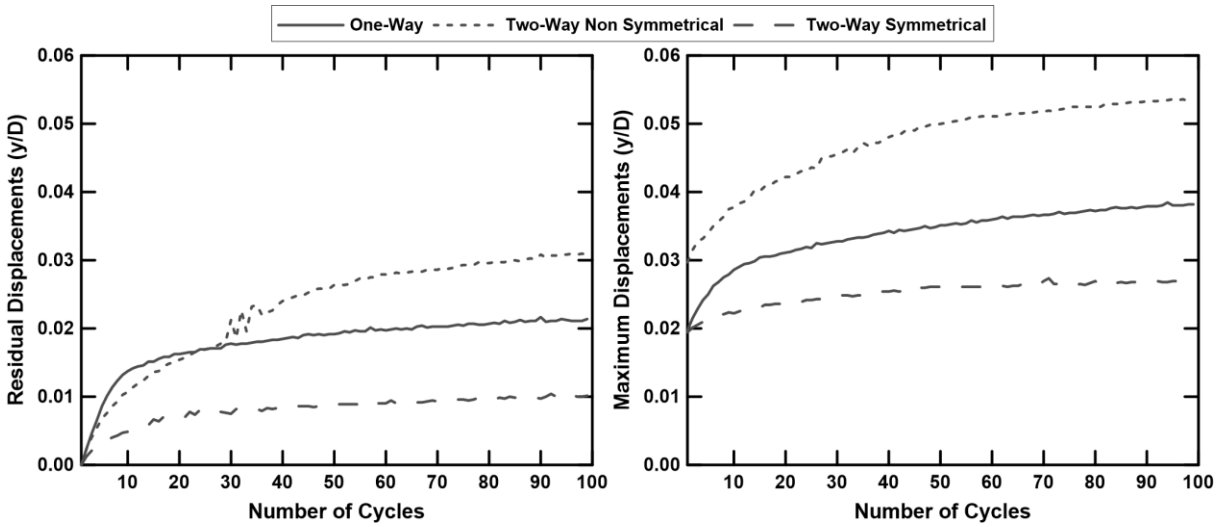

Figure 4.20 Residual and maximum displacement with respect to the number of cycles for three cyclic centrifuge experiments.

A better overview of the residual and maximum displacements with respect to the number of cycles is presented in Figure 4.20, for all the cyclic tests, except for the "storm" which is analyzed separately. As before, the displacements for both graphs are presented from the second cycle of the system, while the

initial value of the residual displacements was set to zero, meaning that all the displacements are measured with the respect to the beginning of the second cycle. The conclusions drawn in Figure 4.19 are confirmed, as the "two-way" non-symmetrical case is the most critical, while the "two-way" symmetrical test accumulates the smallest deformation. It is interesting to observe that at the end of the 100 cycles, the "one-way" curve and the "two-way" symmetrical are getting almost steady. Same behavior is followed by the "two-way" non-symmetrical case, though it is steeper than the other two experimental curves. In all cases, the accumulated displacements after 50 cycles are more than 95% of the final displacements at the 100th cycle. That indicates that the first cycles are the crucial ones, meaning that in an offshore pile in the field, the main cyclic loading's effect are more likely to appear in the early lifetime of the monopile (with the exception of the fatigue effects).

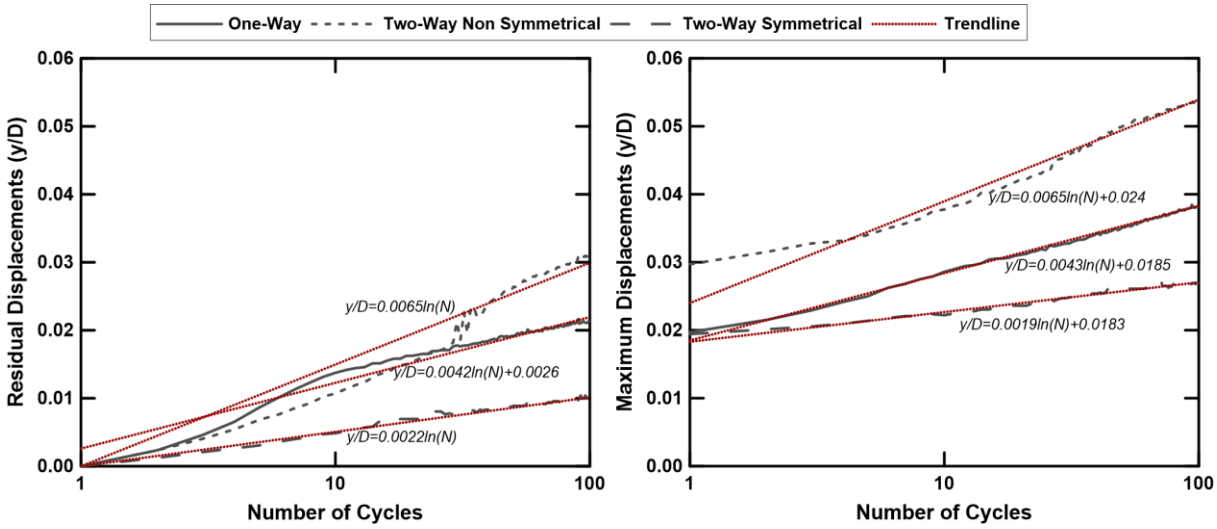

Figure 4.21 Residual and maximum displacement with respect to the number of cycles for three cyclic centrifuge experiments, along with their trendlines in logarithmic scale.

In Figure 4.21, the residual and maximum displacements with respect to the number of cycles are presented in logarithmic scale along with their trendlines. Specifically, logarithmic expressions have been fitted to the normalized displacements (y/D), in order to correlate displacement and number of cycles for each ratio of R_H. Note that especially in the residual displacements, the fitting was not possible to be really accurate for the whole range of cycles, so it was decided to focus on the last cycles, in which the deformations are getting relatively constant. In this way, the derived expressions may be used for more than 100 cycles, although the total number of cycles should remain relatively close to 100 to be reliable enough. In Table 4.1 the logarithmic expressions for the residual and maximum displacements for the three different R_H ratios (0.0, -0.5 & -1.0) are presented. Note that the term N stands for the current number of cycles.

Table 4.1 Logarithmic expressions for residual and maximum displacements for different R_H ratios.

R_H	Residual Displacement (y/D)	Maximum Displacement (y/D)
0.0	$y/D = 0.0042\ln(N) + 0.0026$	$y/D = 0.0043\ln(N) + 0.0185$
-0.5	$y/D = 0.0065\ln(N)$	$y/D = 0.0065\ln(N) + 0.024$
-1.0	$y/D = 0.0022\ln(N)$	$y/D = 0.0019\ln(N) + 0.0183$

The different response of the pile due to the "one-way" and the "two-way" cyclic loading can be approached by hysteretic loops in terms of shear stress & shear strain, as presented in Figure 4.22. Specifically, in an "one-way" loading, the loop will be limited above the horizontal axis (shear strain γ), as the load does not change its direction. Therefore, a relatively small dissipation of energy occurs, along with a low reduction of the soil strength (due to destruction of the soil structure). On the other

hand, a "two-way" loading with the same maximum load as in "one-way" case corresponds to a larger hysteretic loop, as it is extended considerably below the horizontal axis. As a consequence, large dissipation of energy takes place, meaning that the soil degradation is intense, and hence higher accumulated displacement develop compared to an "one-way" case. This phenomenon explains the larger residual displacements observed in the "two-way" non-symmetrical case compared to the "one-way" test. Specifically, both experiments reached the same maximum load, but the "two-way" non-symmetrical case returned to considerably lower minimum value (with opposite sign of the maximum), dissipating considerably larger energy and accumulating larger deformations. This behavior is not observed though when the "one-way" case and the "two-way" symmetrical tests are compared. However, it needs to be considered that the "two-way" symmetrical case reaches a maximum load which is half of the equivalent of the "one-way" case. This maximum load is relatively small, meaning that the response of the soil in this load range can be quite elastic (obviously plastic deformations will occur but in a limited degree). Therefore, the "two-way" symmetrical case is expected to lead to smaller dissipation of energy compared to the "one-way" test and hence smaller residual displacements, as observed in the centrifuge experiments.

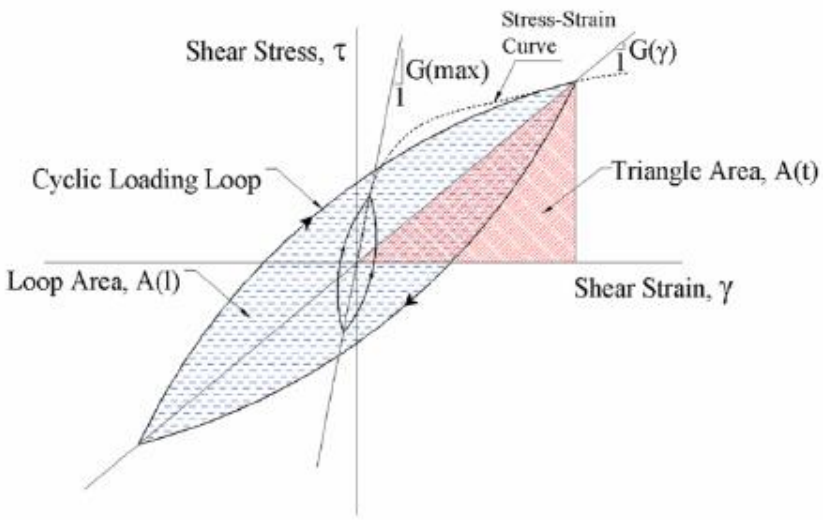

Figure 4.22 Hysteretic loop in terms of shear stress & shear strain (Meidani et al. 2008)

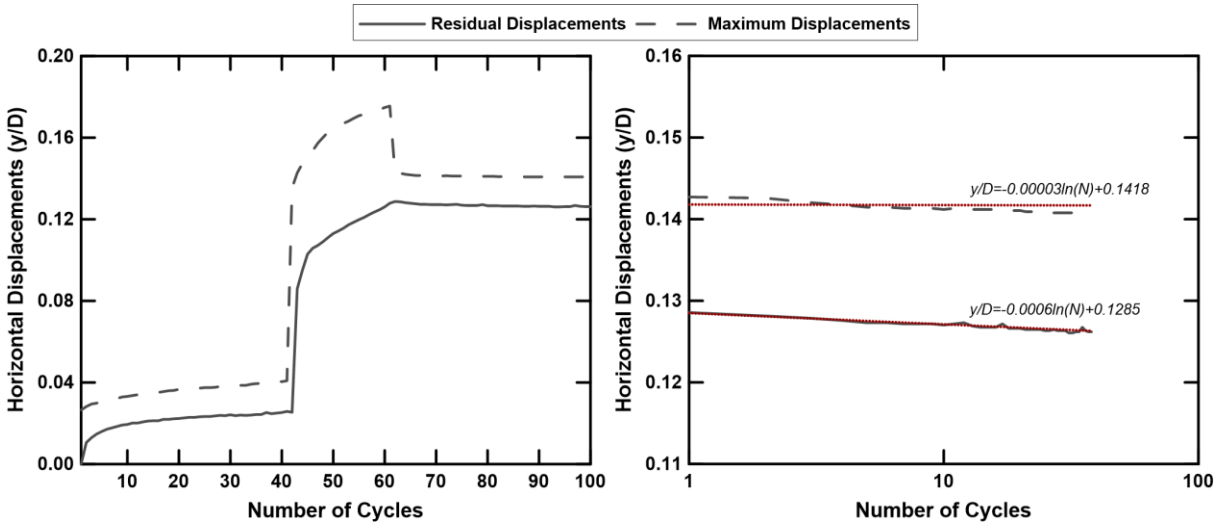

Figure 4.23 Residual and maximum displacements for the "storm experiment" with respect to the number of cycles, along with the trendlines in logarithmic scale for the last 40 cycles (after the "storm event")

In Figure 4.23 the evolution of the residual and maximum displacements with the number of cycles is illustrated for the "storm experiment" in the left graph. In the same figure, the last 40 cycles, after the

"storm event", are presented in logarithmic scale, along with the trendlines fitted to the residual and maximum displacements. The interesting point in this case is the evolution of the soil deformation after the "storm", as both residual and maximum displacements are practically constant. That is attributed to the previous soil history, which is subjected to larger amplitudes, even for a limited number of cycles. This has as a consequence a very stiff behavior of the soil, when it is subjected to loads smaller than the maximum one in its load history and hence negligible deformations occur. The behavior observed in Figure 4.23 can be crucial in real case scenarios, as the monopile in its lifetime will come up against strong current and storm events that will load it with a considerable load for a relatively small period time. This large load will cause large deformations to the monopile, yet if its deflection remains in the SLS (Serviceability Limit State), then the load may be beneficial for the pile. Specifically, the load will eventually return to its initial state, within the typical design magnitude, but the soil will be stiffer, meaning that no considerable deformation will be expected. This conclusion should be further investigated, with more cycles, as it could lead to a more favorable design of a typical offshore monopile.

4.2.2 Stiffness Evolution

The evolution of the stiffness with the number of cycles can dictate the behavior of the monopile against the cyclic loading. This parameter was investigated in this thesis, based on two different approaches of the secant stiffness, stated by Verdure et al. (2003) and Depina et al. (2015). The first one, the external secant stiffness, determines the stiffness of the system based on the maximum load and the total accumulated displacement at the end of each cycle, as described in Eq. (22) by Depina et al. (2015). Therefore, it does not study each cycle separately but instead it focuses on the general load-displacement curve (Figure 4.24). The second approach, the internal secant stiffness, by Verdure et al. (2003) investigates each cycle, independently of the previous load history, as it calculates the stiffness of the *n* cycle, based on its characteristics, as expresses in Eq. (23). The schematic illustration of this approach is also depicted in Figure 4.24.

$$K_{ext} = \frac{H_{max}}{y_{max}} \qquad \textit{Eq. (22)}$$

$$K_{int} = \left(\frac{H_{max} - H_{min}}{y_{max} - y_{min}}\right)_n \qquad \textit{Eq. (23)}$$

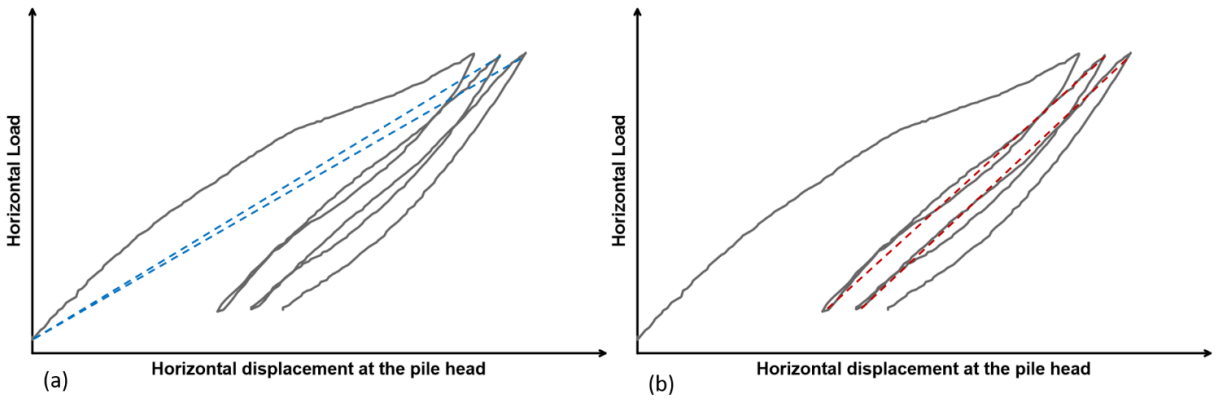

Figure 4.24 Schematic illustration of the external and internal secant stiffness.

Based on the equations 22 & 23, the external secant stiffness and the internal one are presented in Figure 4.25 with respect to the number of cycles. The external secant stiffness by its definition should constantly getting smaller. It is interesting though to observe the rate of this reduction, as after the first 50 cycles, the curves for "one-way" and the "two-way" tests are getting almost horizontal, indicating that the soil-pile response is getting stiffer. The "storm" experimental curve experiences sudden drops in the load changes, which are attributed to the increase of the soil displacements (when the maximum

load goes from 100 to 300 kN) and to the decrease of the load from 300 kN to 100 kN in the last 40 cycles. However, observing the curve after the "storm" event shows an almost horizontal curve, meaning the previous load history has increased considerably the stiffness of the soil. In the internal secant stiffness graph (Figure 4.25), a different behavior is observed for the "one-way" and the "storm" experiments (before the "storm event") compare to the "two-way" tests. Specifically, the internal stiffness in the "one-way" experiments is slightly reducing, after the first 10 cycles in which it reaches a peak. This could be an indication of possible dilation effects, which in the essence lead to reduction of the soil capacity and hence stiffness. On the contrary, the general trend, in the "two-way" tests, is an increase of the stiffness with the number of cycles. That indicates that the samples are getting more densified around the monopile, despite their initial relative density of 80%, without experiencing though considerable dilation effects. Therefore, it seems that the R_H ratio can dictate the evolution of the stiffness with the number of cycles.

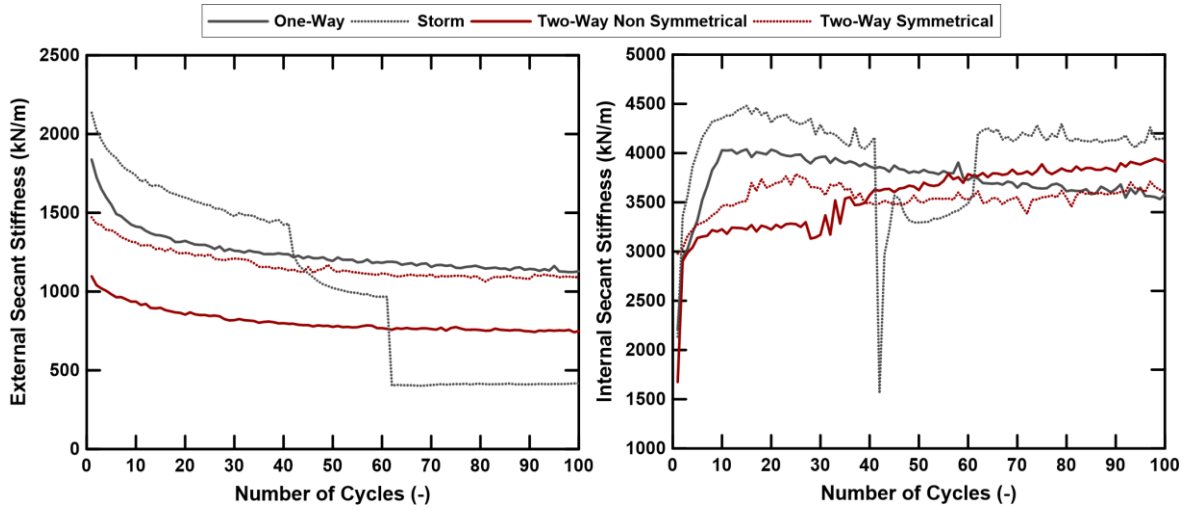

Figure 4.25 External and internal secant stiffness for the four cyclic tests with respect to the number of cycles.

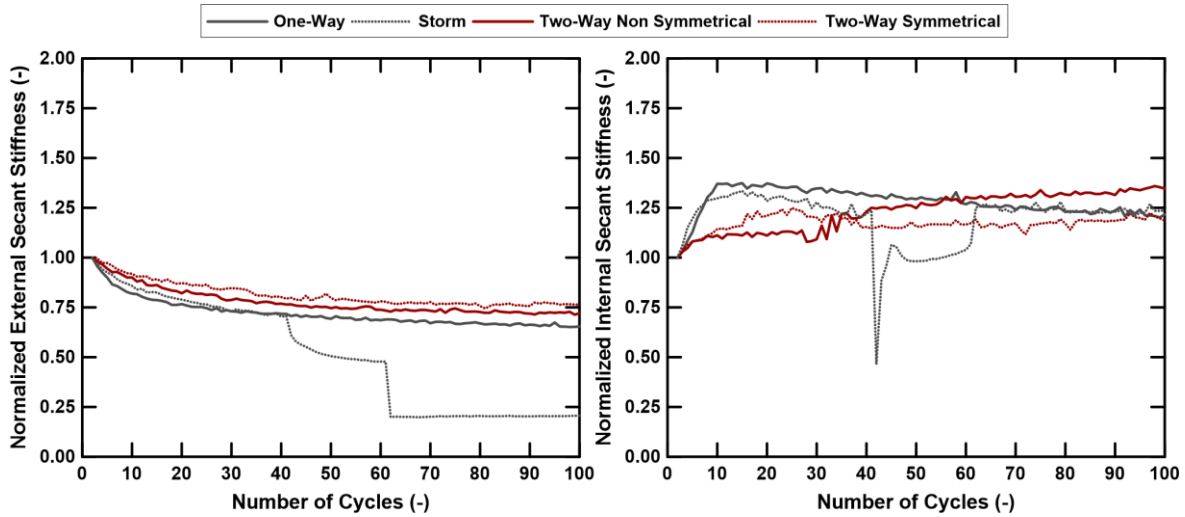

Figure 4.26 Normalized external and internal secant stiffness to the ones of the second cycle for the four cyclic tests with respect to the number of cycles.

To acquire a better overview of the stiffness evolution with the number of cycles, it is normalized based on the first actual cycle after the initial monotonic loading ($k_{ext,n}= K_{ext,n}/K_{ext,2}$ and $k_{int,n}= K_{int,n}/K_{int,2}$) and is presented in Figure 4.26. The normalized external stiffness is decreased with a larger rate for the "one-way" experiments and after 100 cycles it is around 10% smaller than the equivalent stiffness of the "two-way" tests. This difference occurs in the first 20 cycles, as after than point the curves remain almost parallel to each other, meaning the rate of change is practically constant. The "storm" curve

experiences drops, for the reason explained before. The external stiffness evolution can offer a quick overview of the soil-pile system's response as a whole, but it cannot actually give a straightforward image of the behavior of the pile in each cycle. The internal secant stiffness is more appropriate, as it presents the resistance of the soil in each single cycle that is subjected to. In the right graph of Figure 4.26, it is observed that after 100 cycles, regardless of the path they follow, all curves end up in a range from 1.20 after 1.40, meaning that the soil response has actually gotten stiffer by the cyclic load's influence. However, it is interesting that the "two-way" curves present a constant increase in their whole length, while the "one-way" experiments reach a peak relatively fast, in the first ten cycles, and they get reduced slightly cycle by cycle. This behavior can be attributed to the fact that the "one-way" loading concentrates its energy to the one side of the pile, densifying the soil in fast rate. Consequently, a crucial dense state is reached after a very few cycles, followed by dilation effects, explaining the decrease in the stiffness. It needs to be stated that when the soil tends to dilate, the grains tend to loosen up, meaning that an increase of the soil volume is imminent. This change corresponds to larger pressures to the pile by the soil, as it tries to expand its volume in limited space. Therefore, the tendency for dilation will initially highly increase the stiffness of the system before it will gradually drop, as observed in the equivalent experiment. A different behavior is observed, though, in the "two-way" loading as concentration of energy occurs to the whole pile's proximity, leading to uniform soil densification, in a smaller rate. The grains are getting packed in a denser state, without reaching though a crucial density, after which loosening would occur, as no dilation effects have been observed, up to the 100th cycle. Note though that these trend are observed for a total number of 100 cycles, meaning that in the actual number of cycles that a monopile would come up against in its lifetime (more than 10000), a different trend may exist. A general conclusion drawn though is that the cyclic load in dense sands may lead to a considerable increase of the stiffness of the soil-monopile system, at least for a limited number of cycles.

4.2.3 Cyclic p-y Curves

The p-y curves have been derived for the cyclic experiments performed in the centrifuge, meaning the "one-way", the "two-way" non-symmetrical and the "two-way" symmetrical test. The "storm" experiment has decided not to be included in this chapter, due to the constant load changes, that did not allow for a clear schematic illustration of the curves evolution. The extraction of the "p-y curves" has been performed according to the procedure described in section 4.1.2.2 for the monotonic experiments. The data processing was again made using MATLAB 2017b software, as a large number of data required for each curve in all the experiments presented. In Figure 4.27, the evolution of the "p-y curves" for the "one-way" experiment at the strain gauges' positions, is presented. The accumulated deformations can be observed, as the cycles are constantly moving towards to the load direction, above the rotation the point, and in the opposite direction below it. The increase of the stiffness is also illustrated, as the curves are getting denser for the number of cycles. An interesting observation for the extracted "p-y curves" is that the shallower (z/D=1.1) and the deeper (z/D=3.9) one have a considerably increasing minimum and maximum soil pressure with the number of cycles, while the ones in the middle of the pile (z/D=1.7, z/D=2.8) remain between relatively constant soil pressures' limits. Note that below the rotation point (z/D=3.9) much larger passive soil pressures develop comparing to the curves above the rotation point, which may be attributed to the "toe-kick". In Figure 4.28, the evolution of the "p-y curves" for the "two-way" symmetrical experiment at the strain gauges' positions is presented. The same conclusions as with the graphs of Figure 4.27 can be drawn. Specifically, the accumulated deformations are observed, as before, increasing towards to the load direction, above the rotation the point, and in the opposite direction below it. Note that in the equivalent depths of Figures 4.27 & 4.28, smaller deformations are depicted in the "p-y curves" after the end of the 100 cycles in the "two-way" symmetrical experiment compared to the "one-way" case. The stiffness is also increased, as it is illustrated in the graphs, in which the curves are getting denser as the number of cycles escalates. The previous conclusion regarding the shallower (z/D=1.1) and the deeper curve (z/D=3.9) is also confirmed, in which large soil pressures' increase is obvious as the number of cycles rises up, while the middle ones (z/D=1.7, z/D=2.8) are limited into a relatively constant range of minimum and maximum load.

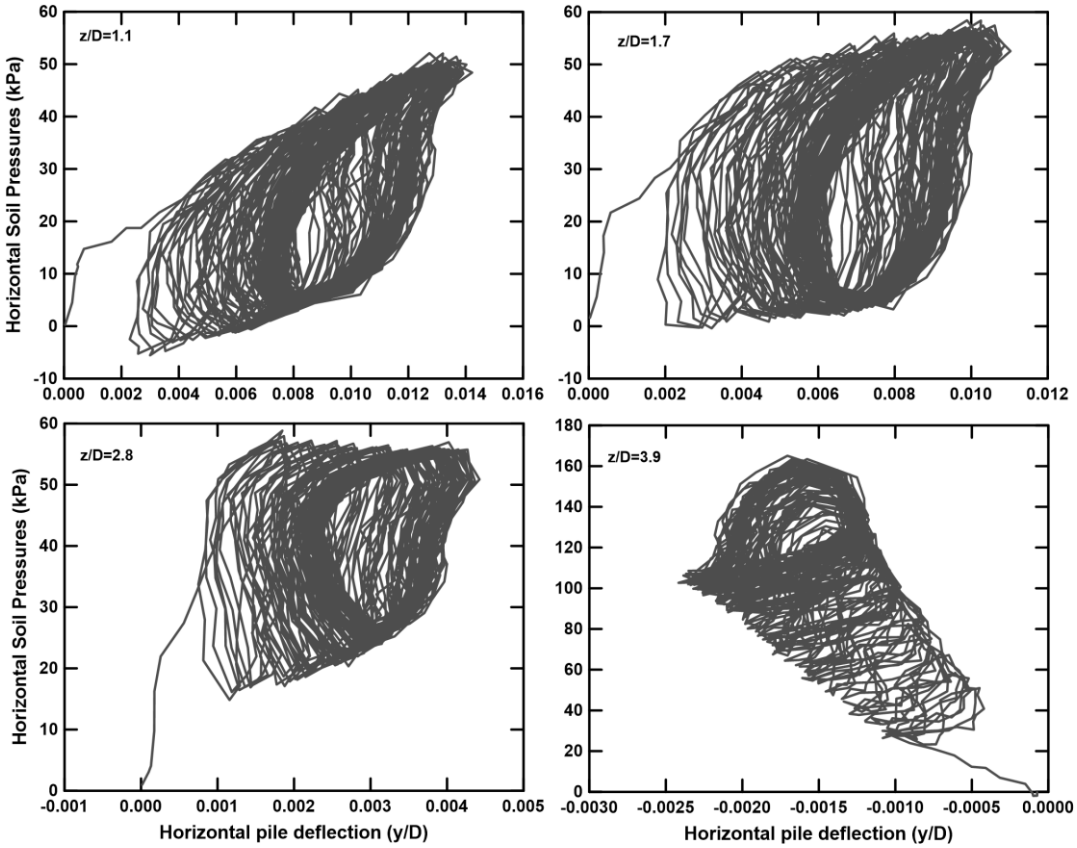

Figure 4.27 Evolution of the "p-y curves" for the "one-way" experiment at various depths in the strain gauges' positions.

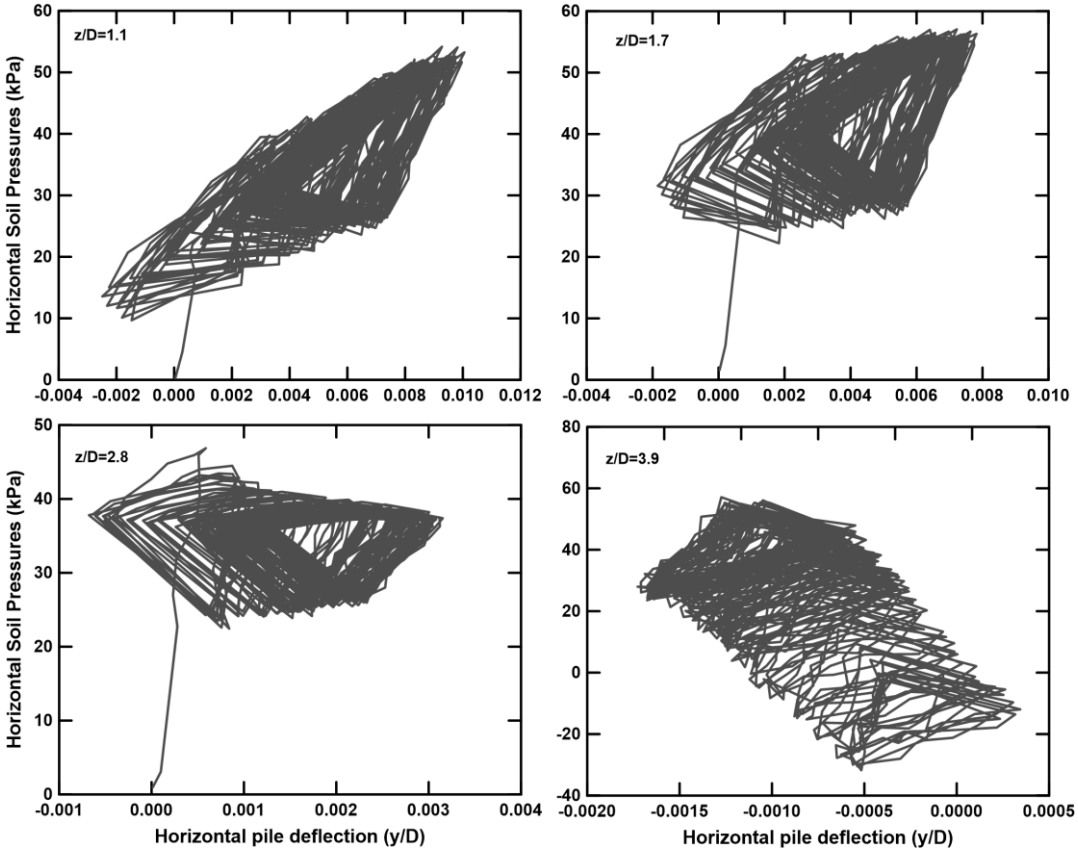

Figure 4.28 Evolution of the "p-y curves" for the "two-way" symmetrical experiment at various depths in the strain gauges' positions.

The evolution of the "p-y curves" for the "two-way" non-symmetrical experiment at the strain gauges' positions follows, which is depicted in the Figure 4.29. These curves experience the larger soil deformations for the three tests investigated in these sections, in the four depths examined. Highest soil pressures appear again below the rotation point (z/D=3.9). The general conclusions drawn by Figures 4.27, 4.28 & 4.29 have to do initially with the stiffness increase as the number of cycles increases, which can be observed by the reduction of the residual displacements as the "p-y curves" progress. It was also interesting the fact that the shallower and the deeper curves (z/D=1.1, z/D=3.9) had a considerably increasing minimum and maximum soil pressure as the cycles were escalating, while the ones in the middle of the pile (z/D=1.7, z/D=2.8) remained between relatively constant soil pressures' limits.

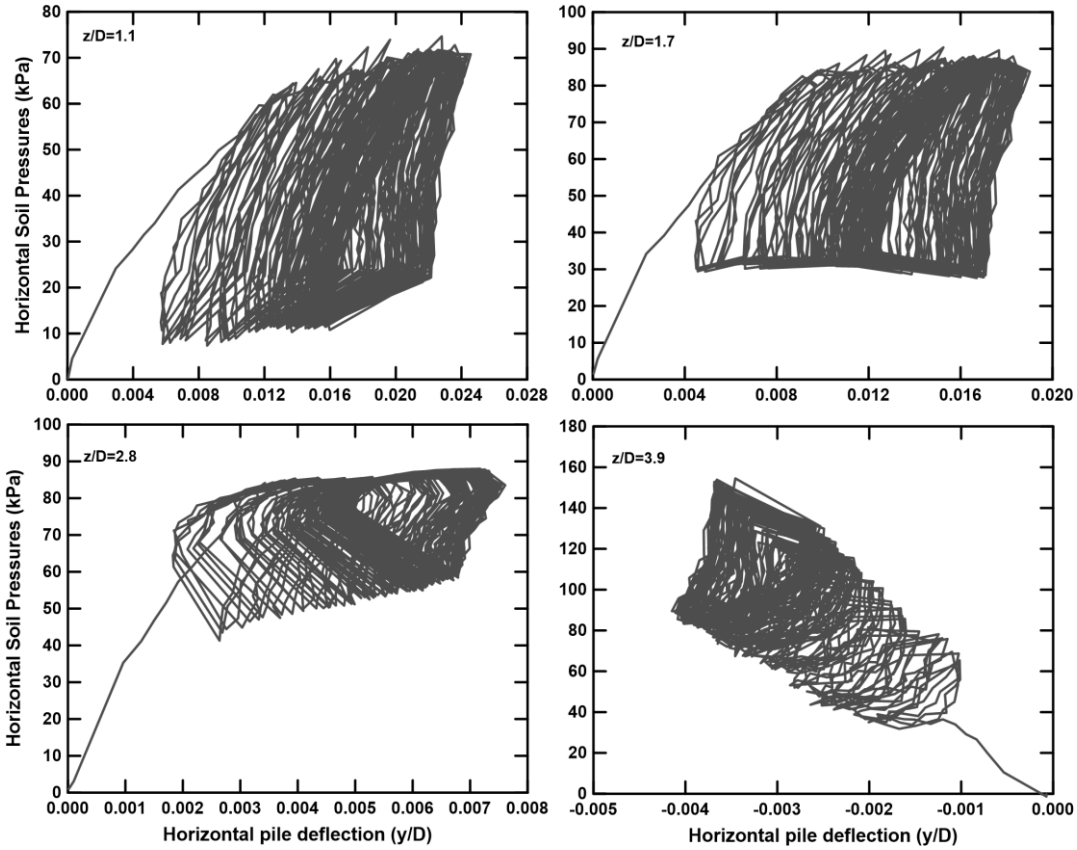

Figure 4.29 Evolution of the "p-y curves" for the "two-way" non-symmetrical experiment at various depths in the strain gauges' positions.

4.3 Numerical Cyclic Analyses

The output of the numerical cyclic tests is presented in the current section, including load-displacement curves, the evolution of the residual and maximum displacements, and the stiffness change with respect to the number of cycles. The results are divided into two main categories, the first one focusing on the load characteristics' influence in the pile's response, and the second group investigating the effect of the scour protection' properties to the monopile's behavior.

4.3.1 Cyclic Characteristics' Influence in the Monopile Response

Four cyclic numerical analyses have been performed for investigating the cyclic characteristics' influence in the monopile response. More specifically, two identical analyses with the ones in the centrifuge have been conducted, the "one-way" and the "two-way" non-symmetrical. Based on them, an evaluation of the numerical model developed is executed. These two analyses have been chosen as the most realistic ones to occur in an offshore pile in field conditions. In addition to them, two extra analyses have been performed, a variation of the centrifuge "storm" event, and a gradual maximum load increase from 25

to 100 kN. The "new-storm" analysis is divided into 4 sets of 25 cycles, with the load pattern going from 0 to 100 kN for the first set, 0 to 300 kN for the second set, again 0 to 100 kN for the third set, finishing with 0 to 300 kN for the last set. The point of this test was to study the load history effect in the stiffness of the soil. The "gradual test" is also distinguished into 4 sets of 25 cycles, with the minimum load being constant at 0 kN and the maximum one going from 25 to 100 kN with a step of 25 kN for each set. The load-displacement curves for the aforementioned analyses are presented in Figure 4.30.

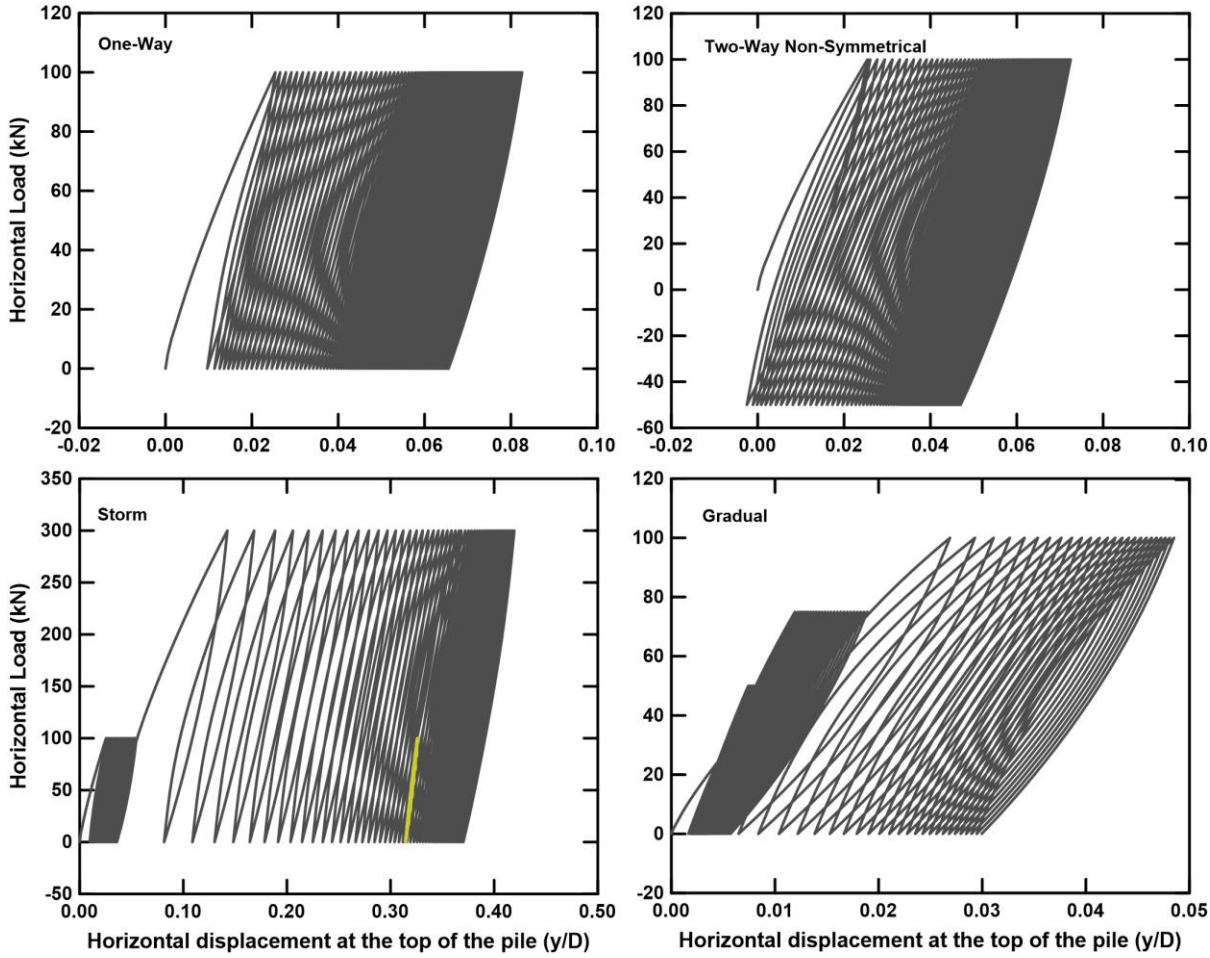

Figure 4.30 Load-displacement curves for the four cyclic numerical analyses conducted in PLAXIS 3D, with respect to the cyclic loading characteristics.

Comparing the "one-way" and the "two-way" non-symmetrical analyses, the first discrepancy between experimental and numerical results is observed. Specifically, the "one-way" analysis leads to larger accumulated displacements than the non-symmetrical case, with the difference being around 25%. In the centrifuge tests though, the opposite observation was made as the higher residual deformations have been measured in the non-symmetrical case, in which the deformation at the end of the 100th cycle was around 30% larger than the equivalent in the "one-way" test. Note that the "one-way" test in the centrifuge ends up in 35% smaller deformation that in the equivalent test in the numerical modelling, while the non-symmetrical case's final residual displacement is 15% larger than the one in PLAXIS 3D. These observations are more likely attributed to the shape of the loading-unloading branch (after the monotonic part) in the experimental and numerical tests, as it is observed that in the numerical analysis, this branch is less steep comparing to the experimental ones. As a consequence, at the end of each cycle in the numerical tests higher maximum deformation occurs. Note that the less steep numerical branch means that the maximum displacement at each cycle is reduced in a faster rate before reaching the residual one at the end of the unloading, comparing to the centrifuge test. This faster rate means that initially, the PLAXIS 3D gives smaller residual displacements both for "one-way" and "two-way" analyses than the ones in the centrifuge. However, in the "one-way" analysis the considerably larger

maximum numerical displacements cancel out the unloading branch's effect described above after approximately 20 cycles. In the non-symmetrical case, though, the unloading branch's effect is enough to keep the deformations of the numerical analysis smaller comparing to the centrifuge equivalent one, as well as the "one-way" numerical analysis.

In Figure 4.31, the evolution of the residual and maximum displacements with the number of cycles is presented for the "one-way" and the "two-way" non-symmetrical analyses. As it was already discussed, the "one-way" load scenario is more critical as it leads to higher accumulated displacements as well as maximum pile deflections. This observation is confirmed in the graphs of Figure 4.31, as the response of the pile in the "one-way" case results to 25% higher residual displacements and 10% larger maximum deformations. It is interesting to state that the deviation between the two load scenarios is much clearer and almost constant at the residual displacements' graph, while in the maximum displacements' one considerably different paths are followed after the first 50 cycles.

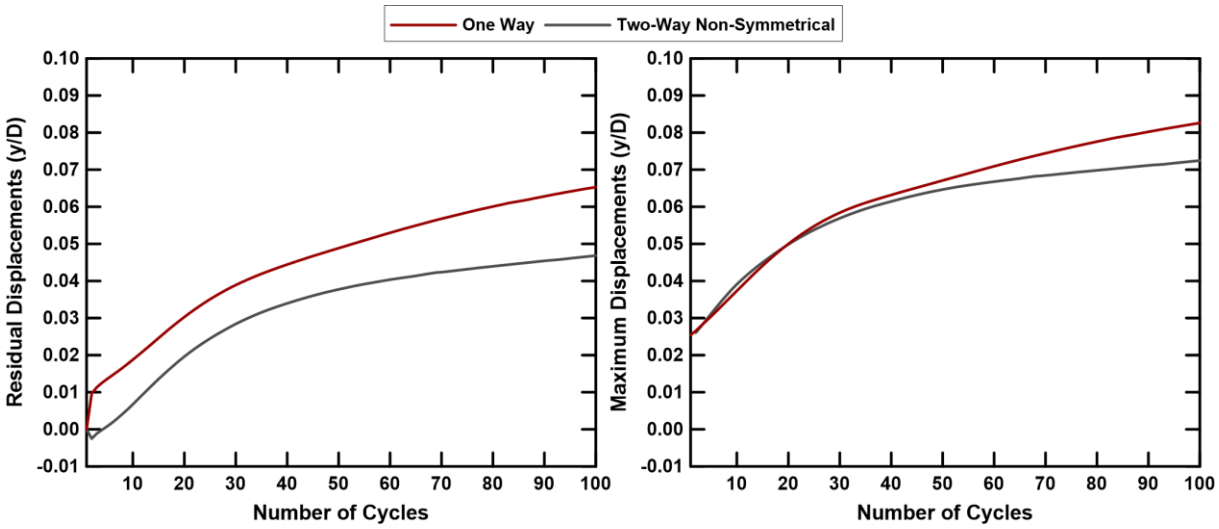

Figure 4.31 Residual and maximum displacement with respect to the number of cycles for the "one-way" and "two-way" non-symmetrical numerical analyses.

Up to now, the "storm" and the "gradual" analyses have not been commented. In essence, these two tests are not suitable for comparison, and hence have not been conducted with this goal. On the contrary, the objective of them is investigating the load history's effect in the monopile response when subjected to cyclic loading. In Figures 4.32 & 4.33 the external and internal secant stiffness (as described in 4.2.2) is presented for the "one-way", "two-way" analyses and the "storm", "gradual" analyses respectively. The stiffness is initially presented in terms of absolute values and then is normalized with respect to the first actual cycle, after the monotonic push of the pile. The external secant stiffness' curves, both for the absolute and the normalized ones, follow almost the same path for the "one-way" and the "two-way" analyses. Specifically, they present a slight divergence after the 60th cycle, yet it does not get larger than 10% in the end of the analyses (100th cycle). Similar observations can be made in the internal secant stiffness, with the absolute values, after the first 30cycles. However, when the stiffness is normalized to the one of the second cycle, after the monotonic push, an interesting trend is observed. Specifically, in both cases, an initial drop is observed in the stiffness, which reaches a bottom after 20 and 10 cycles for the "one-way" and the "two-way" non-symmetrical analyses respectively. Then, in both cases, the internal stiffness constantly grows, with different rates though, as after 100 cycles, the "one-way" test tends to reach the value 1.00 and the non-symmetrical exceeds 1.10. Therefore, it seems that "one-way" cyclic loading does not offer an actual increase in the monopile's stiffness, as after some changes mainly the first 50 cycles the stiffness is getting almost constant at its initial value. On the contrary, a considerable contribution is observed for the non-symmetrical case, as it offers a 10% increase to the stiffness, before the curve starts to get horizontal. These two responses are quite in accordance with the centrifuge tests, although important difference can be seen in specific areas. Specifically, the contribution to the stiffness in the centrifuge tests was higher in the non-

symmetrical case, reaching a value of about 1.35 at the 100th cycle. However, an initial drop was never measured in the centrifuge, as in the numerical analysis. The "one-way" numerical test has presented a quite different behavior, as after an initial drop a slow-rate increase is seen. However, in the centrifuge, the equivalent test produced a curve in which an initial peak was captured and after this point the stiffness was continuously decreasing, yet after the 100th cycle it was well above the initial value, as it stopped at 1.20. However, in both cases the higher contribution of the non-symmetrical case in the stiffness is captured, with the normalized graphs for both external and internal secant stiffness presenting a similar trend both for the numerical and the physical modelling after the first 20-30 cycles. Therefore, it can be concluded that the numerical model does not capture perfectly the response of the monopile as dictated by the centrifuge experiments, yet it is sufficiently accurate in capturing important trends that allow to investigate the scour protection's influence in the pile's stiffness.

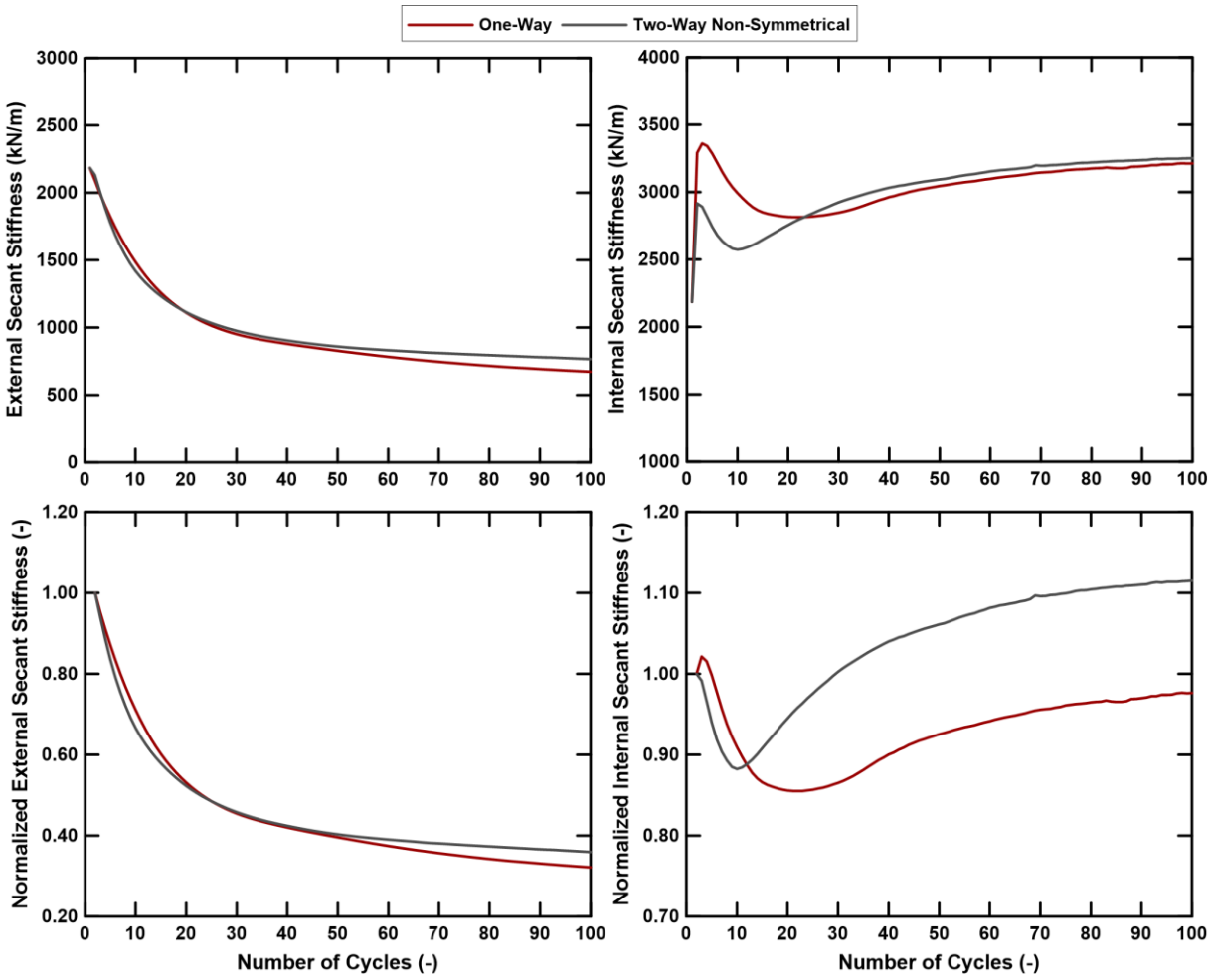

Figure 4.32 Absolute and normalized external and internal secant stiffness for the "one-way" and "two-way" non-symmetrical analyses with respect to the number of cycles.

In Figure 4.33 the evolution of the absolute and normalized external and internal secant stiffness, for the "storm" and "gradual" numerical analyses, is presented. Note that the two cases are not eligible for comparison with each other, so they are presented together only for saving space in this report. Observing the "storm" analysis produces interesting findings after the 50th cycle. Specifically, as it can be seen in the internal secant stiffness, when the maximum load is reduced from the 300 to 100 kN, the soil response is getting very stiff and remains almost constant during the increase of the cycles. On the same context, in the last 25 cycles, in which the load goes up again to 300 kN, a drop is observed in the stiffness up to the last value acquired in the previous set of cyclic loading from 0 to 300 kN. After this drop, the stiffness' evolution remains quite constant, as a slight increase is observed. Note that the same trend was observed in the "storm" experiment performed in the centrifuge, in which though only

the sequence of the maximum load was going from 100 to 300 kN and then finishing in 100 kN. However, it seems by both analyses that the sand has memory of the previous load history when subjected to cyclic loading. Specifically, if the current maximum value of the load pattern of the soil is equal or smaller to the maximum value that the soil has come up against in its lifetime, then a stiffer response is expected by the monopile.

The "gradual" analysis performed in the PLAXIS 3D software (Figure 4.33, grey line) indicates that the previous load history has no actual effect in the soil's behavior, when the current load applied to the pile is simultaneously the maximum one that is has experienced in its lifetime. As it is observed especially in the normalized internal secant stiffness graph, the stiffness of the system drops in each increase of the maximum load (every 25 cycles). During each set though, difference behavior is captured, as in the first one and the last one, the internal stiffness increases with the number of cycles, while in the two middle ones the opposite behavior is observed. This could be attributed to the number of cycles of each set, as the increase of the stiffness may require a minimum number of cycles with constant load in order to occur. More specifically, in the "one-way" and the "two-way" analyses, in which the load pattern was constant, the increase of the stiffness was observed to begin around the 30th cycle. Note that the stiffness curve of the "gradual" test in the last cycles has a considerable angle, indicating that if the analysis was continued, the stiffness would increase respectively.

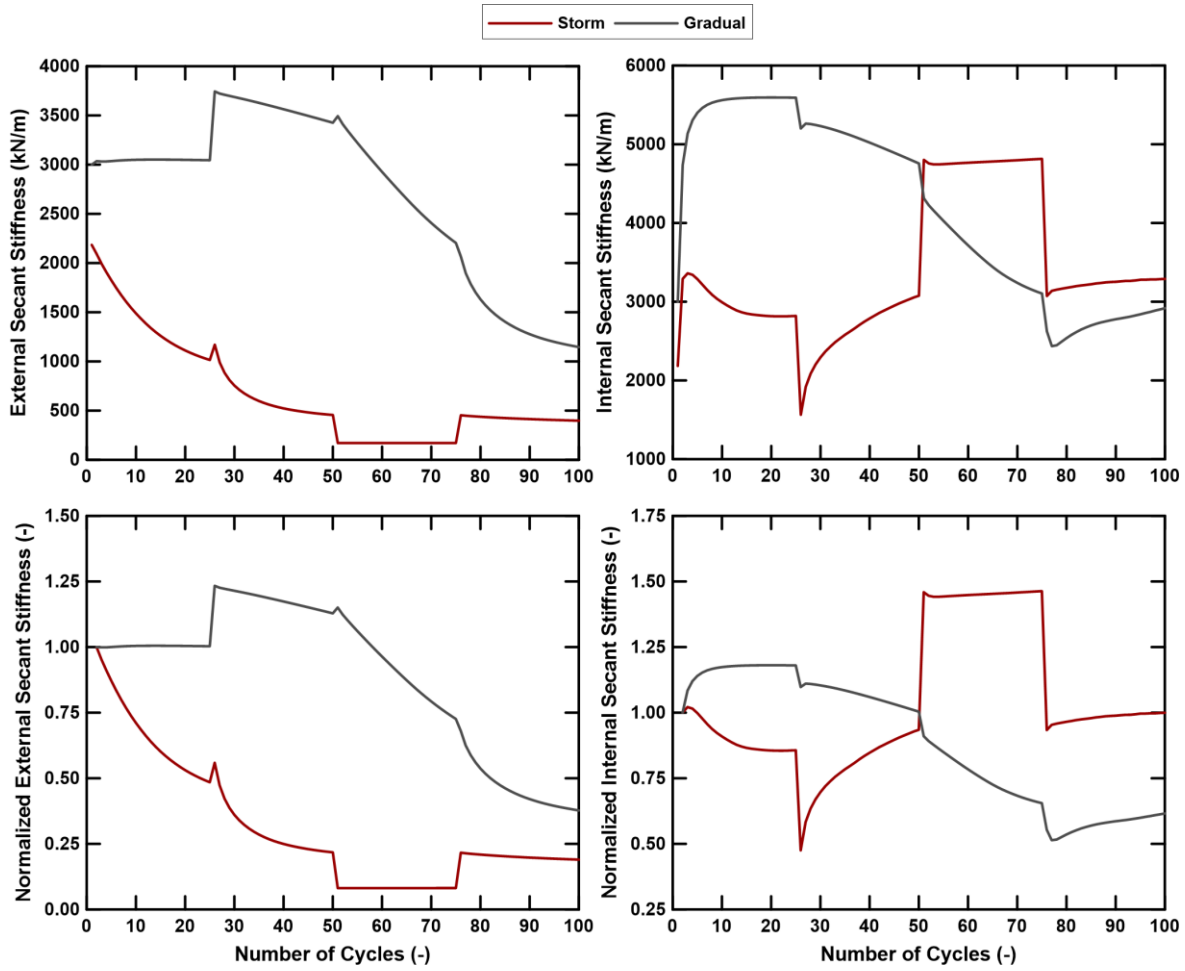

Figure 4.33 Absolute and normalized external and internal secant stiffness for the "storm" and "gradual" numerical analyses with respect to the number of cycles.

4.3.2 Influence of Scour Protection's Properties in the Monopile Response

The main goal of the numerical analyses was the investigation of the scour protection layers' effect in the monopile response under cyclic loading. In all the tests of this section, therefore, the same loading

pattern was applied, an "one-way" loading from 0 to 100 kN, while the two parameters investigated were the scour protection' length and thickness. Note that the thickness corresponds to overburden pressures around the monopile, meaning that this parameter has been modelled by three stress regimes, which are equivalent to different scour protection thicknesses.

4.3.2.1 Scour Protection's Length Effect on the Pile Behavior

In Figure 4.34, the load-displacements curves for the no-protection case and for three different scour lengths (3.0D, 5.0D & 7.0D) are presented. Note that the equivalent of the thickness overburden pressure is equal in all cases to 15 kPa. The positive influence of the scour protection layer in the monopile response can be detected by these curves, as both maximum and residual displacements are considerably lower when the protective layer is applied. Moreover, the area of each cycle is larger in the no-protection case (as shown characteristically in Figure 4.35a for the second cycle of each analysis), meaning that a higher amount of energy dissipates which corresponds to smaller stiffness and larger plastic deformations. The evolution of the dissipated energy (calculated as the area of each cycle) is depicted in Figure 4.35b. It is observed that the not-protected case dissipates more energy in each cycle, compared to the cases that scour protection layers have been applied, explaining the larger accumulation of plastic deformations for the not-protected case. A larger fluctuation of the dissipated energy is observed in the first 20 cycles, possibly due to rearrangement of the sand particles. After this point, the dissipated energy constantly decreases with the number of cycles, meaning that less accumulated deformations occur at each cycle. Specifically, there is a high rate of reduction of the energy dissipation from the 20th to the 40th cycle, showing that the stiffness of the system is getting increased considerably in this range. After the 40th cycle, the rate of reduction is quite low, indicating that no considerable alterations occur to the pile response.

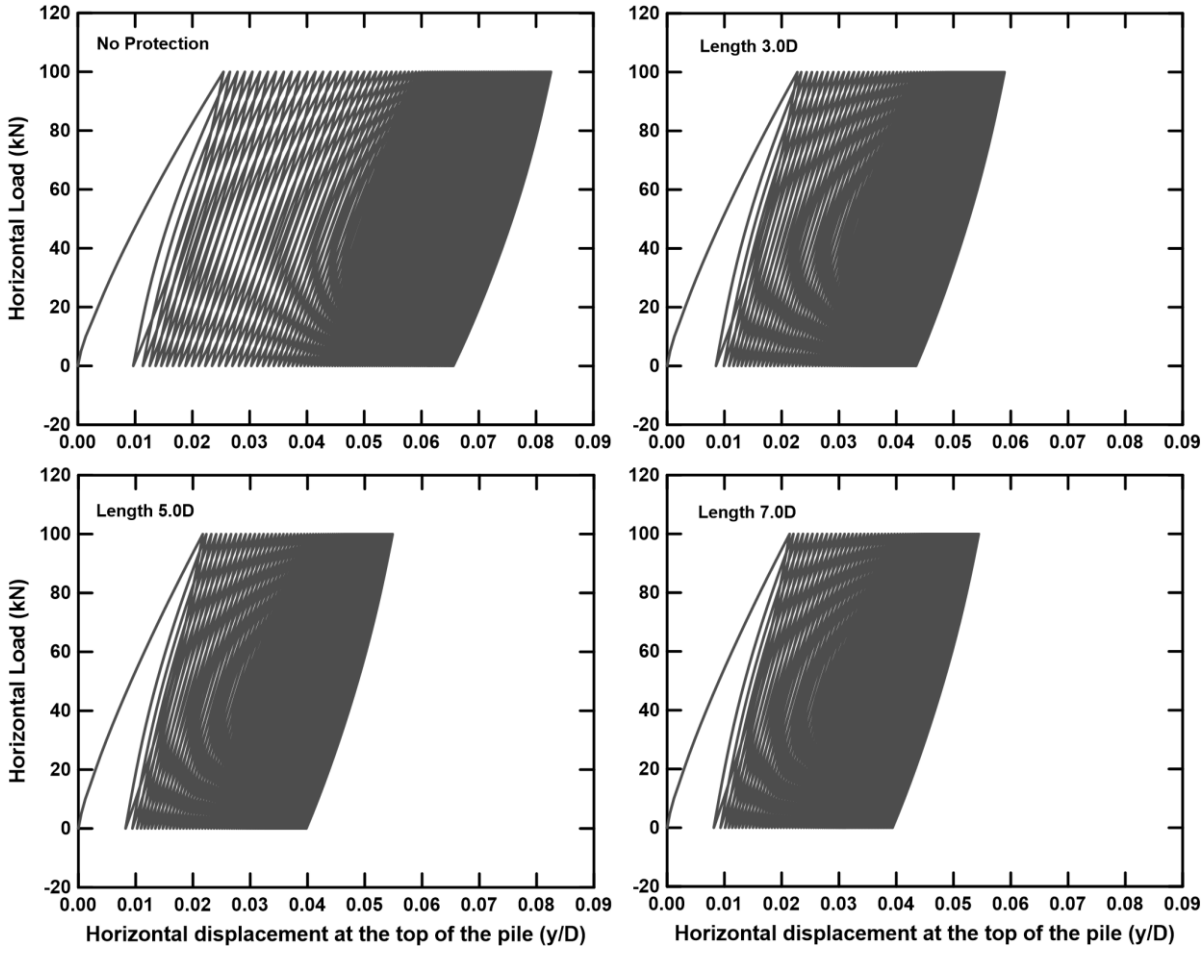

Figure 4.34 Load-displacements curves for the no-protection case and for three different protection lengths.

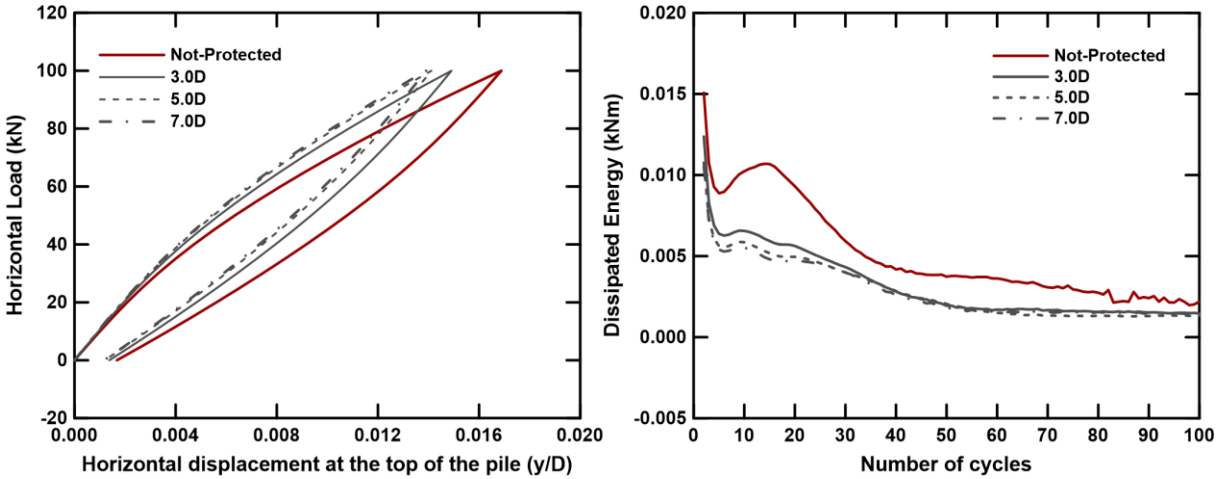

Figure 4.35 (a) Area of the second cycle for the not-protected case and the three cases of different scour protection lengths (b) Evolution of the dissipated energy with the number of cycles for the not-protected case and the three cases of different scour protection lengths.

A better overview of the protection layer's influence, along with a quantification of it, can be extracted by Figure 4.36 in which the evolution of the residual and maximum displacements for the no-protection case and the three different scour lengths is illustrated. More specifically, the residual displacements are considerably reduced due to the scour protection layers in a range of 35 to 40%, while the same percentage is around 30 to 35% for the maximum induced displacements by the cyclic loading. More interesting though is the fact that the scour protection length seems to be of little importance, as the 5D-long protection layer gives approximately 8% smaller deformations compared to the 3D-long layer, while the same percentage is about 1% in the same comparison between 7D and 5D lengths. Taking also into account that in the literature, only a very few cases were found with a scour protection smaller than 3 times the diameter (defined by the currents and waves action in each field), it seems that the protection length is not important, as the minimum one is enough for considerably limiting the deformations (up to 30%). The same trend is observed in Figure 4.37, in which the evolution of the external and internal secant stiffness for the no-protection case and the three different protection lengths is depicted. In absolute values, the protection length at the end of the 100th cycle offers an increase of the external stiffness around 35% and for the internal stiffness approximately 15% compared to the no protection case. One the same context, the stiffness contribution of each protection layer is similar to each other, confirming the findings of Figure 4.36.

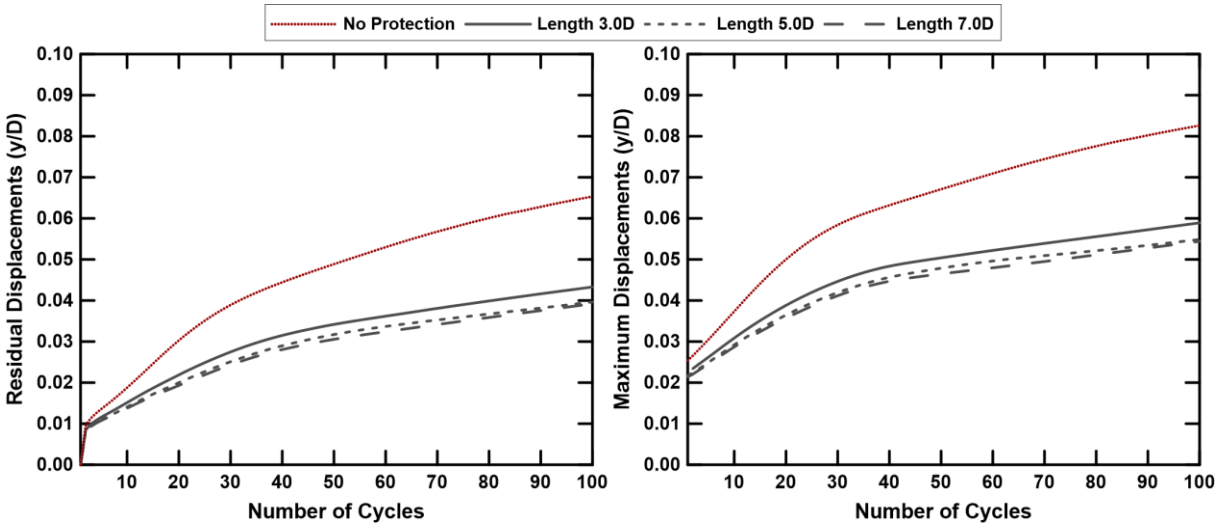

Figure 4.36 Evolution of the residual and maximum displacements for the no-protection case and for three different scour protection lengths.

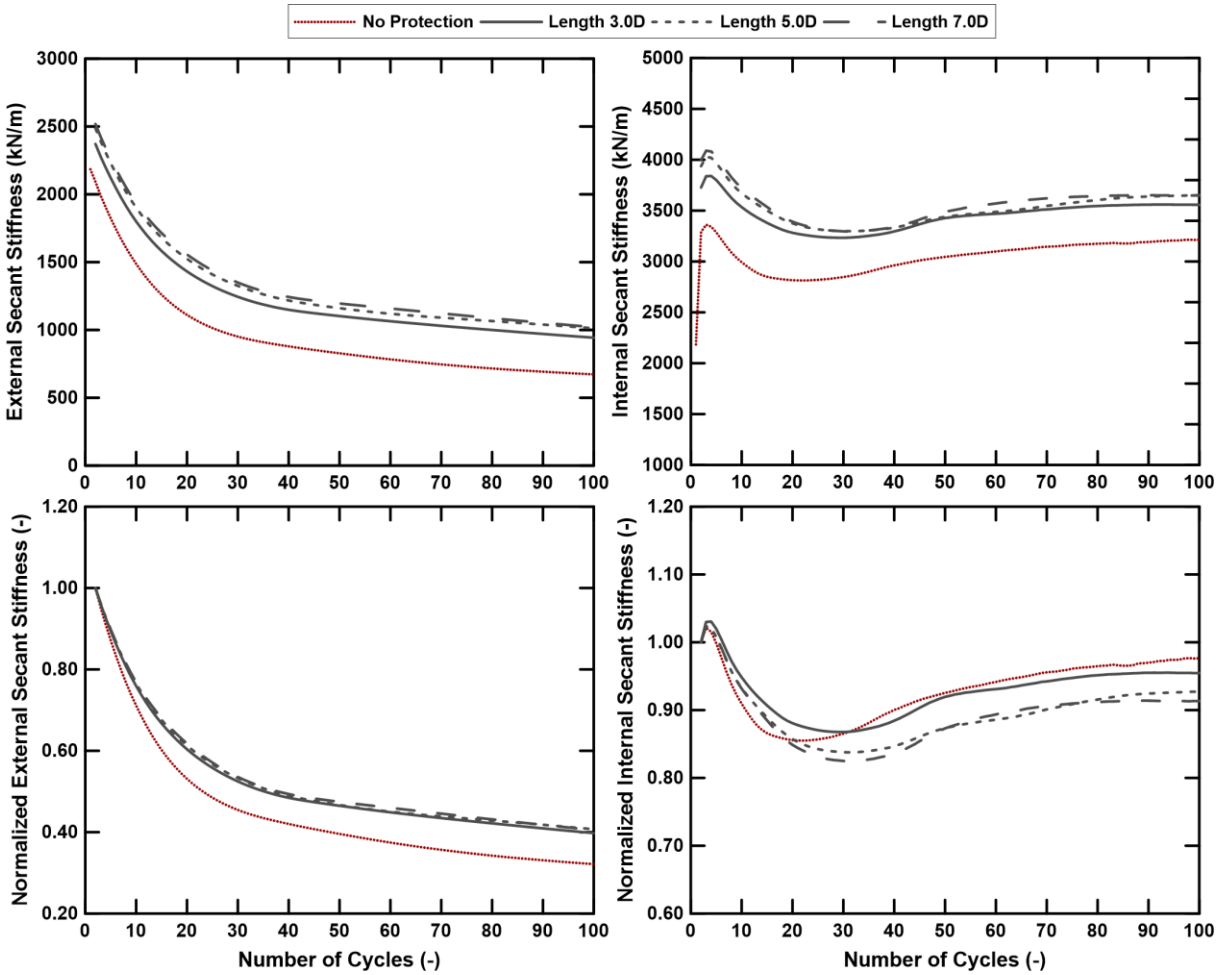

Figure 4.37 Evolution of the external and internal secant stiffness (both absolute values and normalized to the second cycle) for the no-protection case and for three different scour protection lengths.

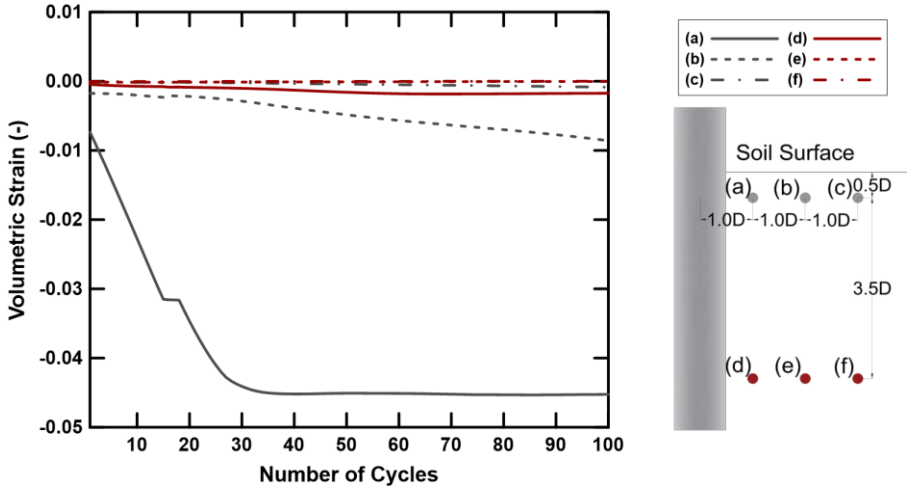

Figure 4.38 Evolution of the volumetric strains with respect to the number of cycles for the Pile_1 (not-protected case) in three different radial positions (1.0, 2.0 & 3.0D) for two depths (0.5 & 4.0D).

In Figure 4.38 the evolution of the volumetric strains with respect to the number of cycles for the no scour protection case is presented at three different radial positions (1.0, 2.0 & 3.0D from the pile axis) for two depths (0.5 & 4.0D). At the shallow points (z=0.5D) intense reduction is observed in the volumetric strain only to the point closest to the pile (r=1.0D) implying soil densification, while the intermediate point (r=2.0D) experiences only a small reduction in the whole range of the 100 cycles. The further point (r=3.0D) is almost unaffected, showing the minimum length of the scour protection is

larger than the influence zone. This observation explains why the increase of the scour protection length had no actual contribution in the stiffness of the system, as the area covered by the minimum length already exceeds the soil zone that dictates the pile behavior. In the deepest points (z=4.0D), it is shown that the closest point to the pile is affected more, though in general much smaller volumetric reduction occurs close to the pile end compared to the one at the pile head.

4.3.2.2 Scour Protection's Thickness Effect on the Pile Behavior

In Figure 4.39, the load-displacements curves for the no-protection case and for three different overburden pressures (15 kPa, 20 kPa & 25 kPa) are presented. Note that in all analyses, a 5D-long protective layer has been applied. As it can be seen, the increase of the protection layer's thickness and hence of the overburden pressure has a positive influence in the monopile's response under cyclic loading, as the deformations are reduced significantly. The mechanism responsible for this behavior, that has already been described in the monotonic centrifuge tests, is the increase of the stress regime around the monopile due to the extra pressure, meaning that the soil is subjected to higher confining pressures and hence can offer higher resistance.

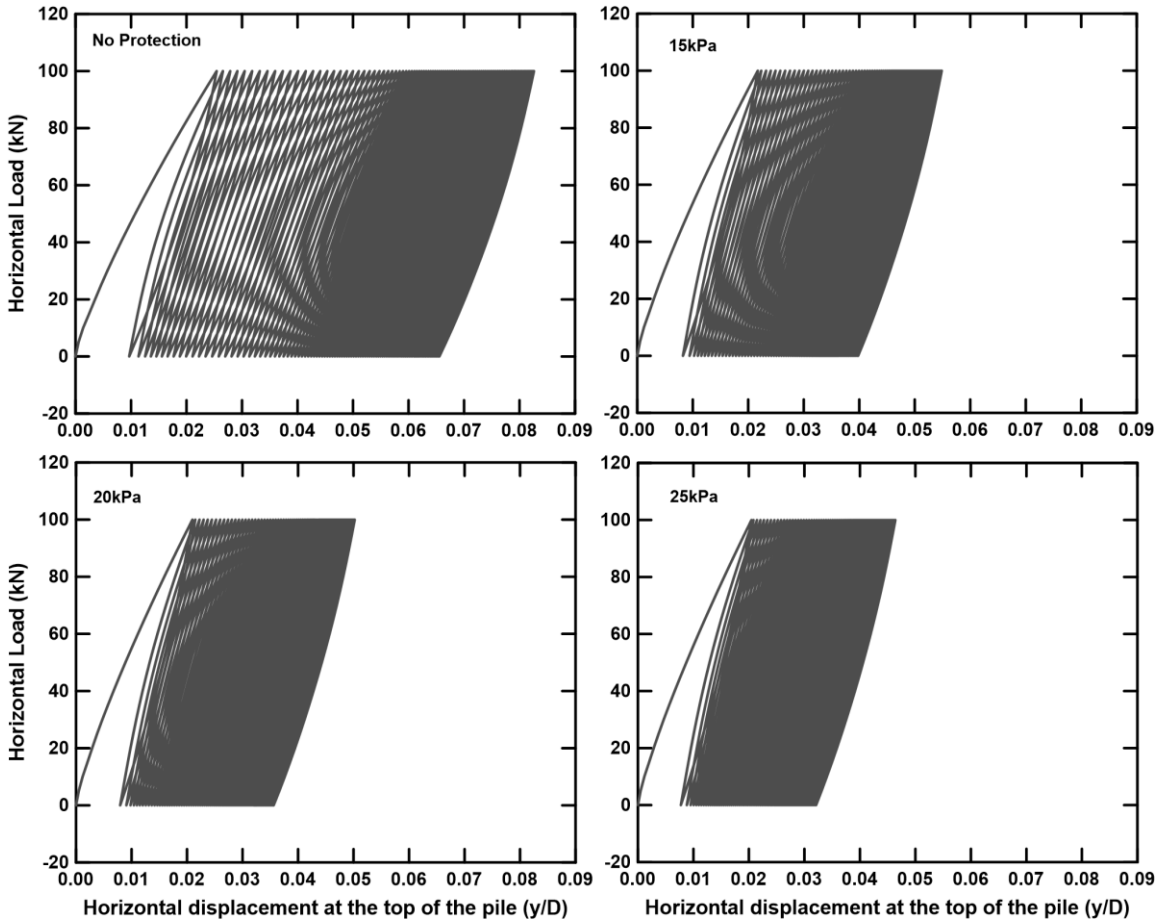

Figure 4.39 Load-displacements curves for the no-protection case and for three different protection overburden pressures.

A quantification of the effect of the overburden pressure in the pile's behavior can be made by Figure 4.40, in which the evolution of the residual and maximum displacements for the no-protection case and for three different overburden pressures is illustrated. As it is observed, the residual displacements are reduced considerably, when the protective layer is applied by at least 40%. However, the interesting part there is that the for a 5 kPa increase in the overburden pressure a reduction of 10% in the accumulated deformations is observed, both when comparing the cases 15 & 20 kPa, along with 20 & 25 kPa. Similar findings are extracted by the maximum displacements curves, in which though the aforementioned percentage is around 5.5%. In essence, that means that the increase of the overburden

pressures, either by increasing the thickness of the layer or by choosing a material with higher unit weight, can significantly improve the monopiles behavior. The same trends are observed in Figure 4.41, in which the evolution of the external and internal secant stiffness for the no-protection case and the three different overburden pressures is depicted. In absolute values, the increase of the pressure for 5 kPa at the end of the 100th cycle offers an increase of the external stiffness around 8% and for the internal stiffness approximately 4%.

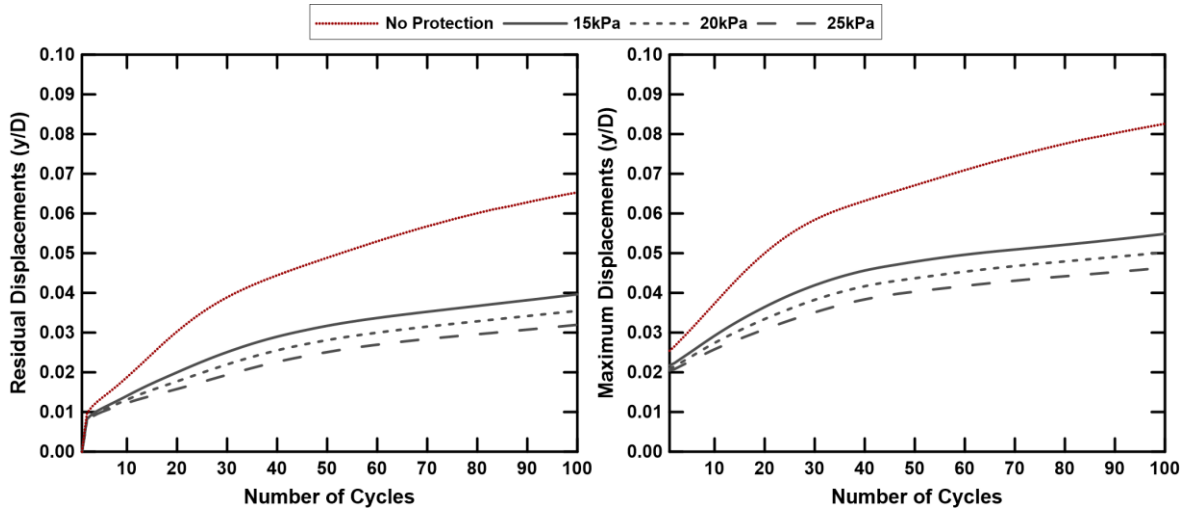

Figure 4.40 Evolution of the residual and maximum displacements for the no-protection case and for three different overburden pressures.

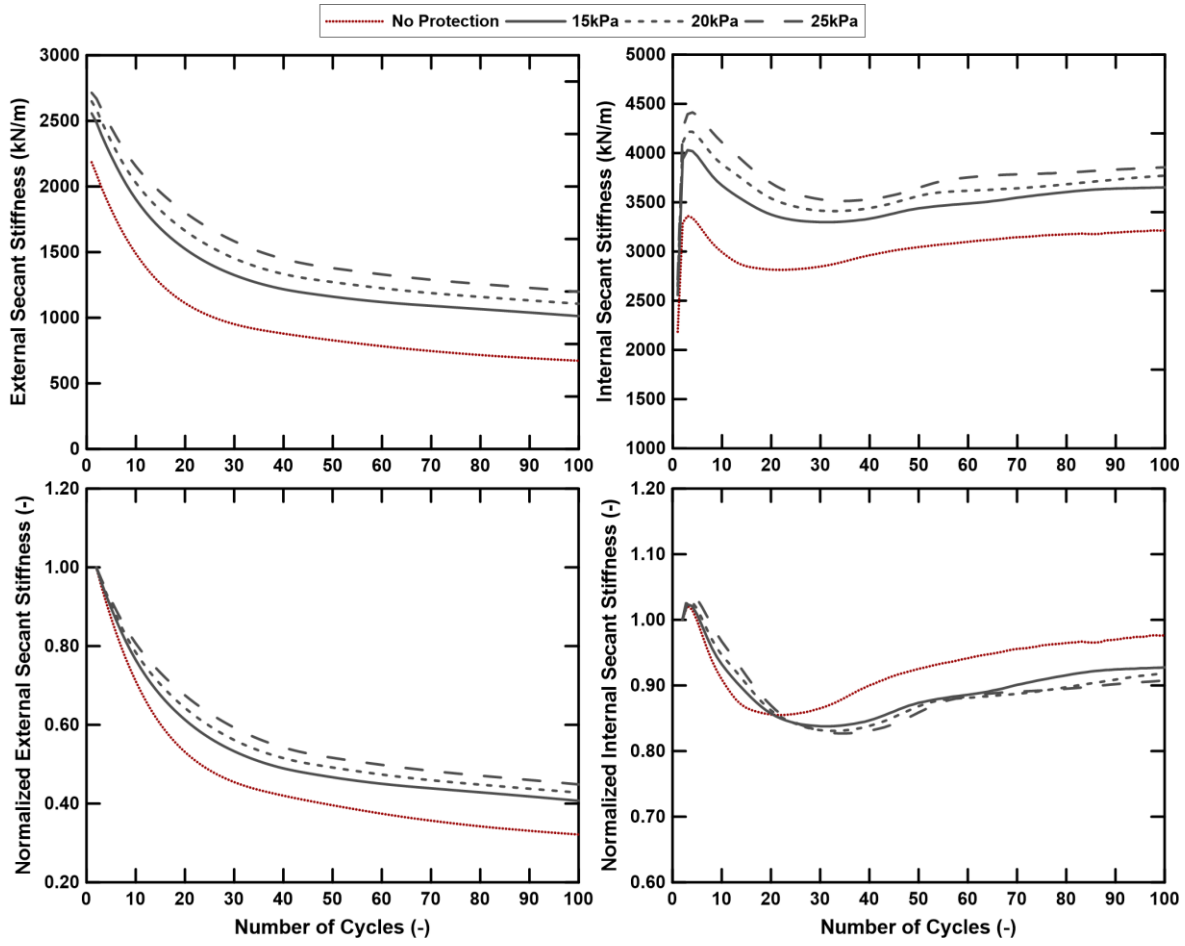

Figure 4.41 Evolution of the external and internal secant stiffness (both absolute values and normalized to the second cycle) for the no-protection case and for three different overburden pressures.

The general conclusion drawn by the numerical cyclic analyses regarding the scour protection layer is its large contribution in limiting the accumulated displacements, along with increasing the stiffness of the soil-pile system. Note that in the modern offshore windfarms, the general trend is to install beforehand a scour protection layer around all piles instead of risking a scour hole formation larger than predicted (which is highly unlikely to be accurate). Since this layer exists almost in all offshore monopiles, taking into account its influence in the pile response can result in reduction of the cost of each monopile, as it could lead to smaller diameters or embedded lengths.

An example is given in Figure 4.42, in which the load-displacements curves are presented for a pile embedded 5.0D deep into the soil, without any protection in the surface, and a pile embedded 4.5D deep into the soil, with a scour protection of 5.0D length and an added effective pressure of 15 kPa in the surface. It is observed that the pile with the smaller embedded length (case b), offers a stiffer response compared to the first pile (case a), which is embedded deeper but without scour protection layer. A better overview of this observation is given in Figure 4.43, where the evolution of the residual displacements with the number of cycles are presented for the two cases. Specifically, it is shown that lower deformations are accumulated for the pile with the scour protection layer and the smaller embedded length. Therefore, by adding a relatively cheap scour protection layer, the length of the pile can be reduced about 1.0 m, potentially lowering the total design cost, as less steel material is needed. It should be taken into account that modern practice in the windfarms includes scour protection layers for all the monopiles, meaning that incorporating its contribution in the stiffness of the system can make a considerable difference in the design. Note also that the vertical capacity of a typical monopile is significantly larger compared to the vertical loads that are applied due to the weight of the wind turbine and of the pile. Therefore, the diameter and the embedded length of the monopile are determined by the lateral resistance against the actions of the wind, waves and currents. Consequently, altering the pile geometry, does not pose a potential danger to the integrity of the monopile, as long as the lateral capacity provided is sufficient. Taking all these into account, it is proposed to further investigate the contribution of the scour protection layer to the behavior of the monopile, and use it as a means for a more economical, yet safe design.

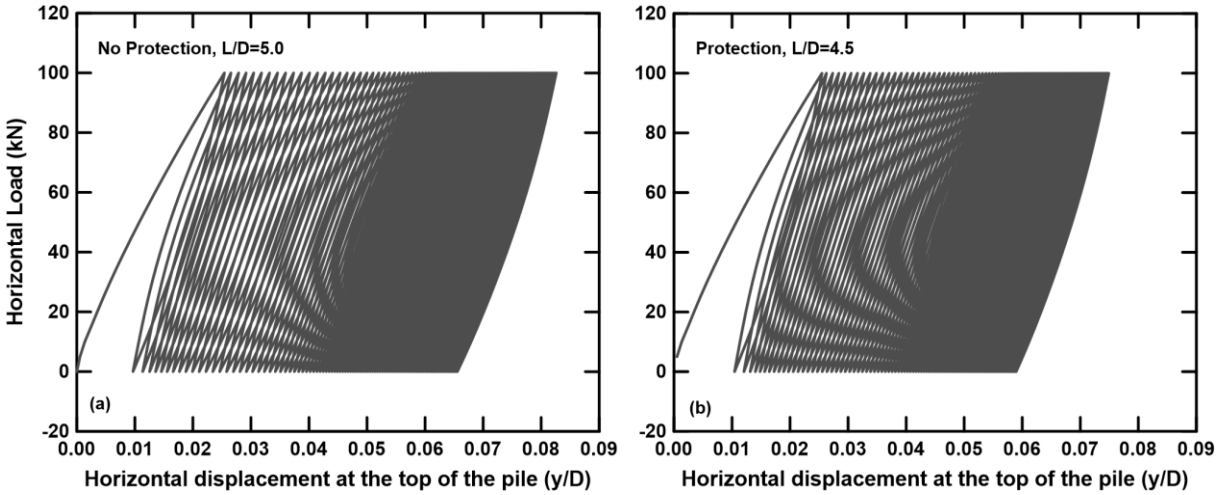

Figure 4.42 (a) Load-displacements curves for (a) a pile embedded 5.0D deep into the soil, without any protection in the surface and (b) a pile embedded 4.5D deep into the soil, with a scour protection of 5.0D length and added effective pressure 15 kPa in the surface.

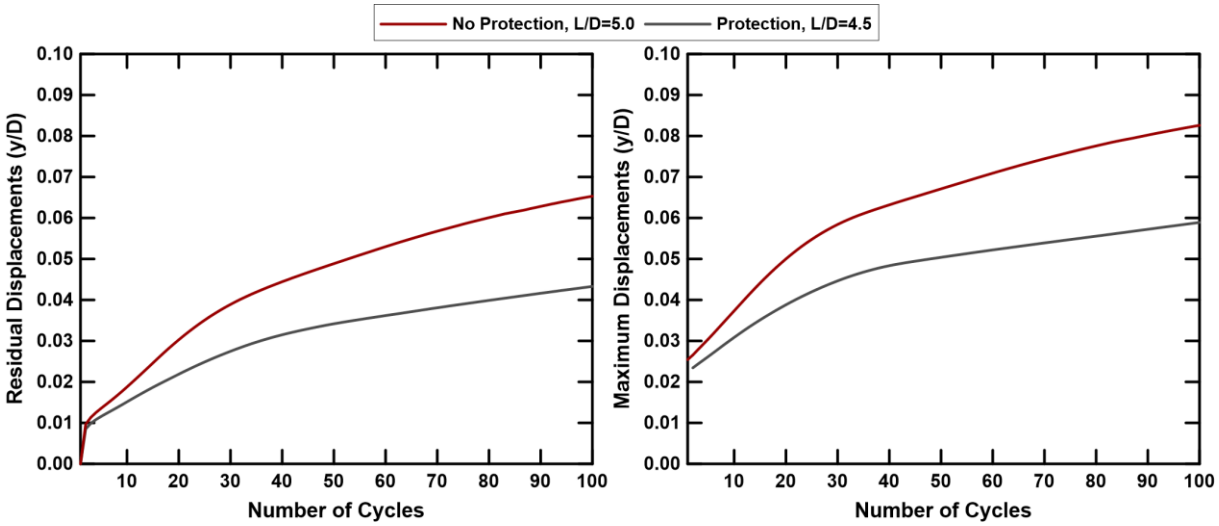

Figure 4.43 Fig. 15 Evolution of the residual displacements for Pile_1 (embedded 5.0D deep and the soil surface was not protected) and the Pile_7 (embedded 4.5D deep and the soil surface was protected with a scour protection of length 5.0D and added effective pressure 15 kPa).

Chapter 5

Conclusions

An experimental and numerical investigation of the behavior of a typical offshore monopile has been performed, with respect to scouring for both monotonic and cyclic loading. The results can be distinguished into three categories, the centrifuge monotonic section, the centrifuge cyclic one and the numerical cyclic section. The conclusion drawn by each category are presented below, followed by recommendations for future research.

5.1 Centrifuge Monotonic Experiments' Conclusions

The conclusions drawn by the set of centrifuge monotonic experiments are presented in this section. More specifically:

1. The increase of the vertical load seems to have a positive, yet almost negligible influence on the lateral capacity of dense sands. Note that the magnitude of the vertical loads investigated is far away from the axial monopile capacity.
2. Soil lateral capacity is significantly reduced by the increase of the scour depth for the same scouring type, as a 0.5D deeper scour hole can lead up to 35% reduction in the soil's resistance at the ULS. A dual mechanism is responsible for this behavior, as the embedded pile length is reduced due to the scour hole and simultaneously the overburden pressures are getting lower due to the soil removal, hence the soil strength is reduced and limited in a smaller area.
3. Scour width can highly dictate the scour effect in the soil-pile system capacity, as the local scour type can offer up to 30% larger resistance compared to the global case for the same depth. However, the distinction between global and local scour seems to be insufficient, as local narrow and local wide cases can differ up to 20% in the ULS. Therefore, it is highly recommended to model at least two different geometries for the local scour case, as in this thesis. The effect of the scour type can be attributed to the different overburden pressures, as removing a small inversed cone of soil will result in a smaller reduction on the confining pressures around the monopile and ultimately on the soil strength, compared to a whole soil layer removal, as in global case.
4. Scour depth is considered to be more crucial than the scour width, as it seems to lead in no-return states when it reaches a value of 2.0D, regardless of the scour type. However, for shallower formed holes, the type of scour can make the difference between structure's integrity and potential failure. Therefore, it is concluded that the scour is a complex phenomenon, and its exact geometry should be taken into account during design.
5. Predicting accurately the scour hole's geometry is highly unlikely, as stated in the literature. Therefore, a valid design against scour should include a series of scenarios with different combinations of scour types and depths, within realistic ranges.
6. A typical scour protection layer can offer extra soil capacity up to 40% in the ULS, which is attributed to the increase of the overburden pressures around the monopile.
7. Piecewise polynomial method seems to be an efficient way to extract soil pressures from discrete bending moment profiles. One the same context, the pile deflection can be extracted sufficiently by applying a 7^{th} order polynomial to the discrete moment profile.

8. API method for extracting the p-y curves highly overestimates the initial response of the soil and its ultimate capacity, leading to non-realistic curves. The failure of the method to capture sufficiently the soil behavior is attributed to the pile rigidity, as the API regulations have been based on long slender piles. A specific weakness of the method is considered to be the assumption of zero shear stress at the tip of the pile, while the experimental data indicate that considerable shear develops at the bottom.

9. The effect of the scour in the p-y curves is profound in the shallower depths, as the local scour formation can lead to stiffer response, up to 40% compared to the global case. In addition to this, the local narrow and the local wide scour diverge up to 20% in the upper soil layers (narrow scour is more favorable). However, in larger depths, the p-y curves are almost unaffected by the scour formation.

5.2 Centrifuge Cyclic Experiments' Conclusions

The conclusions drawn by the set of centrifuge cyclic experiments are presented in this section. More specifically:

1. "One-way" loading proved to be more critical compared to the "two-way" symmetrical one, when the same amplitude is applied to both cases, as the residual displacements were 45% larger in the "one-way" load pattern. In essence, the accumulation of displacements occurs in a lower rate for the "two-way" loading as the change in load direction allows for larger compensation of the maximum soil deformation in each cycle.

2. "Two-way" non-symmetrical experiment was the most unfavorable, since the highest maximum and residual displacement observed in that test. Note that its amplitude was the larger compared to the "one-way" and "two-way" symmetrical (150 kN against 100 kN respectively). Therefore, the larger deformations are most likely attributed to the degradation of the soil structure, due to the largest amplitude, despite the fact that the load effects are not concentrated only in one side of the pile (as in "one-way" load pattern), but in the whole vicinity of the mono-pile ("two-way" load pattern).

3. The different response of the pile due to "one-way" and "two-way" cyclic loading is attributed to the dissipation of energy, calculated by the area of the hysteretic loops (load to shear strain γ). In general, dissipation of energy corresponds to destruction of the soil structure and accumulation of plastic deformations. In "one-way" loading, the loop is relatively small, as the load does not change its direction, leading to low dissipation of energy and hence limited plastification of the soil. A "two-way" loading with the same maximum load as in "one-way" case corresponds to a larger hysteretic loop, as it is extended in a wider range of load, leading to larger plastic deformations.

4. The load history of the sample had a considerable effect in the pile's response under cyclic loading. Specifically, if the current amplitude of the load subjected to the pile is lower than the maximum one that the monopile has experienced, a stiff response is observed, with very low accumulated displacements. On the contrary though, if the current load is the maximum one that has been applied to the pile, then the previous history seems to have no influence in the soil-pile system's response.

5. The internal secant stiffness (load over the displacement differences of each cycle), has been normalized for all experiments to the second cycle, after the monotonic load. At the end of the 100th cycle, the normalized stiffness has increased for all the experiments from a range of 20 to 40%. However, in the "one-way" case a sudden increase is observed in the first 10 cycle and then the stiffness gradually drops, while the "two-way" experiments both present a slight, but yet continuous increase of the stiffness in the whole range of experiment.

6. The difference in the stiffness evolution with respect to the load pattern is attributed to the fact that the "one-way" loading concentrates its energy to the one side of the pile, densifying the soil in fast rate. Consequently, it reaches in a few cycle a very dense state, followed by dilation effects, explaining the decrease in the stiffness. Note that when the soil is in a state to dilate, loosening of the grains is occurring, which corresponds to increase of the soil volume and hence larger pressures

to the pile. Therefore, the tendency for dilation will initially highly increase the stiffness of the system before it will gradually drop, as observed in the equivalent experiment. In the "two-way" loading the energy is concentrated to the whole pile's vicinity, densifying the soil uniformly in a smaller rate. The grains are packed in a denser state, but they do not reach a crucial density, after which loosening would occur, as no dilation effects are observed, up to the 100th cycle.

5.3 Numerical Cyclic Analyses' Conclusions

The conclusions drawn by the set of numerical cyclic analyses are presented in this section. More specifically:

1. A typical scour protection layer (meaning a length of 5.0D and equivalent pressure of 15 kPa) can lead up to 40% smaller residual displacements compared to the no-protection case for the same load pattern. The mechanism responsible for this behavior is the increase of the confining stresses of the soil due to the increase of the overburden pressures by the extra layer, leading to larger soil strength.
2. Scour protection lengths larger than 5.0D seem to not offer actual extra resistance, as the residual displacements remain almost the same. The minimum scour protection length found in the literature (3.0D) leads to 8% larger deformations compared to the most typical one (5.0D), meaning that the scour protection length is not a crucial parameter with respect to the stiffness of the soil.
3. Scour protection thickness, which corresponds to overburden pressure into the soil, has a higher influence on the pile response. Specifically, an increase to the pressure over the soil of 5 kPa lead to smaller deformations of about 10%, in the range of 15 kPa (typical value in the literature) to 25 kPa.
4. Similar findings have been observed in the internal secant stiffness, which was increased in a range of 15 to 25% for the different scenarios of the scour protection geometry. Again, the overburden pressure change had a larger influence in the stiffness, compared to the scour protection's length.

5.4 Recommendations

Recommendations for future research in the topic of scour formation and protection layers are presented in this section. More specifically:

1. The term "local scour" seems to be insufficient, as it cannot be described by a unique geometry. Therefore, further investigation of the local scour case is proposed, in which a parametrical series of analyses should be focused on the width of the local hole and the angle of the slopes.
2. An update of the existing p-y curves is considered a valid area of research, as their applicability on rigid piles cannot be characterized as satisfactory. Therefore, a distinction between slender and rigid piles could be incorporated in the p-y curves method. On the same context, it is proposed to add rotational springs in the existing methodology, as this is likely to better model the effects of the shear stresses developed in the bottom of the rigid piles.
3. Scour type's effect in the p-y curves can be taken into account by degrading the soil resistance in the shallower depths. The reduction rate and the influence area should be further investigated.
4. Scour protection can offer considerable increase in the soil-pile system's stiffness. A deeper investigation should be made in its nature and characteristics with respect not only to the prevention of scour formation, but also to the mechanical properties of the soil around the monopile.
5. Cyclic tests should be performed for a larger number of cycles, for "one-way" and "two-way" loading types. It is proposed to have a series of tests with the same amplitude but different R_H ratios (minimum over maximum load).
6. Hypoplastic model should be deeper evaluated in capturing the hardening and softening of the soil during cyclic load. This evaluation should include a series of laboratory tests, including cyclic ones.

References

[1]. Abdel-Rahman, K., & Achmus, M. (2006). Numerical modelling of combined axial and lateral loading of vertical piles. In Numerical Methods in Geotechnical Engineering - 6th European Conference (pp. 575–581).

[2]. Achmus, M. (2010). Design of Axially and Laterally Loaded Piles for the Support of Offshore Wind Energy Converters. Indian Geotechnical Conference, 322–327.

[3]. Achmus, M., & Thieken, K. (2010). On the behavior of piles in non-cohesive soil under combined horizontal and vertical loading. Acta Geotechnica, 5(3), 199–210.

[4]. Achmus, M., Kuo, Y.-S., & Abdel-Rahman, K. (2009). Behavior of monopile foundations under cyclic lateral load TT. Computers and Geotechnics TA, 36(5), 725–735.

[5]. Alderlieste, E. a. (2011). Experimental modelling of lateral loads on large diameter mono-pile foundations in sand. Civil Engineering, (April).

[6]. Allersma, H. G. B. (1994). The University of Delft geotechnical centrifuge. International Conference Centrifuge 94, 47–52.

[7]. Anagnostopoulos, C., & Georgiadis, M. (1993). Interaction of Axial and Lateral Pile Responses. Journal of Geotechnical Engineering, 119(4), 793–798.

[8]. Annandale, G. W. (2006). Scour technology. McGraw-Hill.

[9]. API. (2007). Recommended Practice for Planning, Designing and Constructing Fixed Offshore Platforms — Working Stress Design. Api Recommended Practice, 24–WSD (December 2000), 242.

[10]. Arnold, M. (2008). Application of the Intergranular Strain Concept to the Hypoplastic Modelling of Non-Adhesive Interfaces. Interface, (1999), 1–6.

[11]. Atkinson, J. H., Richardson, D., & Stallebrass, S. E. (1990). Effect of recent stress history on the stiffness of overconsolidated soil. Géotechnique, 40(4), 531–540.

[12]. Azua Gonzalez, C. (2017). Dynamic Finite Element Analysis of Impact Pile Driving Centrifuge Tests. TU Delft.

[13]. Bauer, E. (1996). Calibration of a Comprehensive Hypoplastic Model for Granular Materials. Soils and Foundations, 36(1), 13–26.

[14]. Bennett, C. R., Lin, C., Parsons, R., & Han, J. (2009). Evaluation of behavior of a laterally loaded bridge pile group under scour conditions. In Structures Congress 2009: Don't Mess with Structural Engineers: Expanding Our Role.

[15]. Brinkgreve, R. B. J., Kumarswamy, S., & Swolfs, W. (2016). PLAXIS Manual, Delft, Netherlands.

[16]. Britta, B., Jan, D., Jürgen, G., F., R. M., & J., W. D. (2012). Response of Piles with Wings to Monotonic and Cyclic Lateral Loading in Sand. Journal of Geotechnical and Geoenvironmental Engineering, 138(3), 364–375.

[17]. Chang, C., & Whitman, R. (1988). Drained Permanent Deformation of Sand Due to Cyclic Loading. Journal of Geotechnical Engineering, 114(10), 1164–1180.

[18]. Chopra, A. K. (2006). Dynamics of structures: Theory and Applications to Earthquake Engineering (5th ed., Vol. 3).

[19]. Davisson, M., & Robinson, K. (1965). Bending and buckling of partially embedded piles. 6th International Conference on Case Histories in Geotechnical EngineeringInternational Conference on Soil Mechanics and Foundation Engineering, 243–246.

[20]. de Jager, R. R., Maghsoudloo, A., Askarinejad, A., & Molenkamp, F. (2017). Preliminary Results of Instrumented Laboratory Flow Slides. Procedia Engineering, 175, 212–219.

[21]. Depina, I., Hue Le, T. M., Eiksund, G., & Benz, T. (2015). Behavior of cyclically loaded monopile foundations for offshore wind turbines in heterogeneous sands. Computers and Geotechnics, 65, 266–277.

[22]. Det Norske Veritas. Design of Offshore Wind Turbine Structures. Technical Report, DNV; 2014. DNV-OS-J101.

[23]. Doherty, P., & Gavin, K. (2012). Laterally loaded monopile design for offshore wind farms. Proceedings of the Institution of Civil Engineers - Energy, 165(1), 7–17.

[24]. Dunnavant, T. W. (1986). Experimental and Analytical Investigation of the Behavior of Single Piles in Overconsolidated Clay Subjected to Cyclic Lateral Loads.

[25]. Garnier, J., Gaudin, C., Springman, S. M., Culligan, P. J., Goodings, D., Konig, D., Thorel, L. (2007). Catalogue of scaling laws and similitude questions in geotechnical centrifuge modelling. International Journal of Physical Modelling in Geotechnics, 7(3), 1–23.

[26]. Germanischer Lloyd. Guideline for the Certification of Offshore Wind Turbines; 2012, GL.

[27]. Goryunov, B. F. (1973). Analysis of piles subjected to the combined action of vertical and horizontal loads (discussion). Soil Mechanics and Foundation Engineering, 10(1), 10–13.

[28]. Gudehus, G. (1996). A comprehensive constitutive equation for granular materials. Soils and Foundations, 36(1), 1–12.

[29]. Gui, M. W., Bolton, M. D., Garnier, J., Corte, J. F., Bagge, G., Laue, J., & Renzi, R. (1998). Guidelines for cone penetration tests in sand. Proceedings of the International Conference on Centrifuge Modelling (Centrifuge '98), 155–160.

[30]. Hajialilue-Bonab, M., Levacher, D., Chazelas, J. L., & Kaynia, A. M. (2014). Experimental study on the dynamic behavior of laterally loaded single pile. Soil Dynamics and Earthquake Engineering, 66, 157–166.

[31]. Hald, T., Mørch, C., Jensen, L., Leblanc, C., & Ahle, K. (2009). Revisiting monopile design using p-y curves Results from full scale measurements on Horns Rev. European Wind Energy Conference.

[32]. Han, J., & Frost, J. D. (2000). Load-deflection response of transversely isotropic piles under lateral loads. International Journal for Numerical and Analytical Methods in Geomechanics, 24(5), 509–529.

[33]. Harris, J. M., & Whitehouse, R. S. (2017). Scour Development around Large-Diameter Monopiles in Cohesive Soils: Evidence from the Field. Journal of Waterway, Port, Coastal, and Ocean Engineering, 143(5), 04017022.

[34]. Heibaum, M. H. (2006). The use of geosynthetics in scour protection, 294, 294–297.

[35]. Hill, D. (2015). SUBSEA PROTECTION: Protection solutions against scouring.

[36]. Hjorth, P. (1975). Studies on the nature of local scour.

[37]. Hoffmans, G. J. C. M., & Verheij, H. J. (1997). Scour Manual. Rotterdam, Netherlands; Brookfield, VT: A.A. Balkema.

[38]. Hosny, M. M. (1995). Experimental Study of Local Scour Around Circular Bridge Piers in Cohesive Soils.

[39]. International Electrotechnical Commission. Wind turbines: Part 3: Design requirements for offshore wind turbines; 2009. IEC61400-3.

[40]. Jones, J. S., Kilgore, R. T., & Mistichelli, M. P. (1992). Effects of footing location on bridge pier scour. Journal of Hydraulic Engineering, 118(2), 280–290.

[41]. K. Rajagopal, & S. Karthigeyan. (2008). Influence of Combined Vertical and Lateral Loading on the Lateral Response of Piles. The 12th International Conference of International Association for Computer Methods and Advances in Geomechanics (IACMAG), (August 2016), 3272–3282.

[42]. Kallehave, D., Thilsted, C. L., & Troya, A. (2015). Observed variations of monopile foundation stiffness. Proceedings of the Third International Symposium on Frontiers in Offshore Geotechnics (ISFOG), 978–1.

[43]. Karthigeyan, S., Ramakrishna, V. V. G. S. T., & Rajagopal, K. (2006). Influence of vertical load on the lateral response of piles in sand. Computers and Geotechnics, 33(2), 121–131.

[44]. Kishore, Y. N., Rao, S. N., & Mani, J. S. (2009). The behavior of laterally loaded piles subjected to scour in marine environment. KSCE Journal of Civil Engineering, 13(6), 403–408.

[45]. Klein, G. K., & Karavaev, V. N. (1979). Design of reinforced-concrete piles for vertical and horizontal loading. Soil Mechanics and Foundation Engineering, 16(6), 321–324.

[46]. Kolymbas, D. (1985). A generalized hypoelastic constitutive model. Proc. XI Int. Conf. Soil Mechanics and Foundation Engineering, 5, 2626.

[47]. Kramer, S. L., & Heavey, E. J. (1988). Lateral load analysis of nonlinear piles. Journal of Geotechnical Engineering, 114(9).

[48]. Kumar Jain, N., Ranjan, G., & Ramasamy, G. (1987). Effect of Vertical Load on Flexural Behaviour of Piles. Geotechnical Engineering, 18(2), 185–204.

[49]. Kuo, Y.-S., & Achmus, M. (2008). Practical Design Considerations of Monopile Foundations with Respect to Scour.

[50]. LeBlanc, C., Houlsby, G. T., & Byrne, B. W. (2010). Response of stiff piles in sand to long-term cyclic lateral loading. Geotechnique, 60(2), 79–90.

[51]. Lee, J., Kyung, D., Hong, J., & Kim, D. (2011). Experimental Investigation of laterally loaded piles in sand under multilayered conditions. Soils and Foundations, Japenese Geotechnical Society, 51(5), 915–927.

[52]. Lengkeek, W., Didderen, K., Driessen, F., Coolen, J. W. P., Bos, O. G., Vergouwen, S., & Raaijmakers, T. (2017). Eco-friendly design of scour protection: Potential enhancement of ecological functioning in designs for scour protection in offshore wind farms, 98.

[53]. Li, F., Han, J., & Lin, C. (2013). Effect of Scour on the Behavior of Laterally Loaded Single Piles in Marine Clay. Marine Georesources and Geotechnology, 31(3), 271–289.

[54]. Li, W., Gavin, K., Igoe, D., & Doherty, P. (2014). Review of design models for lateral cyclic loading of monopiles in sand. In Physical Modelling in Geotechnics - Proceedings of the 8th International Conference on Physical Modelling in Geotechnics 2014, ICPMG 2014 (Vol. 2, pp. 819–825).

[55]. Li, Y., Chen, X., Fan, S., Briaud, J., Chen, H. C., & a, T. (2009). OTC 19906 Is Scour Important for Pile Foundation Design in Deepwater Offshore Technology Conference.

[56]. Li, Z., Haigh, S. K., & Bolton, M. D. (2010). Centrifuge modelling of mono-pile under cyclic lateral loads. 7th International Conference on Physical Modelling in Geotechnics, 2, 965–970.

[57]. Lin, C., Bennett, C., Han, J., & Parsons, R. L. (2010). Scour effects on the response of laterally loaded piles considering stress history of sand. Computers and Geotechnics, 37(7–8), 1008–1014.

[58]. Little, R. L., & Briaud, J.-L. (1988). Full scale cyclic lateral load tests on six single piles in sand. Miscellaneous Paper GL-88-2.

[59]. Madhav, M., & Sarma, C. (1982). Analysis of Axially and Laterally Loaded Long Piles. Proceedings of the 2nd International Conference on Offshore Piling.

[60]. Mašín, D. (2011). PLAXIS implementation of hypoplasticity, 30.

[61]. Mašín, D. (2017). Calibration of sand hypoplastic model on Geba sand data. Internal Report Issued for Royal IHC.

[62]. Matutano, C., Negro, V., López-Gutiérrez, J.-S., & Esteban, M. D. (2013). Scour prediction and scour protections in offshore wind farms. Renewable Energy, 57(Supplement C), 358–365.

[63]. McClelland, B., & Focht, J. A. (1980). Soil modulus for laterally loaded piles. International Journal of Rock Mechanics and Mining Sciences & Geomechanics Abstracts International Journal of Rock Mechanics and Mining Sciences & Geomechanics Abstracts, 17(1), A12.

[64]. McGann, C. R., Arduino, P., & Mackenzie-Helnwein, P. (2011). Applicability of Conventional p-y Relations to the Analysis of Piles in Laterally Spreading Soil. Journal of Geotechnical and Geoenvironmental Engineering, 137(6), 557–567.

[65]. Meidani, M., Shafiee, A., Habibagahi, G., Jafari, M. K., Mohri, Y., Ghahramani, A., & C S Chang, A. (2008). Granule shape effect on the shear modulus and damping ratio of mixed gravel and clay. Iranian Journal of Science and Technology (Vol. 32).

[66]. Meyerhof, G. G., & Sastry, V. V. R. N. (1985). Bearing Capacity of Rigid Piles Under Eccentric and Inclined Loads. Canadian Geotechnical Journal, 22(1), 267–276.

[67]. Mezazigh, S., & Levacher, D. (1998). Laterally loaded piles in sand: slope effect on P-Y reaction curves. Canadian Geotechnical Journal, 35(3), 433–441.

[68]. Mostafa, Y. E. (2012). Effect of Local and Global Scour on Lateral Response of Single Piles in Different Soil Conditions. Engineering, 04(06), 297–306.

[69]. Murchison, J. M., & O'Neill, M. W. (1984). Evaluation of p-y relationships in cohesionless soils. In Analysis and Design of Pile Foundations. Proceedings of a Symposium in conjunction with the ASCE National Convention (pp. 174–191).

[70]. Niemunis, A., & Herle, I. (1997). Hypoplastic model for cohesionless soils with elastic strain range. Mechanics of Cohesive-Frictional Materials, 2(4), 279–299.

[71]. Peder Hyldal Sørensen, S., & Bo Ibsen, L. (2013). Assessment of foundation design for offshore monopiles unprotected against scour. Ocean Engineering, 63, 17–25.

[72]. Prendergast, L. J., & Gavin, K. (2014). A review of bridge scour monitoring techniques. Journal of Rock Mechanics and Geotechnical Engineering, 6(2), 138–149.

[73]. Prendergast, L. J., Reale, C., & Gavin, K. (2018). Probabilistic examination of the change in eigenfrequencies of an offshore wind turbine under progressive scour incorporating soil spatial variability. Marine Structures, 57, 87–104.

[74]. Prendergast, L., Gavin, K., & Doherty, P. (2015). An investigation into the effect of scour on the natural frequency of an offshore wind turbine. Ocean Engineering, 101(0), 1–11.

[75]. Puzrin, A. M., & Burland, J. B. (1998). Non-linear model of small-strain behaviour of soils. Géotechnique, 48(2), 217–233.

[76]. Qi, W. G., Gao, F. P., Randolph, M. F., & Lehane, B. M. (2016). Scour effects on p–y curves for shallowly embedded piles in sand. Géotechnique, 66(8), 648–660.

[77]. Reddy, A. S., & Ramasamy, G. (1973). Analysis of an axially and laterally loaded tapered pile in sand. Soils and Foundations, 13(4), 15–27.

[78]. Reese, L. C., & Matlock, H. (1956). Non-dimensional solutions for laterally-loaded piles with soil modulus assumed proportional to depth. Dallas, Tex.: Association of Drilled Shaft Contractors.

[79]. Reese, L. C., Cox, W. R., & Koop, F. D. (1974). Analysis of Laterally Loaded Piles in Sand. Offshore Technology in Civil Engineering: Hall of Fame Papers from the Early Years, 95–105.

[80]. Reese, L. C., Wang, S., & Long, J. (1989). Scour from cyclic lateral loading of piles. Offshore Technology Conference.

[81]. Reese, L., & Welch, R. C. (1975). Lateral Loadings of Deep Foundations in Stiff Clay. Journal of Geotechnical Engineering, 101(7), 633–649.

[82]. Remaud, D. (1999). Pieux sous charges latérales: étude expérimentale de l'effet de groupe. Confrontation.

[83]. Robertson, I. N., Riggs, H. R., Yim, S. C., & Young, Y. L. (2007). Lessons from Hurricane Katrina Storm Surge on Bridges and Buildings. Journal of Waterway, Port, Coastal, and Ocean Engineering, 133(6), 463–483.

[84]. Shakhirev, V. B., & Yanyshev, G. S. (1969). Calculation of the joint effect of vertical and horizontal loads on single piles. Transactions of the Bashkir Scientific-Research Institute of Construction.

[85]. Soulsby, R. (2004). The Mechanics of Scour in the Marine Environment. Coastal Engineering, 51(1), 101–102.

[86]. Sumer, B. M., & Fredsøe, J. (2012). The mechanics of scour in the marine environment. Advanced Series on Ocean Engineering, 17.

[87]. Sumer, B. M., Fredsøe, J., & Christiansen, N. (1992). Scour Around Vertical Pile in Waves. Journal of Waterway, Port, Coastal, and Ocean Engineering, 118(1), 15–31.

[88]. Taheri, O., Moayed, R. Z., & Nozari, M. (2015). Lateral Soil-Pile Stiffness Subjected to Vertical and Lateral Loading Lateral. Journal of Geotechnical and Transportation Engineering, 1(2), 30–37.

[89]. Tokyo Sokki Kenkyujo. (2018). Strain Gauge Product Information. Retrieved from http://www.tml.jp/e/product/strain_gauge/index.html

[90]. Trochanis, A. M., Bielak, J., & Christiano, P. (1991). Three-dimensional nonlinear study of piles. Journal of Geotechnical Engineering, 117(3), 429–447.

[91]. Uesugi, M., Kishida, H., & Tsubakihara, Y. (1989). Friction between sand and steel under repeated loading. Soils and Foundations, 29(3), 127–137.

[92]. Verdure, L., Garnier, J., & Levacher, D. (2003). Lateral cyclic loading of single piles in sand.

[93]. von Wolffersdorff, P.-A. (1996). Hypoplastic relation for granular materials with a predefined limit state surface. Mechanics of Cohesive-Frictional Materials, 1(3), 251–271.

[94]. Wang, J., & Qi, C. (2008). P-y curves of piles in saturated degradation sands with residual pore water pressures. In Proceedings of the International Offshore and Polar Engineering Conference (pp. 690–697).

[95]. Wentian, F. (1986). Analysis of Slender Piles under Simultaneous Axial and Transverse Loading. Journal of Southwest Jiaotong University, 1.

[96]. Whitehouse, R. J. S. (1997). Scour at marine structures: a manual for practical applications. Scour at marine structures: a manual for practical applications.

[97]. Whitehouse, R. J. S. (2006). Scour at coastal structures. In 3rd Int. Conf. on Scour and Erosion (pp. 52–59). Amsterdam, Curnet, Gouda, Netherlands.

[98]. Whitehouse, R. J. S., Harris, J. M., Sutherland, J., & Rees, J. (2011). The nature of scour development and scour protection at offshore windfarm foundations. Marine Pollution Bulletin, 62(1), 73–88.

[99]. Wilson, D. W. (1998). Soil-Pile-Superstructure Interaction in Liquefying Sand and Soft Clay. Transportation Research Record, 1569(September), 190.

[100]. Wind Europe. (2017). Wind in power 2017_Annual combined onshore and offshore wind energy statistics.

[101]. Yang, K., & Liang, R. (2006). Methods for deriving p-y curves from instrumented lateral load tests. Geotechnical Testing Journal, 30(1), 31–38.

[102]. Zaaijer, M. B. (2006). Foundation modelling to assess dynamic behavior of offshore wind turbines. Applied Ocean Research, 28(1), 45–57.

Appendix

A. Centrifuge's Scaling Laws

The centrifuge modelling is based in achieving the same stress field in the model and the prototype, by increasing the gravity level in the model. More specifically, through rotating, the centrifuge carrier (where the sample is placed) is subjected in an acceleration of N times the field gravity (g). The vertical stresses are then calculated as expressed in Eq. (24).

$$\sigma_m = \rho N g z = \sigma_p \qquad \textit{Eq. (24)}$$

Based on the aforementioned equation, all the parameters of the model, such as its dimension, the load etc. can be extracted into the prototype magnitude. Correlating the model and the prototype is based on a series of scaling laws by Garnier et al. (2007). These are presented briefly in the following table:

Appendix Table 1 Scaling Laws for the model and prototype correlation

Parameter	***Model/Prototype***
Time	1/N
Frequency	N
Displacement	1/N
Velocity	1
Acceleration	N
Length	1/N
Area	$1/N^2$
Volume	$1/N^3$
Mass	$1/N^3$
Force	$1/N^2$
Strain	-
Bending Moment	$1/N^3$

As already mentioned, in the certain project the acceleration of the centrifuge was 100g. Therefore, the value N is equal to 100 and all the measurements from the centrifuge were extracted to the prototype model through the aforementioned equations.

B. Experimental Sequence Investigation

The scour holes in the samples inserted in the centrifuge has been formed in 1g conditions, as this enabled for a faster execution of each experiment. However, it would be more realistic to excavate the scour hole at 100g, as this simulates the natural phenomenon more accurately. Removing the soil in 1g and 100g conditions has an impact in the magnitude of the overburden pressure reduction, which is more profound when the sample is accelerated in the centrifuge. To investigate whether this detail can influence the outcome of the centrifuge experiments, two different scenarios have been studied in numerical model of PLAXIS 3D (section 3.2). In the first scenario (1g) the model has been created including a global scour formation in the initial phase. Note that in the initial phase, PLAXIS software calculates the original stress regime of the model. Therefore, in this way the possible influence of the removed soil (due to the simulation of the global scour) in soil strength and stiffness is ignored, as the previous stress history is not modelled. In the second scenario (100g) a different sequence is followed. Specifically, in the initial phase, the whole soil model is inserted (without any scour) and the field stress is calculated accordingly. Then, an extra phase is modelled, in which the scour hole formation takes place. Therefore, the stress history is taken into account in the second model. In both scenarios, a

prescribed displacement is subjected to the pile and the load-displacement curves are extracted for two different scour depths, 1.5D and 2.0D for global type (Appendix Figure 1). It is evident that a different path is given by PLAXIS 3D analyses for the 1.0g and 100g conditions for the same scour depth, meaning that the sequence of the actions performed in the centrifuge may affect the results. However, the maximum difference is limited to 10% (with the 100g scenario offering larger lateral resistance comparing to the 1g scenario) and around the ULS the same value is about 6%. Consequently, it seems valid to perform the experiments similar to the first scenario, meaning that the scour formation is executed at 1g conditions, before the sample is accelerated in the centrifuge, knowing that the possible error around the ULS area is in satisfactory limits.

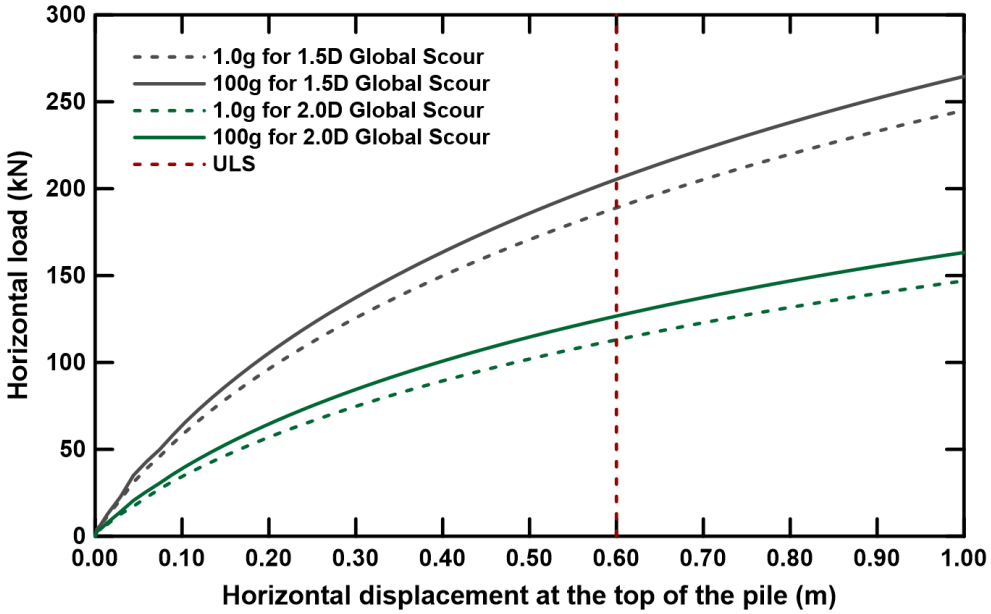

Appendix Figure 1 Load-displacement curves for global scour formation at 1g and 100g for two scouring depths, 1.5D and 2.0D

C. Intergranular Strain Concept

Intergranular strain concept was introduced by Niemunis & Herle (1997) to improve the hypoplastic model's performance in the small-strain stiffness. The initial model by von Wolffersdorff (1996) led to excessive deformations, when small-strain behavior was simulated, rendering the hypoplasticity at the time incapable of performing cyclic analyses. However, the extended model of the Niemunis & Herle (1997), by the addition of five extra parameters, offered a realistic approach in the simulation of small-strain tests.

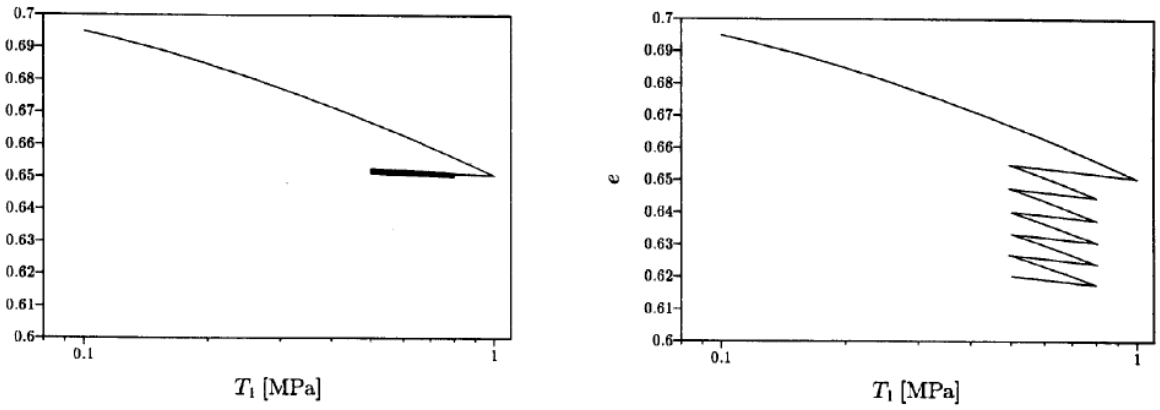

Appendix Figure 2 Oedometric compression (left: extended model, right: initial model) (Niemunis & Herle 1997)

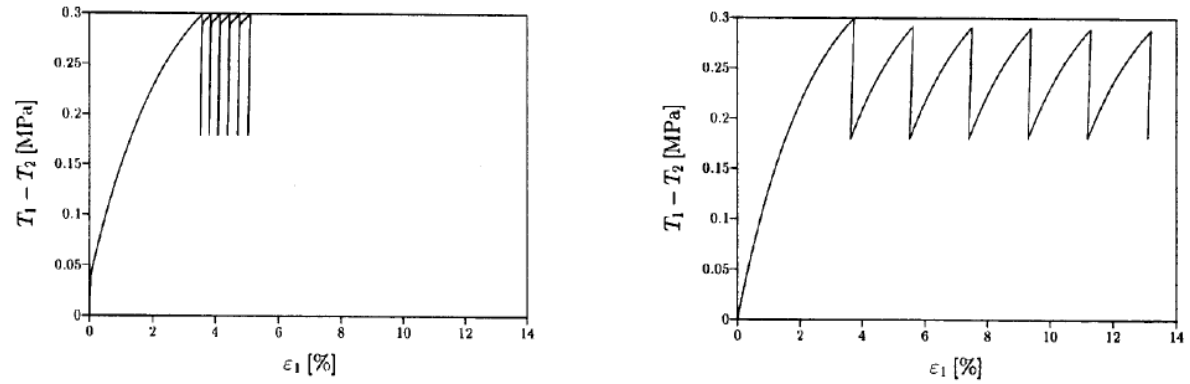

Appendix Figure 3 Drained triaxial compression with the same deviatoric stress cycles (left: extended model, right: initial model) (Niemunis & Herle 1997)

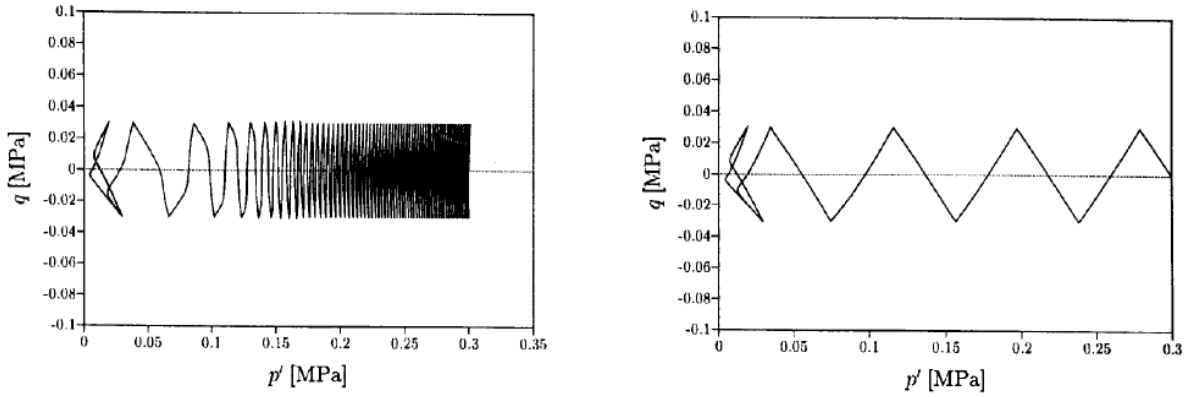

Appendix Figure 4 Undrained triaxial compression with symmetric deviatoric stress cycles (left: extended model, right: initial model) (Niemunis & Herle 1997)

In the figures above (Appendix Figures 2, 3 & 4), three standard laboratory tests are presented (oedometric compression, drained & undrained triaxial compression) both for the initial model (von Wolffersdorff 1996) and the extended one (Niemunis & Herle 1997). It is clearly observed that the initial model over predicts the accumulation of deformations, under the effect of cyclic loading, as in a very small number of cycles, excessive strains occur. On the other hand, the extended model with the addition of the ISC, produces more realistic curves with considerably smaller strains. However, in order to have a valid evaluation of the extended model's efficiency, a comparison between experimental laboratory tests and numerical simulated ones should be done. In Appendix Figure 5, a monotonic and a cyclic test for limited number of cycles without shear stress reversal ("one-way" cyclic loading) are presented, both for experimental tests (Uesugi et al. 1989) and numerical ones, performed in the extended PLAXIS model and presented by Arnold (2008). The same data is also given in Appendix Figure 6 for a monotonic and a cyclic test for limited number of cycles with shear stress reversal ("two-way" cyclic loading, again both for experimental tests (Uesugi et al. 1989) and numerical ones (Arnold 2008). A reasonable match is observed between the experimental and the numerical model, both for the monotonic and the cyclic approach. Small deviations are observed in the exact magnitude and the shape of the cyclic curves at the points of changing the load direction, but the main trend is captured sufficiently good. The conclusion drawn therefore is that the extended model seems to simulate accurately enough the cyclic behavior of the soil. Note though that the cyclic tests presented are limited in a very small number of cycles, not allowing for a more robust inference.

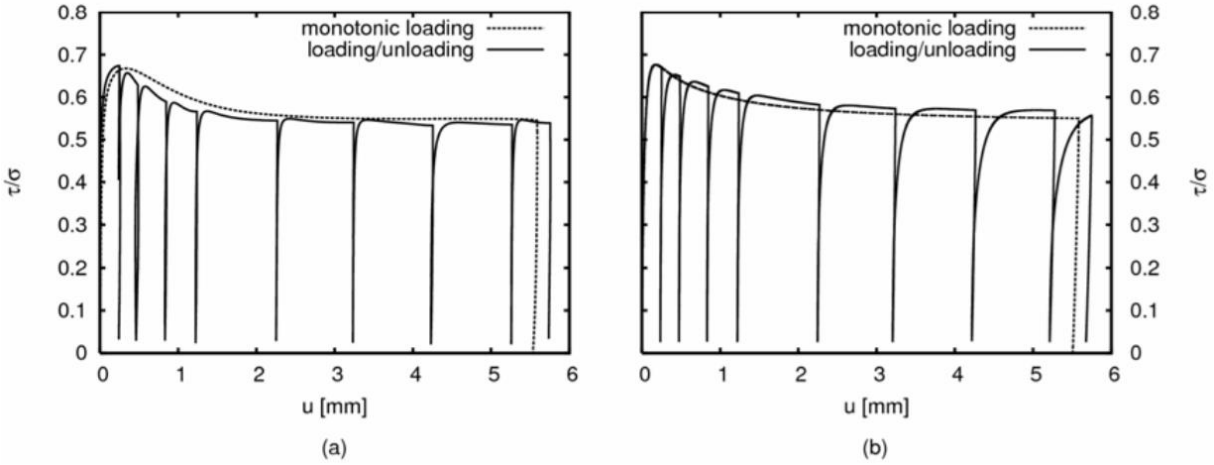

Appendix Figure 5 Cyclic tests without shear stress reversal (a) Test results by Uesugi et al. (1989)*, (b) Numerical simulation by Arnold (2008)*

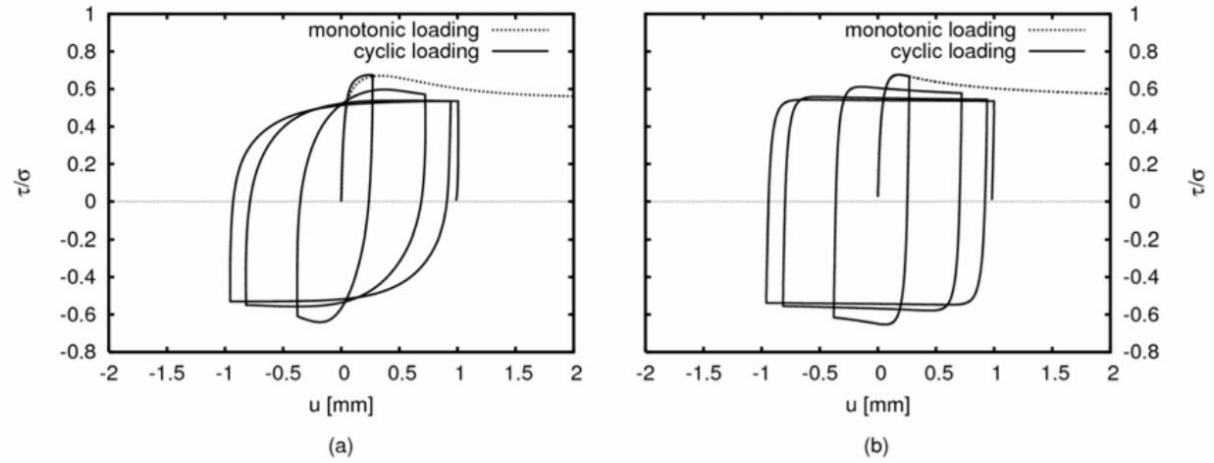

Appendix Figure 6 Cyclic tests with shear stress reversal, (a) Test results by Uesugi et al. (1989)*,(b) Numerical simulation by Arnold (2008)*

D. Model Calibration

As stated, the numerical model calibration has been based on the work of Dr. David Mašín for the Geba sand. The data of the laboratory tests he has performed after the request of the Royal IHC is confidential, so it cannot be presented in this thesis. The parameters of the calibration performed by Mašín (2017) have been set to the PLAXIS 3D model. However, an exact match could not be captured between the numerical and the physical modelling. Therefore, a second calibration has been executed by the author, based on the centrifuge experiments, both for monotonic tests and the cyclic ones. In total, 12 monotonic calibration analyses have been conducted for the monotonic match and 15 for the calibration of the cyclic tests results. The combination of the parameters that fitted best the centrifuge experiments has been chosen, as presented in 3.2.3. Note that the soil parameters of the model with physical meaning, the internal friction angle φ and the three states of void ratio (maximum, critical and minimum), have been kept the same as in David Mašín's calibration. Specifically, these values have a unique value for a specific sand, despite the nature of the problem. On the contrary, the hypoplastic model contains a lot of parameters that have not a very straightforward physical meaning, so it was considered valid to calibrate the model by running parametrical analyses based on this set of analyses (n, a, β, m_R, m_T, R_{max}, β_r, χ). The outcome of the calibration is presented in the two following graphs, Appendix Figures 7 & 8.

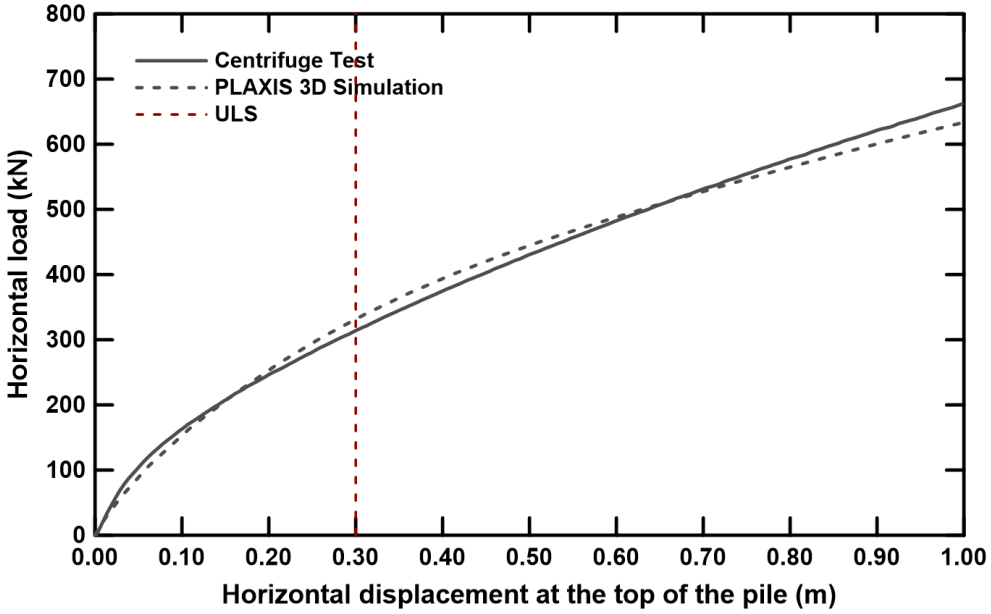

Appendix Figure 7 Calibration test with the load-displacement curves for the no-scour centrifuge experiment and the equivalent numerical analysis.

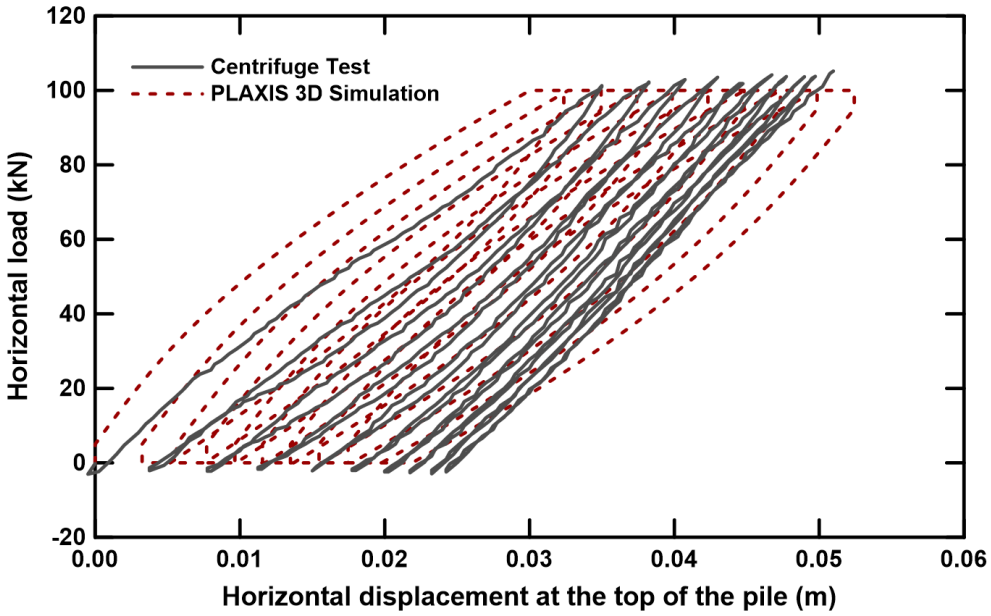

Appendix Figure 8 Calibration test with the load-displacement curves for 10 cycles of the "one-way" centrifuge experiment and the equivalent numerical analysis.

E. IFR & Interface Analyses

In the Appendix Figure 9, the IFR impact on the lateral capacity of the soil is presented. More specifically, three different values of the IFR have been chosen, with the 77.5% and 50% being more realistic and the 10% being an extreme low value. In the centrifuge experiments it was not feasible to see inside the pile and define this parameter, so this set of extra analyses has been conducted for this reason. As it can be seen, the impact of this parameter is not considerable in the lateral capacity of the soil, especially between the first two realistic values. This can be attributed to the fact that the lateral capacity is mobilized by normal soil stresses, while the shear stresses offer mainly to the vertical capacity to the pile, which is not the case in these analyses. Therefore, it can be concluded that IFR parameter is not going to affect the results and with this in mind, it was chosen to have a pile filled with soil in its interior up to a distance of 0.5D from the new soil surface that occurs for every scour depth. This corresponds to a IFR value of about 75% for all cases.

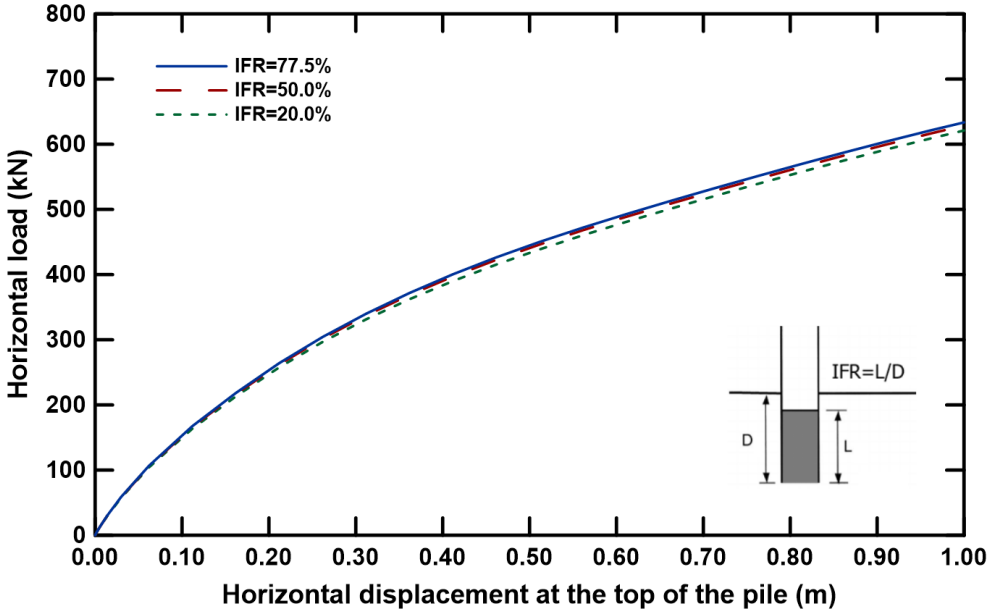

Appendix Figure 9 Load-Displacement curves for different incremental filling ratios.

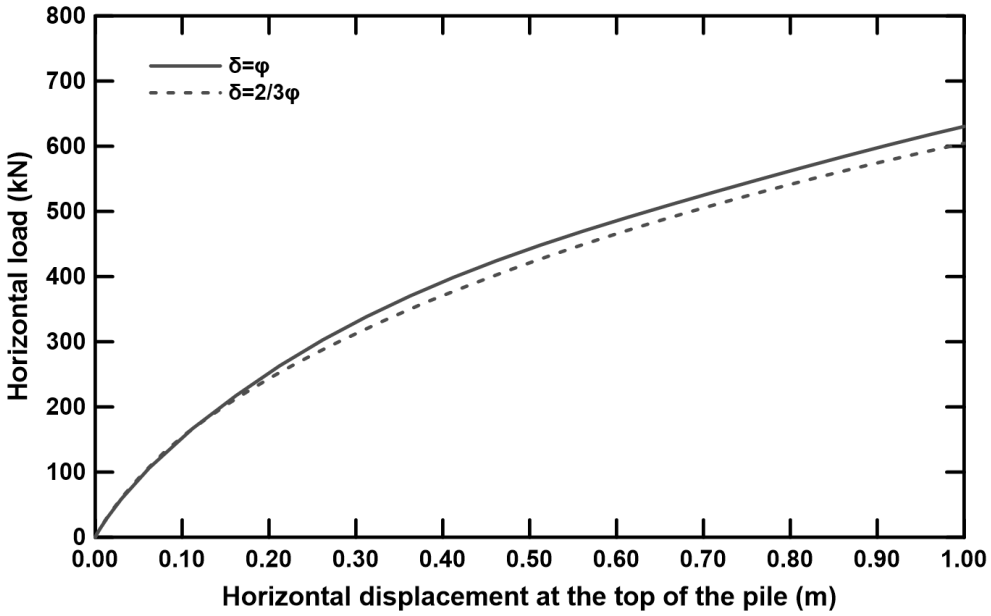

Appendix Figure 10 Load-Displacement curves for different interface properties.

In the Appendix Figure 10, the interface properties' impact on the lateral capacity of the soil is presented. More specifically, two different values of the properties have been chosen, δ=φ and δ=2/3φ. As it was already mentioned, the pile due to the installation of the strains and the glue for water-sealing was really rough in its external surface. On the same context, due to the cables of the strains in the interior of the pile, equally rough internal surface is expected. Therefore, the δ=φ case is considered to be the more realistic value for defining the interface properties. As it can be seen in the graph below, the δ=φ case offers higher soil resistance than the δ=2/3φ case. However, their difference, especially in the area of failure (about 0.60 m displacement at the top of the pile) is small, less than 5%. Consequently, it was chosen to use the interface with properties δ=φ, as this case was considered more realistic and in any case the influence of this parameter is not at any point critical in the horizontal soil capacity.

F. P-y Curves Assumptions

Acquiring the p-y curves requires at least two integration constants, as explained in section 4.1.2.2, which can be either a measures displacement or rotation at any point of the pile. The centrifuge set-up allowed for only one known point, the pile' head displacement. Therefore, a second point was missing in order to extract the p-y curves. A common point used in the literature is the rotation at the pile head or the point where no deflection occurs, which the constant rotation point of a rigid pile. It was decided to make an assumption for the second point, the rotation one, based on PLAXIS simulations (with the model described in section 3.2.1) by modelling 4 experiments, the no-scour one and the global scour cases for 1.0, 1.5 & 2.0D. In Appendix Figure 11 the pile deflection for a constant interval of 0.10 m displacement at the pile head is presented for a no-scour case and three scour depths (1.0, 1.5 & 2.0D). The PLAXIS simulations confirm the very rigid response of the monopile, as almost no deformation occurs in the pile axis. Regarding the rotation point, it is obviously getting deeper as the scour hole increases. However, the ratio between the distance of the rotation point form the new soil surface and the current embedded pile length is around 70% for all cases. Therefore, this value has been used in the MATLAB code implemented for deriving the p-y curves.

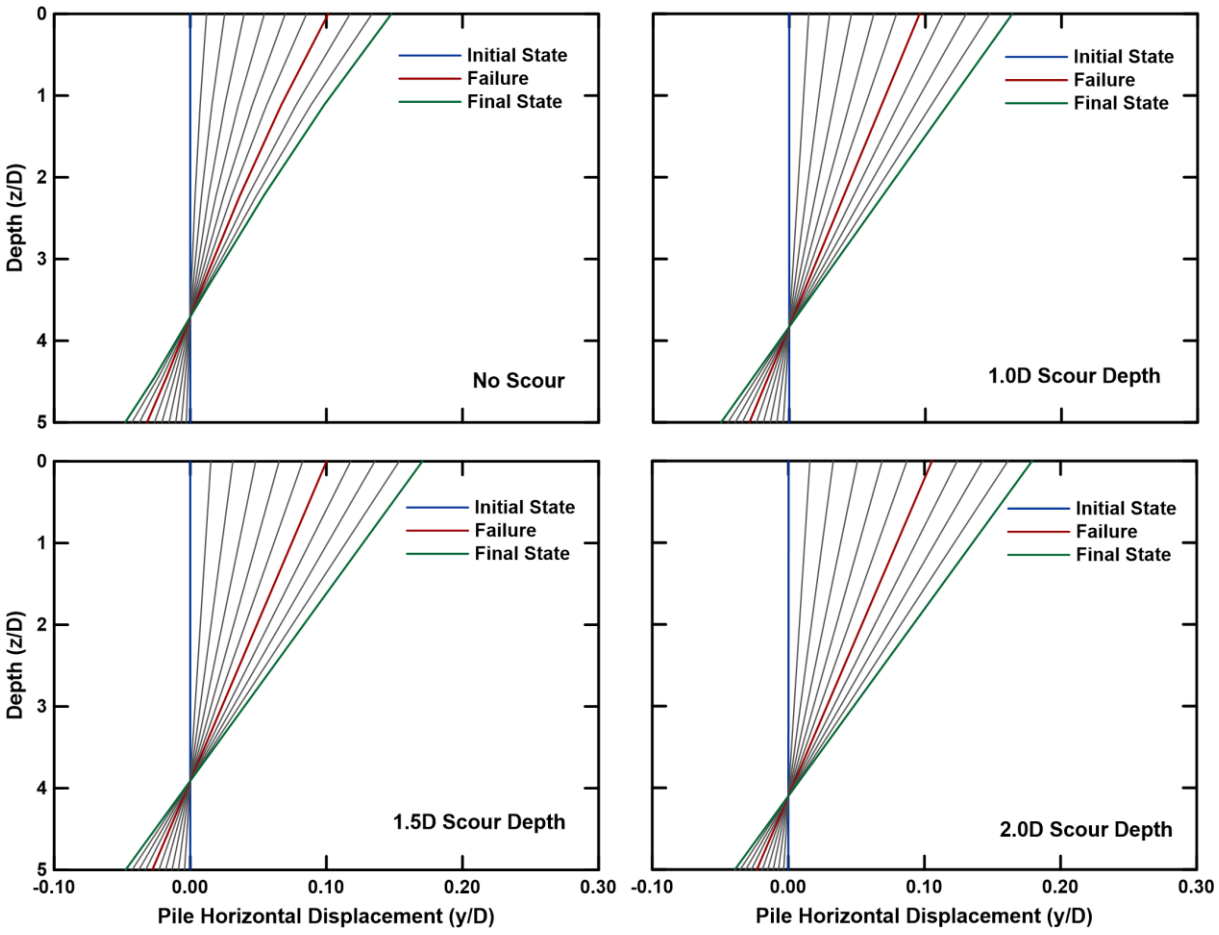

Appendix Figure 11 Evolution of the pile deflection during the monotonic push for the no-scour case and the three scour depths (1.0, 1.5 & 2.0D) for a constant interval of 0.10 m pile head displacement.